Mass transfer and catalytic reaction in a three-phase monolith reactor

Serbetcioglu, Serpil

Award date:
1993

Awarding institution:
University of Bath

MASS TRANSFER AND CATALYTIC REACTION IN A THREE-PHASE MONOLITH REACTOR

submitted by Serpil Serbetcioglu

for the degree of PhD

of the University of Bath

1993

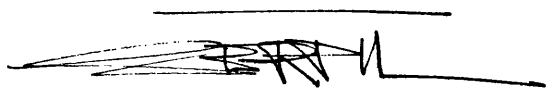

ProQuest LLC
789 East Eisenhower Parkway
P.O. Box 1346
Ann Arbor, MI 48106-1346

Dedicated to Rob.

Thank you for your patience and support.

SUMMARY

For the production of siloxane fluids, the viability of using a multi-channel monolith as a catalyst support system in a three-phase reactor, has been studied.

The reaction kinetics of the condensation polymerisation reactions of partially endblocked and linear polydimethylsiloxanes were first of all studied in a spinning basket, semi-batch reactor. The catalyst was a tripotassium phosphate (K_3PO_4) in the form of pellets and also applied as a coating onto the surface of ceramic monolith support systems. For temperatures in the range of 370 to 420K and fixed purge gas flowrate, the reaction was shown to be first order with respect to concentration of hydroxyl groups for C_{OH} = 20 to 170 $molm^{-3}$.

Although calculated values of the reaction rate constant based on the external surface area were similar, when the values were compared on a reactor volume basis then it was evident that higher reaction rates could be achieved with a monolith support system.

A single channel (15mm *i.d.*) flow reactor was also employed to study the reaction kinetics of the condensation polymerisation reactions representing a single channel in a multi-channel system. Mass transfer coefficients were determined under reaction conditions in gas-liquid, cocurrent, trickle flow, down a catalyst coated tube. The solid-liquid interface mass transfer coefficients under reaction conditions were shown to be much higher than that expected for laminar liquid flow conditions.

Making use of an experimentally determined kinetic expression and a correlation for mass transfer a one dimensional model describing mass transfer and surface reaction was developed and compared favourably with experimental data. The model was used to predict the performance of a multi-channel reactor operating under similar

conditions as that experienced for a commercial packed-bed reactor. The simulation showed that the monolith support system with K_3PO_4 catalyst can achieve higher conversion than a commercial packed bed reactor.

ACKNOWLEDGEMENTS

The work presented in this thesis was carried out under the supervision of Dr. S.T. Kolaczkowski of the school of Chemical Engineering, University of Bath. The author wishes to express her gratitude to Dr. S.T. Kolaczkowski for his constant encouragement, valuable advice, guidance and personal interest in all aspects of this work.

The author would also like to thank the members of staff in the Inter Schools Workshop, and the chief technician, Mr. T. Walton for their active support and help during the construction and commissioning of the experimental rig.

The author is indebted to Dr. S. Perera for her valuable help and guidance on catalyst coating process.

The author is grateful to Dow Corning Ltd. for the making of a financial contribution to support this project and for the provision of technical advice.

The author expresses her appreciation to Ege University, Turkey, for the award of a research studentship supporting her during the period of study.

TABLE OF CONTENTS

NOMENCLATURE

A	pre-exponential factor in Arrhenius equation	$m^3_l\ m^{-2}_e\ s^{-1}$
A_s	free channel area	m^2
a	geometric external surface area of the inside channel wall coated with catalyst per unit free volume of the channel. (The surface area assumed to be smooth).	m^{-1}
C_A	concentration of reactant A	mol m^{-3}
C_B	concentration of reactant B	mol m^{-3}
C_{OH}	concentration of hydroxyl groups	mol m^{-3}
$(C_{OH})_o$	concentration of hydroxyl groups at the beginning of the reaction	mol m^{-3}
D	diffusion coefficient	$m^2\ s^{-1}$
D_p	degrees of polymer	
d_i	inside channel diameter	m
d_p	pellet diameter	m
E	activation energy	J mol^{-1}
F	factor in titration analysis	
F_l	molar liquid flowrate	mol s^{-1}
F_{OH}	molar flowrate of hydroxyl groups	mol s^{-1}
Go	Goucher number	
g	gravitation constant	$m^2\ s^{-1}$

k_c	reaction rate constant based on mass of catalyst	$m^3_l\ g^{-1}\ s^{-1}$
k_m	mass transfer coefficient	$m^3\ m^{-2}\ s^{-1}$
k_o	overall rate constant	$m\ s^{-1}$
k_r	reaction rate constant based on geometric external surface area	$m^3_l\ m^{-2}_e\ s^{-1}$
k_s	reaction rate constant	$m^3\ s^{-1}$
k_t	reaction rate constant based on total area	$m^3_l\ m^{-2}_t\ s^{-1}$
j	number of the section of the axial length	
L	reactor length	m
L_p	inclined plate length	m
N_c	cell density	$cell\ m^{-2}$
N_{OH}	number of moles of hydroxyl groups	mol
$(N_{OH})_o$	number of moles of hydroxyl groups at the beginning of the reaction	mol
N_p	number of particles	
n	reaction order	
n_s	number of sampling	
P	absolute pressure	bar
R	gas constant = 8.341	$J\ mol^{-1}\ K^{-1}$
Re	Reynolds number	
(R_{OH})	reaction rate per unit bed volume in terms of OH	$mol\ m^{-3}_{bed}\ s^{-1}$
r_A	reaction rate in terms of reactant A	$mol\ m^{-3}\ s^{-1}$

$(r)_e$	reaction rate based on external surface area	mol m_e^{-2} s^{-1}
$(r)_c$	reaction rate based on unit mass of catalyst	mol kg^{-1} s^{-1}
rpm	revolutions per minute	
Sc	Schmidt number	
S_c	geometric external surface area per unit bed volume	m_e^2 m_{bed}^{-3}
S_e	geometric external catalytic surface area	m_e^2
Sh	Sherwood number	
S_p	total surface area per unit mass of bed	m^2 kg^{-1}
S.R.	speed of rotation	rpm
s_v	volume of the sample	m^3
T	temperature	K
T_{in}	inlet temperature	K
t	reaction time	s
V	volume	m^3
V_{tit}	voume of the titrant	m^3
V_v	volume of the trapped volatile fluids	m^3
v	liquid velocity	m s^{-1}
W_{bed}	mass of the bed	kg
W_c	mass of the catalyst	kg
W_{nap}	mass of 2-naphthol	g
w_s	mass of a sample	g

X_{OH}	conversion of hydroxyl groups	
x_{OH}	molar fraction of hydroxyl groups	
x_w	wall thickness	m
z	axial direction	m

Greek letters

α	angle	
ϵ_m	bed void fraction of a monolith support	
ϵ_p	bed void fraction of a packed bed	
$\Re$	overall rate in terms of molar flowrate	mol m^{-2} s^{-1}
δ	liquid film thickness	m
μ	viscosity	kg m^{-1} s^{-1}
ν	kinematic viscosity	m^2 s^{-1}
υ	volumetric flowrate	m^3 s^{-1}
ρ	density	kg m^{-3}
μ	viscosity,	kg m^{-1} s^{-1}
σ	surface tension	N m^{-1}
ϕ	sphericity	

Subscripts

b	bulk
bed	catalytic bed
c	catalyst
e	geometric external surface area
f	functional group
g	gas
l	liquid
i	inside
OH	hydroxyl groups
o	overall
s	catalytic surface
t	total surface area

LIST OF FIGURES

LIST OF PLATES

LIST OF TABLES

CHAPTER 1

LITERATURE SURVEY

INTRODUCTION

The literature survey is presented in six different sections. The first section describes the siloxane polymers, their use and commercial development. The second section reviews general polymerisation reactions and mechanisms and then describes the mechanism and kinetics of dimethylsiloxane polymerisation. In the third section a commercial process for the condensation polymerisation of polydimethylsiloxanes is described and the properties of the Dow Corning 200 Fluid and its applications are also presented. In the fourth section the different types of three-phase reactors and the factors influencing the design of a three-phase reactor are discussed. The fifth section describes monolith support reactors and reviews the advantages and disadvantages of monolith supports. This section also reviews the work done on two-phase flow in monolith support systems and the applications of monolith reactors in three-phase systems. In the last section conclusions are drawn from the literature survey.

1.1 SILICONE POLYMERS

Silicon follows oxygen as the second most abundant element in the earth's crust. However elementary silicon is not found in the free state in nature. It occurs as silica (SiO_2) in sand and quartz and as metal silicates in most rocks. The industrially

important silicon-containing materials include both those which occur naturally like clay, asbestos, and mica and those which are extracted or synthesised such as elemental silicon, glass, and the silicones (Pearce, 1972).

The "silicones" are synthetic polymeric materials with a structure consisting of alternating silicon-oxygen atoms with one or more organic groups on each silicon. The term "silicone" is commonly used to describe both the polymers and the industrial products formulated from them. However, silicone has no place in scientific nomenclature therefore, the term "siloxane or polysiloxane" is used as scientific terminology to describe organo-silicon molecules.

1.1.1 DEFINITION OF SILOXANES

The chemical constitution of siloxanes may be represented by the generic polymer formula

$(R_nSiO_{[(4-n)/2]})_m$ where, $0<n<4$ and $m>2$.

At the extremes, if $n = 0$, and $m=2$ the formula reduces to that of silica and the compound is inorganic; if $n = 4$, the formula is that of tetraorganosilane, which is virtually an organic compound. Between these limits it is difficult to decide whether siloxanes should be described as organic or inorganic polymers. From the stand point of physical properties, they possess inorganic characteristics due to the high percentage of ionic character in the Si-O bonds, and organic characteristics due to the substitute groups and to the low intermolecular forces resulting from their shielding of siloxane skeletons (Barry and Beck, 1962). Polymer nomenclature is inherently complex and

difficult to use and, as a result, that of siloxanes is simplified by the use of the letters M, D, T, and Q to represent functional monomer units. The basic structural units and their equivalent symbols of polyorganosiloxane are shown in Table 1.1 (Hurd, 1946).

Table 1.1 Formulas and symbols for siloxanes (Hurd, 1946)

n	Formula	Functionalism	Symbol
3	$R_3SiO_{0.5}$	monofunctional	*M*
2	R_2SiO	difunctional	*D*
1	$RSiO_{1.5}$	trifunctional	*T*
0	SiO_2	tetrafunctional	*Q*

The organic group (-R) is used to indicate the methyl group (CH_3). Primes, *eg*, *D'*, are used to indicate substitutes other than methyl. In commercial siloxanes, the R groups may be any of the following: methyl, longer alkyl, fluoroalkyl, phenyl or vinyl.

1.1.2 TYPES AND FORMS OF SILOXANES

The most widely used type of siloxanes is siloxane fluids. The siloxane fluids which comprise the equilibriated end-blocked polysiloxanes differ from those which contain terminal silanol groups and are therefore capable of further polymerisation. Being equilibriated, they are mainly linear polysiloxanes although those of very low viscosity may contain small amounts of cyclic polysiloxanes (Fordham, 1960). Dimethylsiloxanes, the most important members of the class of silicone fluids, have been made in viscosities that range from 10^{-6} to 10 $m^2 s^{-1}$ at room temperature. Their

viscosity depends upon the length of the molecular chains. Dimethylsiloxanes are conventionally represented as being built up of long rows of difunctional units *D* terminated at both ends by monofunctional units *M*, as $M(D)_yM$. The ratio of *M* to *D* in the chain controls the average molecular weight and the viscosity of the product. This structure is represented as follows:

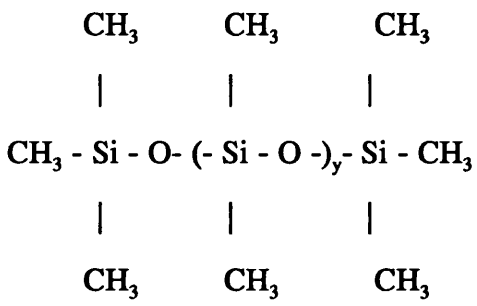

Silicone rubbers are made from high-molecular-weight fluids compounded with fillers and curing agents. The degree of crosslinking determines the consistency of the cured rubber. Increasing the degree of crosslinking produces silicone resin used in the formulation of paints, water repellents, moulding compounds and electrical insulation.

In addition to dimethylsiloxanes, there are also other commercially available siloxane fluids which are mainly phenylmethyl and fluorinated siloxanes. Phenylmethyl compounds withstand higher temperatures than do dimethylsiloxanes. Fluorosiloxanes resist chemicals that attack dimethylsiloxanes. These chemicals include chlorinated solvents and most hydrocarbon fuels.

Some important characteristics of siloxanes are summarised as follows (Schiefer and Pape, 1982):

(a) Siloxanes are available in a variety of forms, from free-flowing liquids to rigid solids, including every intermediate form such as greases, gels, and soft and hard rubbery solids.

(b) Siloxanes resist change (*i.e.* they are chemically inert, thermally stable, and water resistant). They repel water, yet permit the transmission of water vapour. They withstand most chemicals, weather, ozone, sunlight, including ultraviolet radiation.

(c) They have low surface energy. This enables them to be used for the control and prevention of foaming in vessels and reactors, and as release agents to prevent materials from sticking to processing equipment such as conveyor belts.

(d) Most siloxanes are nontoxic and do not react with other chemicals. These properties have led to the development of compounds for food-processing applications, and medical-grade siloxanes as well.

1.1.3 COMMERCIAL DEVELOPMENT OF SILOXANES

The commercial development of siloxanes is described in a number of references *e.g.* Barry and Beck (1962), Fordham (1960) and Kirk and Othmer (1982). In summary, in 1863 Friedel and Crafts reported the synthesis of tetraethylsilane, the first organosilicon compound. This stirred the interest of many researchers, who, armed only with difficult and poorly rewarding synthetic methods, provided by the turn of the century the science with a foundation of about 27 compounds. The work of Kipping and his colleagues at Nottingham, England (1901-1944), made possible by the discovery of the Grignard reagent, contributed monumentally to the knowledge of organosilicon

chemistry. The work was fruitful beyond these ends, for in their experiments on the condensation of silanols they obtained polydimethylsiloxanes. In spite of his accurate perception of their Si-O-Si chain structure, Kipping named the products "silicones", since he had expected elimination of water from silanediols to give silicon analogues of ketones ($R_2Si=O$). Though they were not then considered significant, those compounds were the prototypes for today's commercially important polysiloxane fluids, rubbers and resins. The term "silicones" has persisted as a trivial name.

Although the scientific interest in silicones can be traced to the nineteenth century, industrial interest did not begin until the early 1930s. The methyl silicones, which for both economic and technical reasons dominate commercially, were initially chosen for investigation and development because of their general stability and inertness.

In the United States Corning Glass Works pioneered work on organosilicon polymers. Their objective was to develop resins as varnishes and as partners for glass fibre in high temperature electrical insulation. A number of interesting silicone fluids were obtained as rewarding by-products of that work. This was complemented by a series of polydimethylsiloxane fluids developed by McGregor and his co-workers (under Corning Glass Works sponsorship) in 1938 and succeeding years. In the same period, the General Electric Company had similar interests but first chose to work with silicate esters. Somewhat later Union Carbide Corporation began a programme of organometallic research, which included organosilicon chemistry. Expansion to pilot-plant production by Corning and General Electric was followed by the formation of Dow Corning Corporation in 1943, a joint effort by Corning Glass and Dow Chemical Company. In 1942 the silicone knowledge of Corning Glass Works and the industrial organics experience of the Dow Chemical company were brought together to expedite production of the first commercial silicone sealing compound for aircraft.

Until 1953 almost the entire world production of all types of silicones was based in the U.S.A. at the plants of the Dow Corning Corporation and the General Electric Co. Since then there has been very rapid growth in the installation of silicone manufacturing facilities in the world. There are now four basic manufacturers of silicones in the United States: Dow Corning, General Electric, Union Carbide, and Stauffer-Wacker Silicones. There are also large producers in the UK, France, Germany, Japan, and Russia and small manufacturers in Belgium, Italy and Czechoslovakia.

1.1.4 USES OF SILOXANES

Siloxanes are widely employed in the chemical process industries. In various forms, they appear as process aids, construction and maintenance materials, and raw materials for processes.

The use of siloxanes in chemical processing is growing due mostly to (Scheiefer and Pape, 1982):

(a) An increasing awareness among chemical and petroleum engineers of the capabilities of this relatively young class of synthetic materials.
(b) The declining price differential between siloxanes and hydrocarbon-based synthetic materials.
(c) The compatibility of siloxanes with the environment. While not biodegradable, the basic siloxane molecule often breaks down into harmless materials found naturally in the environment.

Silicone polymers as a generic type are thus intermediate in composition between the purely inorganic silicates and organic polymers used in almost every industry. They are the only class of semi-inorganic polymers which have achieved commercial importance (Pearce, 1972). The reason for the widespread use lies in the fact that silicones are not a single product but a group of highly diverse materials made in the form of oils, resins, rubbers, greases and emulsions.

The variations of the physical and chemical characteristics of silicones, from vapours to solids and from reactive chemicals to inert polymers, permit many unique combinations. This has resulted in several hundred products and many more applications in over twenty major industries. Tables 1.2 and 1.3 summarise applications of silicones (Meals and Lewis, 1959).

1.2 POLYMERISATION REACTIONS

There are two types of classification describing polymerisation reactions: one classification divides polymers into condensation and addition polymers (Carothers, 1929) and the other divides them into step and chain polymers (Flory, 1953). In this section the principles of these classifications of polymerisation are reviewed in order to select an appropriate reaction mechanism, for the polymerisation of polydimethylsiloxane.

1.2.1 CONDENSATION AND ADDITION POLYMERS

Polymers were originally classified by Carothers (1929) into condensation and addition polymers on the basis of whether or not the repeating unit of the polymer contains the same atoms as the monomer.

Table 1.2: Product groups of silicones (Meals and Lewis, 1959)

Product groups	
CHEMICALS	**GREASE**
Intermediates	Lubrication
RUBBER	Dielectric
Moulding and extrusion	Mechanical
Cloth coatings and tape	**ADHESIVES AND SEALANTS**
Wire and cable	Electrical
FLUIDS	Mechanical
Dielectric	**RESINS**
Hydraulic damping	Electrical insulation
Lubricants	Laminating and moulding
Antifoam	Release agent
Water repellents	Protective coatings and paints
Release	Water repellents
Polish	
OILS	
Textile treatments	
Paper treatment	
Polish manufacture	
Release and antifoam agents	

Table 1.3: Specific applications of silicones (Meals and Lewis, 1959)

Specific applications
RELEASE AGENTS
Rubber and plastics
Glass
Food
Metal casting
SURFACE TREATMENTS
Paper
Glass and glass fibres
Masonry and ceramics
MISCELLANEOUS
Cosmetics and drugs
Pharmaceuticals
Additives
Consumer products

Polymerisation reactions can be classified to be condensation polymerisation according to the following conditions:

(a) if a small molecule (or molecules) such as water is eliminated during the reaction,

(b) if polymerisations proceed by a series of stepwise reactions,

(c) if any atom other than carbon is present in the backbone of the organic polymer, and

(d) if the polymers contain functional groups as part of the polymer chain.

Addition polymerisations are those in which none of these conditions takes place in the polymerisation.

Some naturally occurring polymers such as cellulose, starch, wool and silk are classified as condensation polymers since their synthesis can be postulated from certain hypothetical reactants by the elimination of water.

1.2.2 POLYMERISATION MECHANISMS

Carother's original distinction between addition and condensation polymers was amended by Flory (1953), who placed emphasis on the *mechanisms* by which the two types of polymer are formed; condensation polymers are usually formed by the stepwise intermolecular condensation of reactive groups whereas addition polymers ordinarily result from chain reactions involving some sort of active centre.

Step polymerisation proceeds by a series of stepwise reactions. The size of the polymer molecules increases at a relatively slow rate until eventually large polymer molecules containing large numbers of monomer molecules have been formed. The high molecular weight polymer is obtained only near the very end of the reaction. Any two molecular species can react with each other throughout the course of polymerisation. Step polymerisation can be schematically represented by one of the individual reaction steps

A-mer + B-mer $\rightarrow$ (A+B)-mer

with the realisation that species so connected can be any molecules containing A-mer and B-mer groups.

Chain polymerisation requires an initiator to start the reaction. The initiator produces a reactive species which may be a free radical, cation, or anion that is added to a monomer molecule. Polymerisation occurs by the propagation of the reactive centre by successive additions of large numbers of monomer molecules in a chain reaction. This happens in a matter of a second or so at the most. High molecular weight polymer molecules are achieved from the beginning of the reaction, and almost no species intermediate between monomer and high molecular weight polymers are found. The only thing that is accomplished by allowing the reaction to proceed somewhat further is an increased yield of polymer. Monomers can react only with the propagation reactive centre, not with monomers. The growth of the polymer chain ceases when the reactive centre is destroyed by one of a number of possible termination reactions. Hence to describe the mechanism of chain reaction requires three different steps: initiation, propagation, and termination. Some of the differences between the mechanisms of chain and step polymerisation are summarised in Table 1.4 (Billmeyer, 1984).

Table 1.4: Distinguishing features of chain and step polymerisation mechanisms (Billmeyer, 1984).

Chain Polymerisation	Step polymerisation
Only growth reaction adds repeating units one at a time to the chain	Any two molecular species present can react.
Monomer concentration decreases steadily throughout reaction.	Monomer disappears early in reaction: at D_p* 10, less then 1% monomer remains.
High polymer is formed at once; polymer molecular weight changes little throughout reaction	Polymer molecular weight rises steadily throughout reaction.
Long reaction times give high yields but have a small effect on molecular weight.	Long reaction times are essential to obtain high molecular weights.
Reaction mixture contains only monomer, high polymer, and about 10^{-8} part of growing chains.	At any stage all molecular species are present.

* Degrees of polymer

1.2.3 KINETICS OF STEP POLYMERISATION

The rate of step polymerisation is the sum of the rates of reactions between molecules of various sizes, that is, the sum of the rates for reactions such as:

monomer + monomer $\xrightarrow{k_1}$ dimer

dimer + monomer $\xrightarrow{k_2}$ trimer

dimer + dimer $\xrightarrow{k_3}$ tetramer

trimer + monomer $\xrightarrow{k_4}$ tetramer

etc.

The kinetics of such a situation with innumerable separate reactions would normally be difficult to analyse. However, Flory (1939) stated that all of these reactions are chemically identical and their reaction rates may differ only in so far as reactivity affected by molecular weight. Having studied the kinetics of polyesterification reactions and comparing them with several non-polymer forming esterifications, Flory (1939) confirmed that polyesterification and esterification reactions follow similar courses and concluded that the reaction rate is not affected by either increase in molecular weight or increase in viscosity.

On the basis of these results, together with the assurance provided by theoretical considerations, Flory (1953) concluded that at all stages of the polymerisation the reactivity of every like functional group is the same. The reactivity of these functional groups was assumed to be independent of the size and molecular weight of the molecule to which they are attached. This principle of equal reactivity simplifies immensely the kinetic treatment of polymer reactions for it permits total disregard of the complex

array of molecules participating in the polymerisation. Instead, the polymerisation process may be regarded merely as a reaction between functional groups without differentiating according to the sizes of the molecules to which they are attached. In other words, the reaction rate constant may be considered to be the same regardless of the sizes of the molecules involved in a given process. Rate expressions are most conveniently set down, therefore, in terms of the concentrations of functional groups and a single reaction rate constant may be used for all reactions in which the same chemical process is involved.

In reactions such as step polymerisations (which are reversible), the by-product water must be removed as it is formed. The kinetic expressions become less meaningful at higher molecular weights because the high viscosity of the polymer makes it physically more difficult to remove the water (Stevens, 1975). From a practical viewpoint, in order to obtain high yields of high molecular weight product, such polymerisations are run in a manner so as to continuously shift the equilibrium in the direction of the polymer (Odian,1981). This may be accomplished by the removal of water under reduced pressure. Under these conditions the kinetics of the polymerisation can be handled by considering the reactions to be irreversible (Odian, 1981).

Carothers (1929) developed a simple equation for relating degree of polymerisation D_p (defined as the average number of repeating units of all molecules present) to fractional conversion of monomer. If one assumes that there are (N_o) molecules initially and (N) molecules after a given reaction period, the amount reacted is $(N_o\text{-}N)$. The fractional conversion X is then given by

$$X = \frac{N_o - N}{N_o} \qquad (1.1)$$

The degree of polymerisation is equal to

$$D_p = \frac{N_o}{N} = \frac{1}{1 - X} \qquad (1.2)$$

This simple equation demonstrates one fundamental aspect of step polymerisation *i.e.* very high conversions are required to achieve high molecular weights (Stevens, 1975). It is possible to relate the average degree of polymerisation in a step process to polymerisation rate in the following manner.

If it is assumed that the reaction is first order with respect to one of the functional groups, then the rate equation is expressed as:

$$-\frac{dC_f}{dt} = kC_f \qquad (1.3)$$

where:

C_f is the concentration of the functional group, at any time.

k is the reaction constant which is assumed to be the same for each reaction.

t is the reaction time.

The integration of equation (1.3) gives

$$\frac{C_f}{C_{fo}} = e^{-kt} \qquad (1.4)$$

where $(C_f)_o$ is the concentration of the functional group at the beginning of the reaction. If it is assumed that the reaction occurs at constant volume, then substituting for $N = V C_f$ and $N_o = V(C_f)_o$ into equation (1.4) and combined with equation (1.2) to yield

$$D_p = e^{kt} \qquad (1.5)$$

Thus, knowing the reaction rate constant, the degree of polymerisation at time t can be calculated.

1.3 DESCRIPTION OF A COMMERCIAL CONDENSATION POLYMERISATION PROCESS AND ONE OF ITS PRODUCTS

1.3.1 THE REACTION OF POLYDIMETHYLSILOXANES

The principal reaction under study in this thesis and occurring in a commercial process was the polymerisation of linear polydimethylsiloxanes to form endblocked polydimethylsiloxanes of stable viscosity and low silanol (SiOH) content. One of the steps of the polymerisation reactions of dimethylsiloxanes may be represented as follows:

a $HO\text{-}(Si(CH_3)_2\text{-}O)_x\text{-}O\text{-}Si(CH_3)_2\text{-}OH$ +

b $Si(CH_3)_3\text{-}O\text{-}(Si(CH_3)_2\text{-}O)_y\text{-}Si(CH_3)_2\text{-}OH$ →

c $Si(CH_3)_3\text{-}O\text{-}(Si(CH_3)_2\text{-}O)_z\text{-}Si(CH_3)_3$ + H_2O

Since water molecules are eliminated during the reaction and the polymer contains the functional groups (-OH) the polymerisation reaction can be classified as a condensation polymerisation.

On the basis of the literature review it was decided to assume that the mechanism of the condensation polymerisation of linear polydimethylsiloxanes may be classified as step polymerisation and the reaction rate may be expressed in terms of the concentration of hydroxyl groups (-OH) which are the functional groups of the reactant polymer.

1.3.2 DESCRIPTION OF A COMMERCIAL REACTOR

Unfortunately, there was little information in the literature on commercial reactors of the polymerisation reactions or their configurations. However some information was provided by Dow Corning Ltd describing a process to obtain high molecular weight polydimethylsiloxanes (Elms, 1989). This is schematically illustrated in Figure 1.1. The two reactors are packed with catalyst and may be operated either in parallel (for a low viscosity fluid requiring short residence time) or in series (for a high viscosity fluid requiring longer residence time). When operated in series the reactants flow down the first reactor and then through a water-siloxane separator. They are then fed back into the top of the second reactor which is identical to the first reactor.

Pressure drop in the reactors affects removal rates of volatile by-products (*e.g.* water), hence reaction rates. The ability to process and produce high viscosity products is throughput-limited by pressure drop. The process also suffers from undesirable side reactions which can adversely affect the quality of the polymers produced. This is suspected to occur as a result of variations in the residence time of the fluid in the reactors.

1.3.3 DESCRIPTION OF DOW CORNING 200 FLUID

The commercial process described above could be used to produce a class of silicone fluids called Dow Corning 200 Fluid (DC 200). This is a water-clear silicone fluid available in viscosities ranging from 0.65 x 10^{-4} m^2 s^{-1} to 60 m^2 s^{-1}.
Table 1.5 presents the physical properties of a typical DC 200 Fluid. The reaction studied in this thesis produced products which could be described by this class of fluid. Some of the important features of this fluid are summarised as follows (provided by Dow Corning Ltd, 1991):

(a) Little change in physical properties over a wide temperature span (a relatively flat viscosity-temperature slope from 233 K to 473 K).
(b) Excellent water repellency.
(c) Good dielectric properties over a wide range of temperature and frequencies.
(d) Low surface tension (readily wets clean surfaces to impart water repellency and release characteristics).
(e) Low toxicity.

Dow Corning 200 Fluid of viscosities above 10 x 10^{-4} m^2 s^{-1} also exhibits heat stability, oxidation resistance, very low vapour pressures, and high flash point.

1.3.4 APPLICATIONS OF DOW CORNING 200 FLUID

Its unique combination of outstanding properties suits DC 200 Fluid for a variety of application functions , as well as for a wide range of products and processes. The main applications of DC 200 Fluid may be summarised as follows:

(a) As a release material: Being used alone or as part of compounded formula, it provides a non-toxic, non-carbonising mould release for rubber, plastics, and metal die castings.

(b) As a foam preventive: Extremely small amounts of the fluid effectively control foam in many processing operations, especially in non-aqueous systems.

(c) As a mechanical fluid: Excellent viscosity-temperature characteristics, thermal and chemical stability, shear-breakdown resistance, compressibility, and rubber compatibility make DC 200 Fluid outstanding for mechanical/hydraulic uses.

(d) As a surface-active material: Added to vinyl plastisols and liquid springs, DC 200 Fluid improves the flow characteristics, de-aerates and lubricates the surface of the completed part.

(e) As a lubricant: The fluid provides excellent lubrication for most plastic and elastomeric surfaces.

(f) In cosmetic and skin preparations: DC 200 Fluid is an important ingredient in hand creams, skin protectors, suntan lotions, and hair grooming aids because it forms a non-greasy, protective film which resists water and water-borne irritants, yet allows the skin to breathe.

(g) In polishes and chemical specialities: DC 200 Fluid is used in most automobile and furniture polishes for its ease of application, high gloss with minimum rubbing, and a durable water-repellent film.

(h) In electrical/electronic equipment: With excellent dielectric properties, DC 200 Fluid is widely used both insulating and damping applications.

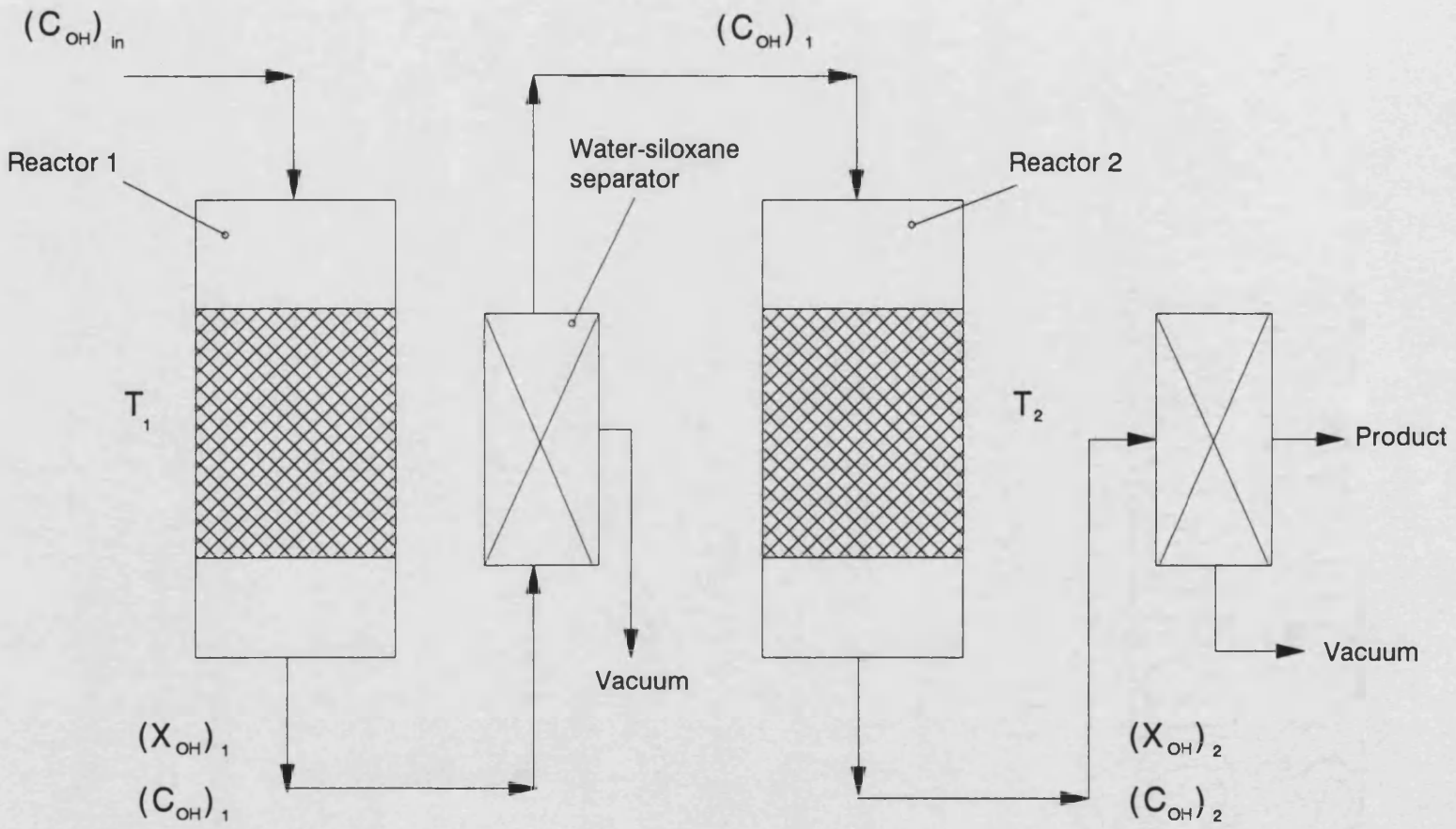

Figure 1.1 Schematic flow diagram of a commercial process for the condensation polymerisation of polydimethylsiloxanes (provided by Dow Corning Ltd, 1992)

Table 1.5 Physical properties of silicone fluids known as DC 200 (Supplied by Dow Corning Ltd., 1992)

Viscosity $m^2 s^{-1}$	Freezing point	Boiling point		Flash point	Thermal conductivity	Refractive index	Specific gravity	V.T.C*
at 298 K	T K	T K	N m^{-2} x 10^{-3}	T K	kg kcal $sec^{-1}cm^{-1}K^{-1}$	at 298 K	at 298 K	
0.00065	205	99.5	101	272	0.24 x 10^{-7}	1.375	0.761	0.31
0.002	189	230	101	352	0.26 x 10^{-7}	1.390	0.871	0.48
	Pour point							
0.005	208	70-100	0.066	375	0.28 x 10^{-7}	1.397	0.918	0.55
0.50	218	>200	0.066	547	0.36 x 10^{-7}	1.402	0.955	0.59
		Volatility						
		T, K	%					
1.00	218	473	<0.26	588	0.37 x 10^{-7}	1.403	0.968	0.60
2.00	220	473	<0.26	588	0.37 x 10^{-7}	1.4031	0.971	0.62
5.00	223	473	<0.26	588	0.38 x 10^{-7}	1.4033	0.972	0.62
10.00	223	473	<0.26	588	0.38 x 10^{-7}	1.4035	0.973	0.62

* Viscosity temperature coefficient

$$\frac{(\nu)_{311K} - (\nu)_{366K}}{(\nu)_{311K}}$$

1.4 THREE-PHASE REACTORS

Reactions can be classified in several ways, *i.e.*, on the basis of mechanism, with respect to operating conditions or according to the phases involved such as:

(a) homogeneous reaction, if only one phase is involved,
(b) heterogeneous reaction, if more than one phase actively participates in the reaction.

Heterogeneous reactions can be complicated by the fact that before substances in different phases can react, they must migrate to at least the interface. Consequently, in addition to chemical affinity, certain physical factors which affect the rate of mass transfer between phases also affect the overall rate of heterogeneous reaction.

A three-phase reactor is a system in which reaction takes place between gas, liquid and solid phases. The solid-phase can be either catalyst or inert. The application of these reactors is of increasing importance in the petrochemical and other industries. In most applications, the reaction takes place in the presence of a solid catalyst. In some cases, the liquid (or gas) is an inert medium and the reaction takes place between the gas (or liquid) and solid surface.

Three-phase reactors as used in industry can be classified into two main categories:

(a) fixed-bed reactors in which the solid catalyst is stationary, and
(b) gas-liquid-suspended solid reactors in which the solid catalyst is suspended and is in motion.

1.4.1 FIXED-BED REACTORS

In this type of reactor, the fluid phases flow through a fixed-bed of catalyst particles. The various modes of operation of fixed bed reactors are:

(a) trickle-bed reactor,
(b) cocurrent up-flow (bubble-bed) reactor, and
(c) segmented-bed reactor.

The reactor in which liquid is generally the dispersed phase and flows downward in the form of rivulets or a thin film and the gas is the continuous phase and flows either cocurrent or countercurrent is called a **trickle-bed reactor**. The trickle bed operation is normally carried out under cocurrent down flow condition; hence, flooding is not a problem in such a reactor. The trickle flow operation gives a lower pressure drop than bubble flow operation (Shah, 1979). The trickle-bed reactor is one of the most widely used three-phase reactors, especially in hydroprocessing operations, in which a variety of reactions between hydrogen, an oil phase, and a catalyst have been examined. Since the liquid flows as a thin film, overall resistance of the liquid film would be smaller than that obtained in other types of three-phase reactor. However, at very low liquid flowrates, flow maldistributions such as channelling and incomplete catalyst wetting may occur. In a trickle bed reactor operating in trickle flow it is possible to identify (Lemcoff et al., 1988) three types of zone which may adversely affect the performance of the reactor:

(a) Zones where the catalytic surface is covered by a thin trickling film which may not completely wet the surface.

(b) Zones where the catalyst particles locally covered by thick pockets of stagnant liquid.

(c) Zones where the catalyst particles are not irrigated by the liquid flow.

The hydrodynamic regimes have been examined by using various experimental procedures: visual and/or optical observations, electroconductimetric and thermoconductimetric tests and pressure drop measurements. For cocurrent gas-liquid down flow over a packed bed, various flow regimes can be obtained. Several studies have shown that the flow regime is related to liquid distribution, pressure drop, hold-up, and mass and heat transfer in three-phase reactors (Larkins et al., 1961; Weekman and Myers, 1964; Turbin and Huntington, 1967; Satterfield, 1975; Goto and Smith, 1975; Charpentier, 1976; Ng, 1986).

A number of flow maps have been published for down flow trickle bed reactors (Weekman and Myers, 1964; Sato et al., 1973; Charpentier and Favier, 1975; Specchia and Baldi, 1977; Scardi et al., 1979; Tosun 1984; Ng, 1986).

These flow regimes are widely accepted by authors mentioned above, to be classified into the following four flow regimes in trickle bed reactors illustrated in Figure 1.2a-d (Ng, 1986).

(a) **Trickling flow regime:** This regime is also known as the channelled flow or gas continuous flow regime. The liquid trickles over the packing surface in laminar flow, and the gas phase flows continuously through the remaining voids

in the bed (Figure 1.2a). Here the flow in one phase is not significantly affected by the flow in the other phase and there is minimum interaction between the two phases.

(b) **Pulsing flow regime:** The pulsing behaviour refers to gas and liquid slugs traversing the column alternately at high gas and liquid flow rates. Pulses always begin at the bottom of the bed, as the gas velocity is higher there due to lower pressure. Figure (1.2b) represents what one may see in a pilot-scale column; the packing particles are not shown. This regime appears to be one of "high interaction" between phases, due presumably to a high shear stress at the gas/liquid interface.

(c) **Spray flow regime:** Transition to the spray flow regime occurs when the gas flow rate is high while the liquid flow rate is kept at a low value. The liquid phase travels down the column in the form of droplets carried by the continuous gas phase (Figure 1.2c).

(d) **Bubble/dispersed bubble flow regime:** The bubble flow regime appears at high liquid flow rates and low gas flow rates. There is high interaction between the two phases. The entire bed is filled with the liquid and the gas phase is in the form of slightly elongated bubbles (Figure 1.2d). If the gas flow rate is increased, the bubbles become highly irregular in shape. This is referred to as the dispersed bubble regime.

The reactor with cocurrent up-flow operation of both gas and liquid is generally referred to as a packed bubble-column reactor (Hofmann, 1978). In this reactor, the gas phase is the dispersed phase while the liquid is a continuous phase. This type of reactor is

preferred when a relatively small amount of gas is to be processed with a large amount of liquid and also when a large residence time for the liquid is desired (Ramachandran and Chaudhari, 1983). This up-flow reactor gives better mixing and liquid distribution and higher transfer coefficients than the down flow reactor at equivalent conditions. However it also gives higher pressure drops and poorer conversion due to the axial mixing.

In the segmented fixed-bed reactors the catalyst is packed in vertically-suspended baskets and both the liquid and gas flow either cocurrent upward or downward or in a countercurrent mode. In a vertically-segmented bed, the three phases can be transported without plugging the reactor. The segmented bed reactor allows better flexibility of liquid to catalyst ratio, thus allowing better variations in homogeneous and heterogeneous reaction rates when both are possible (Shah, 1979). The high liquid-to-solid (catalyst) ratio may allow more homogeneous reactions which may not be desirable. Table 1.6 gives some practical examples of fixed bed reactors (Shah, 1979).

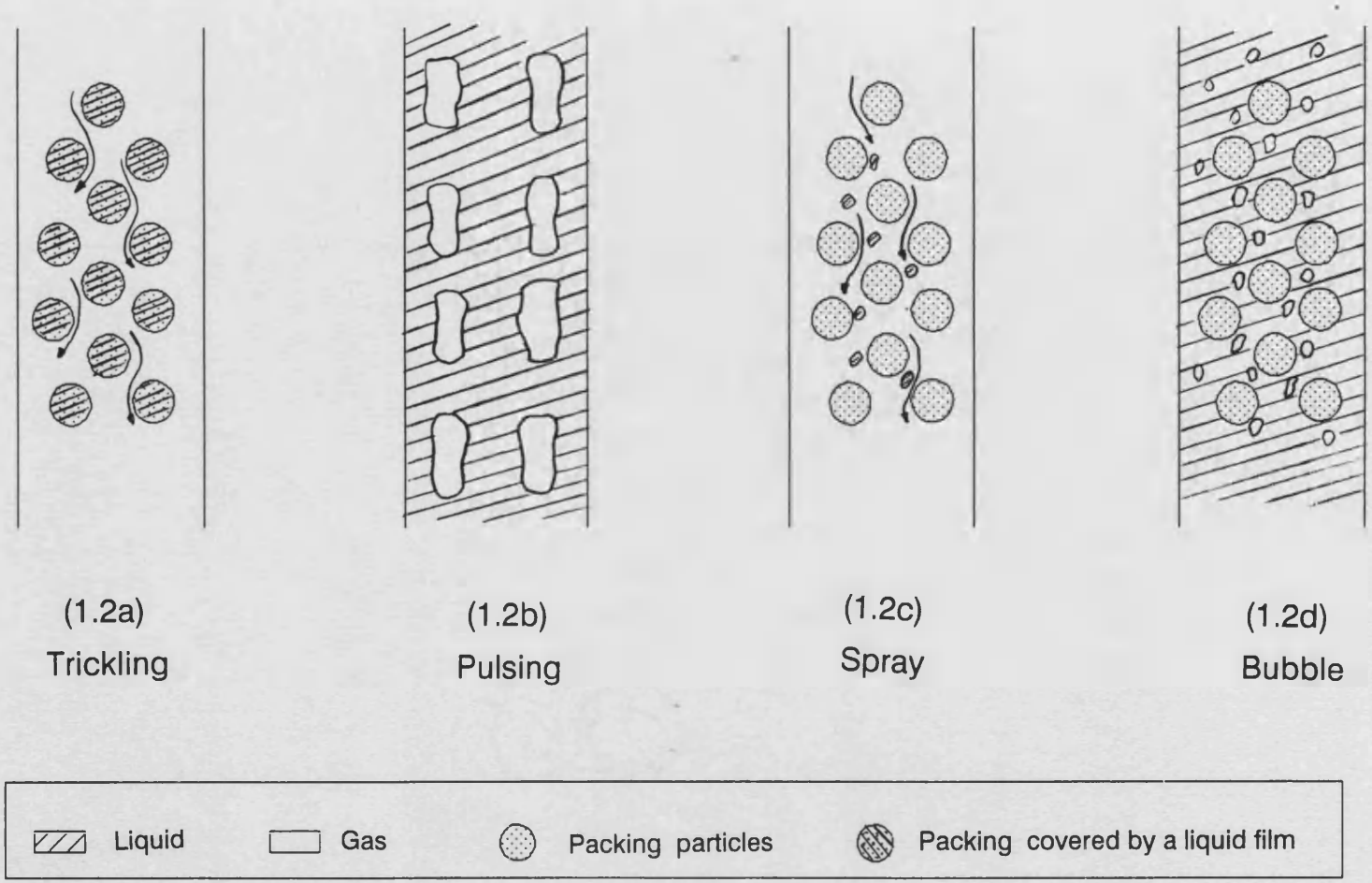

Figure 1.2 Flow pattern in trickle-bed reactors (Ng, 1986).

Table 1.6: Practical examples of fixed-bed reactors (Shah, 1979)

1. Trickle-bed reactor
a. Catalytic hydrodesulphrisation
b. Catalytic hydrotreating
c. Catalytic hydrocracking
d. Catalytic hydrogenation
e. Production of calcium acid sulphite
f. Synthesis of butynediol
g. Production of sorbitol
h. Oxidation of formic acid in water
i. Oxidation of sulphur dioxide in slurries of activated carbon
j. Hydrogenation of aniline to cyclohexylaniline
2. Cocurrent- up-flow (bubble-bed) reactor
a. Coal liquefaction
b. The Fischer-Tropsch process
c. Selective hydrogenation of phenylacetylene and styrene
d. Catalytic hydrodesulphrisation
3. Segmented-bed reactor
a. Coal liquefaction
b. Fermentation reactions

1.4.2 GAS-LIQUID-SUSPENDED SOLID REACTORS

This type of reactor can be subdivided into five categories as follows:

(a) agitated gas-liquid-suspended solid reactors,
(b) non-agitated three-phase slurry reactors,
(c) non-agitated three-phase cocurrent up flow fluidised bed reactors,
(d) non-agitated three phase countercurrent-flow reactors, and
(e) pulsating three-phase reactors.

The agitated and non-agitated slurry reactors are batch reactors in which the liquid does not flow through the reactor. They are used when a small quantity of product is required. The continuous three-phase fluidised-bed reactor is used for Fischer-Tropsch and catalytic coal-liquefaction processes. The pulsating three-phase reactor has been examined only at the laboratory level. The agitated and non-agitated slurry reactors are batch reactors in which the liquid does not flow through the reactor. These reactors are used when a small quantity of product is required. The major advantages of the gas-liquid-suspended solid reactors are that they give better flexibility of mixing, heat recovery, and temperature control. These reactors, however, give poor conversion due to axial mixing.

1.4.3 FACTORS INFLUENCING THE DESIGN OF A TRICKLE-BED REACTOR

In order to design a trickle-bed reactor the following aspects need to be carefully considered:

(a) hydrodynamics (flow regimes in the reactor),

(b) reaction kinetics and transport processes,

(c) gas and liquid hold-ups,

(d) pressure drop across the reactor, and

(e) residence time distribution.

The effects of these factors on the reactor performance are summarised below based on reviews published by Satterfield (1975), Shah (1979), Herskowitz and Smith (1983), Lemcoff et al. (1988), and Gianetto and Specchia (1992).

The performance of trickle bed reactors does not only depend on the reaction kinetics but also depends on the hydrodynamics and transport processes. The mixing characteristics and transport processes within a three phase reactor depend strongly on the flow regime. Different flow regimes may exist in a three-phase reactor, depending on the gas and liquid flow distributions, the packing properties, pressure drop, and holdup. The flow regime plays a very significant role in reactor scale-up. If data obtained in a pilot scale reactor are to be used for scale-up, then the flow regime in these two reactors must be the same. Uniform flow distribution is important in order to reproduce experimental data. Maldistribution can cause channelling or by-passing, which may adversely affect the performance of the reactor.

Since more than one phase is present in a three-phase system, the movement of the material from phase to phase must be considered in the rate equation. Thus the global rate expression will incorporate mass transfer terms in addition to the intrinsic kinetic term. The intrinsic kinetics should include the detailed mechanism of the reaction, the kinetic expression and heat of reaction associated with each step of the mechanism.

Two important parameters characterising mass transfer are mass transfer coefficient and interfacial area. Both these parameters depend on the flow conditions and nature of the packing.

In a pilot scale trickle bed reactor, the holdup of a phase, which is usually defined as the volume of the phase per unit reactor volume, may play an important role in changing the nature of the apparent kinetics of the reaction. When homogeneous and catalytic reactions occur simultaneously, the liquid holdup plays an important role in determining the relative rates of homogeneous and catalytic reactions.

The pressure drop across the reactor is an important parameter because the pumping costs could be a significant portion of the total operating cost. Additionally, some of the transport variables such as gas-liquid and liquid-solid mass transfer coefficients can be correlated to the pressure drop using the analogy between mass and momentum transfer processes. Significant pressure drop may also cause large undesired changes in the partial pressure of the reacting gas within the reactor.

As the fluid passes through the reactor the exchange of mass between the fluid elements occurs both on a microscale as well as on a macroscale. The mixing process on a macroscale is characterised by the residence time distribution of the fluid elements. Usually, only the macromixing is considered to have a significant effect on reactor performance. In a three phase reactor the residence time distribution for each flowing phase is measured separately. The reactor performance must take into account the role of residence time distribution, which is normally measured by tracer techniques.

1.5 MONOLITH SUPPORT REACTORS

Since the late 60's the use of monolithic supports for catalysts has been studied and used mainly in automotive emission control and for the purification of industrial waste gases. Most of the development of monolithic materials has been directed towards high-temperature applications required in those areas. However, there is a growing interest from the chemical industry to find applications for monoliths as a catalyst support in chemical processes. These applications often require high surface area monoliths.

1.5.1 DESCRIPTION OF MONOLITH SUPPORT SYSTEMS

Monolith support systems are composed of a large number of parallel channels, available in a variety of shapes, including the circle, hexagon, square, triangle and sinusoid and in a variety of hydraulic diameters. Monolith catalyst supports with hexagonal shaped passages resemble, and often are referred to as honeycombs. The channels in honeycomb structures, have hydraulic diameters of 1 to 7 mm (Kesselring, 1986). The length of the channels typically ranges from 1 cm to 1 m, and monoliths with diameters up to 2 m have been formed (DeLuca and Campbell, 1977). The monoliths can be stacked to produce any desired length of bed.

Monoliths may be made from a variety of materials *e.g.* low surface area ceramics such as mullite ($3Al_2O_3 \cdot 2SiO_2$) or cordierite ($2MgO \cdot 5SiO_2 \cdot 2Al_2O_3$) or metal monoliths that have been developed to overcome thermal shock and material stability problems sometimes encountered in the use of ceramics.

In order to achieve a high catalytic total surface area, coating material, such as γ-Al_2O_3, is required on the monolith. This washcoat strongly adheres to the ceramic support and provides a large surface area. At the same time, because the washcoat is thin (10-20 μm) the catalytic material which subsequent impregnates it is close to the main flow of reactants (Kesselring, 1986).

Ceramic monoliths have been manufactured by different techniques. However, of these techniques the corrugation and extrusion manufacture methods are the most frequently used (Deluca and Campell, 1977). The manufacturing procedure has a great effect on the physical properties of the monoliths.

Table 1.7 gives the physical properties of the most common monolith material (DeLuca and Campbell, 1977).

Table 1.7 Physical properties of a typical cordierite monolith support (DeLuca and Campbell, 1977).

Major composition	$2MgO{\cdot}5SiO_2{\cdot}2Al_2O_3$
Melting temperature	1523 K
Density of web material	1600 kgm^{-3}
Thermal expansion	1.0×10^{-6}
Thermal conductivity at 25°C	9.2 $W\ m^{-1}K^{-1}$
Specific heat at 25°C	0.84 $kJ\ kg^{-1}K^{-1}$
Average pore diameter	6 μm
Compressing strength -Parallel to channels -Perpendicular to channels	 $1.24 \times 10^7\ Nm^{-1}$ $1.37 \times 10^6\ N\ m^{-2}$

1.5.2 CATALYST COATING ON MONOLITHS

DeLuca and Campbell (1977) discussed the catalyst preparation methods by dividing them into the following four groups:

(a) Catalyst incorporation during manufacturing of monolithic supports.
(b) Deposition of active material directly onto the monolithic supports.
(c) Washcoating (i.e., laying down a high surface area coating) the monolith first and then catalysing.
(d) Depositing the washcoat and the active material at the same time.

Between these groups the most widely used method of coating a catalyst on a monolith support consists of first washcoating the monolith with a high surface area material and then depositing on this layer the active material. Monoliths are usually made with a surface of only 0.1 - 1.0 $m^2 g^{-1}$. A large surface area is obtained by coating the monolith surface with 5 - 20 % w/w of high surface area oxides. This coating gives a total surface area of 2.5 - 40 $m^2 g^{-1}$ based on total support weight (DeLuca and Campell, 1977). The desired properties of the washcoat are high uniformity, high surface area, good adherence to the monolith and good thermal stability. The thermal stability of the washcoat is often improved by adding small amounts of different oxides. The most common washcoat material is γ-Al_2O_3 (Kesselring, 1986).

1.5.3 THE ADVANTAGES OF A MONOLITH CATALYST SUPPORT

In applications such as gas-liquid contactors with cocurrent flow or in a trickle bed reactor the monolith support system offers several potential advantages over a packed bed system. These are summarised below:

(a) In a trickle-bed reactor, more than one phase is involved in the reaction. Interface mass transfer is therefore important between the gas and the liquid or between the liquid and the catalyst. The size of a catalyst particle affects the rate of mass transfer and the rate of reaction which takes place at the catalyst surface. In a packed bed system, if the size of the particles is decreased then a high surface area can be obtained, however the pressure drop increases in the reactor. One of the advantages of the monolithic support is the availability of a large external surface area to volume ratio, (over 2000 $m^2 m^{-3}$, Mazzarino and Baldi, 1987) offering the possibility of depositing the catalytic materials on it. Therefore a low pressure drop (10 -100 times lower than in packed beds, Mazzarino and Baldi, 1987) is achieved during the operation without loss in the geometric surface area.

(b) The design of a trickle-bed reactor is complicated by potential non-uniform liquid distribution. The size and shape of the particles is one of the important factors that affects the ability to achieve uniform liquid distribution in the bed. At low liquid flow rates only a part of the outer surface of the catalyst particles may be covered with the flowing liquid, hence incomplete catalyst wetting may occur which reduces the performance of the reactor. It is easier to accomplish uniform flow distribution and better contacting in a monolith support system than in a packed bed (Satterfield and Ozel, 1977).

(c) In a monolith support system, the uniformity of passageways is likely to minimize axial dispersion and hence enhance selectivity. Radial mixing between neighbouring channels could also be minimised.

(d) In two phase systems with liquids containing fine solids, such as those derived from liquefaction of coal, bed plugging may be minimized or avoided in a monolith support system (Satterfield and Ozel, 1977).

(e) In a cocurrent up-flow mode the maximum allowable liquid and gas flow rates through a conventional packed bed reactor are frequently limited by the desire to avoid fluidisation which can, for example, cause grinding of the catalyst. The use of monoliths may permit considerably higher flow rates to be utilized (Satterfield and Ozel, 1977).

(f) By their nature, particles are free to move when disturbed by pressure surges, shrinkage during the life of the catalyst or other mechanical actions. Therefore, special care must be taken with fixed bed particulate catalysts to avoid attrition or settling. It is also very difficult to have a particulate catalyst system in a horizontal reactor tube because of the tendency of the catalyst to "sag" away from the top of the tube, providing a by-pass channel. A monolith support system could be operated in a variety of positions without concern for "catalyst sag" (DeLuca and Campbell, 1974).

(g) In a metallic monolith, good thermal conductivity can be achieved (Mazzarino and Baldi, 1987).

(h) In a monolith support it is possible to obtain a high catalyst effectiveness in the presence of very fast reactions by superficial coating on a non porous support (Mazzarino and Baldi, 1987).

1.5.4 THE DISADVANTAGES OF A MONOLITH CATALYST SUPPORT

Some possible disadvantages of the monolith catalyst support system are listed below:

(a) The restricted radial communication of flow elements may make the contactors more sensitive to hot spots than conventional packing (Satterfield and Ozel, 1977).

(b) Suitable methods of obtaining good initial distribution on a large scale need to be developed (Satterfield and Ozel, 1977).

(c) If used as a catalytic reactor under conditions in which the effectiveness factor approaches unity, approximately twice the vessel volume will be needed, since the solid fraction of monolith packing is typically about one-half that of conventional packing (Satterfield and Ozel, 1977).

(d) The lack of sufficient information in the literature (Mazzarino and Baldi, 1987).

(e) The high cost of the available supports due to specific design for severe operating conditions (Mazzarino and Baldi, 1987).

1.5.5 TWO PHASE FLOW IN A MONOLITH SUPPORT SYSTEM

The prediction of flow patterns is a central problem in two phase gas-liquid flow in pipes since design parameters such as pressure drop and heat and mass transfer are strongly dependent on the flow pattern. In a two-phase system the flow patterns must be known in order to model the physical phenomena as closely as possible.

Several flow patterns are possible in gas-liquid two phase flow. These flow patterns and the transition between different flow regimes have been reviewed in a vast number of papers over the last 30 years. Hewitt and Hall (1970); and Bergles et al. (1981) reviewed two-phase flow patterns in a tube extensively in their books.

Satterfield and Ozel (1977) studied the characteristics of two-phase flow (air and water) in monolith catalyst structures. Particular emphasis was placed on the effect of gas and liquid flowrates on pressure drop. They took a large number of still photographs under a variety of inlet conditions in a piece of precision bore glass capillary tubing (0.2 cm id and 102 cm long). They interpreted the results in terms of liquid distribution, of the conditions under which slug-type flow occurs in contrast to annular flow and in terms of the relative contributions to the pressure drop of contrictions, hydrodynamic friction, and gravity head.

Hatziantoniou and Andersson (1982) studied two phase segmented flow (slug flow) and mass transfer, in a single channel monolith . The length and diameter of the channel were 0.17 m and 2.35 mm respectively. The inner wall of the channel was coated with a solid layer of benzoic acid. They studied the mass transfer of benzoic acid into a two-phase water/air mixture. Experiments were performed at room temperature and atmospheric pressure. They compared the solid-liquid mass transfer in the channel under slug flow conditions with continuous liquid flow (Skelland, 1974) and concluded that the solid-liquid mass transfer is much enhanced by introducing slugs of gas into the liquid flow. The presence of slugs in the flow decreases the axial dispersion and increases the radial mixing in the channel.

1.5.6 APPLICATIONS OF MONOLITH REACTORS IN THREE-PHASE SYSTEMS

Over the last 16 years there has been a number of studies exploring the use of monoliths in three phase reactors.

Satterfield and Ozel (1977) performed an exploratory study to assess the viability of using stacked monolith structures as gas-liquid contactors or in trickle bed reactors. Measurements were made of pressure drop during two-phase downward flow through a vertical 25.4 mm diameter stack of monolith sections that were 122 cm high. Individual sections were either 76 or 152 mm long, and contained either 200 or 360 cells per square inch. They concluded that the pressure drop is very sensitive to the nature of liquid distribution at the inlet to the bed. Also the monolith support may have considerable potential in trickle bed reactors, and the comparison with conventional catalyst supports shows that, on an equivalent basis, the pressure drop for two phase flow in monoliths is an order of magnitude or more below that for conventional packing.

Liquid-phase hydrogenation of aqueous nitrobenzoic acid was performed in the presence of a palladium catalyst by De Vos et al. (1982). The reaction conditions were 100-1000 kPa and 300-370 K. The monolith specimen was specially designed for cross flow processing with inflow of hydrogen in separate channels perpendicular to the inflow of the liquid phase. The catalyst consisted of a number of thin, porous plates, separated by corrugated planes. These planes were placed at a 90° angle to the corrugated planes immediately above and below. If the gas and liquid inflows are separated 90°, gas and liquid will not be mixed in the same channels and will moreover, penetrate the catalyst plates from different sides. The carrier specimens consisted of 19 parallel 50 x 50 mm porous plates, 0.2 mm thick, and 19 supporting corrugated plates situated between the plates. The height of the specimen was 35 mm and its mass was 15 g. The BET surface area was 44 $m^2 g^{-1}$. They concluded that this type of

catalyst support was found to give better availability of the active surface of the catalyst, lower external mass transfer resistance, and a lower pressure drop compared to an ordinary trickle bed of pellets.

Hatziantoniou and Andersson (1984) have performed liquid phase hydrogenation of nitrobenzoic acid in a honeycomb monolith reactor. The catalyst used was palladium on a ceramic monolith structure. The reactions were performed at 100-400 kPa and 300-350 K. The monolith specimens consisted of 24 parallel porous and plane plates and 24 supporting corrugated plates located between plane plates. The plates form 427 vertical channels with a cross-sectional area of 2.0 mm^2 per channel. The height of the specimen was 198.5 mm and its mass was 68 g. The BET surface area of the monolith was 14.7 $m^2\ g^{-1}$. The flow through the monolith was segmented gas-liquid flow (slug flow) in order to enhance mass transfer conditions. The authors also compared the monolith catalyst reactor with a typical laboratory trickle bed reactor under corresponding reaction conditions. The comparison favoured the monolith catalyst reactor. The advantages of the monolith catalyst were the short diffusion length in the solid catalyst (0.15 mm in monolith used, compared to 2.5 mm for a typical trickle bed), good contact between gas-solid and liquid-solid, uniform flow distribution, low axial dispersion and low pressure drop.

Hatziantoniou et al. (1986) have also studied mass transfer and selectivity aspects of a honeycomb monolith catalyst reactor compared to a slurry reactor, in liquid phase hydrogenation of nitrocompounds. The reactor type was similar to that used by Hatziantoniou and Andersson (1984) above. The reaction conditions were 500-1000 kPa and 343-373 K. The flow through the monolith was segmented two-phase flow. The mass transfer of hydrogen directly from the gas plugs to the channel wall was found to be the dominating transport step. The selectivity aspects on the use of

monolith catalyst reactor were illustrated by comparing the yield of aniline in hydrogenation with the monolith catalyst and with ground monolith catalyst in slurry hydrogenations. The decreased selectivity of aniline formation found in the hydrogenations in the monolith catalyst was explained by the influence of the film transport resistance near the channel wall.

Mazzarino and Baldi (1987) carried out the hydrogenation of α-methylstyrene to cumene in the liquid phase on a honeycomb monolith support coated with palladium. Three different operating modes were tested: single liquid phase (saturated with hydrogen), two phase downward flow, and two phase upward flow. The reaction was carried out at 303-323 K and 100 kPa total pressure. The monolith was 38 mm in diameter and 50 mm in length and consisted of 499 channels. For saturated single phase flow the conversion was measured for the monolith and a packed bed system containing palladium-alumina pellets. They concluded that the monolith catalyst support was a good alternative to the packed pellet bed especially when the reaction was very fast and limited by diffusion inside the pores of the catalyst pellets.

Table 1.8 gives recent important applications of monoliths as catalyst supports in three phase reactors.

Table 1.8 Recent important applications of monoliths as catalyst supports in three-phase reactors.

Authors	Reactions	Reactor types and remarks	Flow type	Conclusions
De Vos et al. (1982)	Liquid phase hydrogenation of aqueous nitrobenzoic acid with a Pd catalyst	The reactor consist of a number of a thin porous plates separated by corrugated planes and operated in cross flow mode; the hydrogen was fed in separate channels perpendicular to the inflow of liquid; the two reactants thus penetrated the catalyst plates from different sides.	Cross-flow	The effectiveness factor was determined to be much higher than in corresponding hydrogenations in a trickle bed. Cross-flow increased the availability of the active catalyst surface and reduced the liquid film resistance.
Hatziantoniou and Andersson (1984)	Liquid phase hydrogenation of nitrobenzoic acid with a Pd catalyst	The monolith support consisted of parallel porous and plane plates and supporting corrugated plates; the gas flowed cocurrently downwards with the liquid feed was pulsated whilst gas flow was continuous, forming the segmented gas-liquid pattern.	Segmented two-phase flow	The advantages of the monolith were determined to be: short diffusion length, good gas-solid and liquid-solid contact, uniform flow distribution, and low pressure drop.
Hatziantoniou et al. (1986)	Liquid phase hydrogenation of nitrocompounds with a Pd catalyst	Reactor type was similar to that used by Hatziantoniou and Andersson (1984) above.	Segmented two-phase flow	The selectivity aspects of the monolith catalyst reactor was compared with the slurry reactor. The decreased selectivity of aniline formation in the monolith catalyst support was due to the influence of the film resistance near the surface.
Mazzarino and Baldi (1987)	Hydrogenation of α-Metilstyrene to Cumene	A honeycombe ceramic support was used for the catalyst; three different modes were tested *ie* single phase saturated with hydrogen, two-phase downward and two-phase upward flow.	Single liquid and two-phase downward and upward	It was concluded that the monolith catalyst was a good alternative to the packed bed of particles in presence of a very fast reaction.
Irandoust and Andersson (1988)	Hydrogenation of 2-ethyl-hexanal	Reactor type was similar to that used by Hatziantoniou and Andersson (1984) above.	Segmented two-phase flow	The enhanced mass transfer between phases was detarmined due to the very high interfacial surface area in combination with a short diffusion length.
Irandoust et al. (1989)	Hydrogenation of anthraquinones	Reactor scale up was explored for a similar system to that describe in earlier work *eg* Hatziantoniou and Andersson (1984).	Bubble flow Slug flow	It was concluded that the scaling up of monolith three-phase reactors with downward slug flow was very straightforward. The flow in the narrow monolith channels was viscosity dominant, which gave an easily predictable flow behaviour.

1.6 CONCLUSIONS

(a) On the basis of the literature review the mechanism of the dimethylsiloxane polymerisation reaction is proposed to be a condensation polymerisation with stepwise reactions.

(b) Although the step polymerisation reactions are reversible, from the practical viewpoint of obtaining high yields of products such polymerisations are run in a manner so as to continuously shift the equilibrium in the direction of products. In the case of condensation polymerisation reactions this is accomplished by removal of the by-product, water, from the system. Under these conditions the kinetics of the polymerisation of dimethylsiloxanes can be practically handled by considering the reactions to be irreversible.

(c) From the concept of equal reactivity of functional groups (Flory, 1953) the reaction rate can be expressed in terms of the concentration of the functional hydroxyl group, (-OH) *ie.*

$$-\frac{dC_{OH}}{dt} = kC_{OH}$$

(d) Although the chemistry of the condensation polymerisation reactions are discussed in the literature, fundamental kinetic data to aid reactor design is scarce and in the literature surveyed there was no evidence that work had been done on the condensation polymerisation reaction of dimethylsiloxane fluids in monolith supports. There was also no information on how to coat the monolith with the catalyst of interest, hence a coating method needed to be developed.

(e) Since it is necessary to select a reactor system in which a low pressure can be maintained, to enhance the removal of water and any low molecular weight species formed as by products, a cocurrent trickle down flow reactor was selected for subsequent experiments.

(f) There are numerous potential advantages to be exploited from the use of a monolith catalyst system for the reaction of interest. These are summarised as follows:

-large external surface area to volume ratio,
-low pressure drop,
-uniform flow and residence time distribution,
-better contacting,
-minimised radial mixing and axial dispersion,
-good selectivity,
-avoidance of bed plugging and grinding of the catalyst, and
-availability in variety of bed positions.

(g) Since it is important to ensure uniform flow distribution at the inlet to a monolith reactor, it was decided to perform experiments in a single channel system in which a uniform and known flow of gas and liquid could be achieved.

CHAPTER 2

SEMI-BATCH REACTOR EXPERIMENTS

INTRODUCTION

Chemical reaction kinetic experiments were performed with the catalyst in the form of pellets and coated on monolith support systems. The catalyst in the form of pellets as used by Dow Corning Ltd, was used to provide a reference base with which to compare the monolith system. Experiments were performed in a spinning basket, semi-batch reactor. Preliminary experiments were initially undertaken in order to establish appropriate experimental conditions. Experiments were then performed to determine reaction kinetic data for both the pellet and monolith support systems. Experiments were done using both multi-channel and single channel monolith support systems.

This chapter is presented under the following headings:

2.1 Method of measurement and data analysis
2.2 Selection of an experimental method
2.3 Theoretical analysis
2.4 Experimental studies
2.5 Experimental results
2.6 Discussion of the results
2.7 Conclusions

2.1 METHOD OF MEASUREMENT AND DATA ANALYSIS

The successful design of a reactor lies primarily with the reliable determination of experimental parameters. Jordan (1968) classified the methods of measurement and data analysis which affect both the mode of experimentation and the method of design. Rase (1977) reviewed Jordon's (1968) classifications and concluded that there were at least four approaches to the problem of exploring and determining the kinetics and mechanism of the reaction. These are summarised as follows:

(a) Fundamental kinetic studies: In this method, the kinetics and mechanism of the reaction are evaluated using the best method of operation and analysis without regard to the industrial practicality of the method or the apparatus. Every effort is made to determine the reaction type and order and to find an equation (or equations) which describes the system accurately.

(b) Empirical kinetic studies: In this method, reaction kinetics are obtained using a scale model of the actual reactor (in fact, for many fixed-bed catalytic reactors the experimental reactor will be the same size as one tube in the production reactor). The experimental procedures and the analysis of the data do not attempt to discover the fundamental kinetics and mechanism of the reaction. Instead, the work measures the response of the system to changes in the more obvious external parameters. An overall result is achieved not a view of fundamental kinetics.

(c) Rate equation combined with scale-up: Reaction systems that are complex, and strongly influenced by mass and heat transfer, may not readily yield to methods 1 or 2. A third method for the investigation of chemical reaction kinetics is to build a suitable apparatus, which will be a scale model of the large apparatus, conduct an experimental program designed to study the effects of several variables, and correlate

the results graphically or by a simple equation. In this method it is not necessary to determine the reaction rate constant. This method is preferred for complex reactions which have many constituents in the feed and product and if it is essentially impossible to conduct a fundamental kinetics determination within a reasonable length of time.

(d) Graphical or regression techniques combined with scale-up: This method is a combination of the above in which a scale-down version of the actual reactor is used. Experiments are selected to obtain data which show the response of the system to changes in operating parameters. Regression analysis techniques are applied to develop equations for predicting conversion and yields as functions of the operating variables.

2.2 SELECTION OF AN EXPERIMENTAL TECHNIQUE

In order to study reaction kinetics there are various types of three-phase reactor which could be used to investigate the chemical kinetics of a reaction in a scientific way so that reproducible results of a fundamental nature are obtained. The experimental reactors should be operated in such a way that only chemical effects are measured, and physical effects such as heat transfer, mass transfer, and residence time distribution are either eliminated or minimised.

The criteria used to evaluate the different types of laboratory reactor are listed by Jordan (1968), Weekman (1974), Rase (1977), Shah (1979) and Fogler (1983) as follows:

- physical and chemical nature of feed,
- nature of catalyst and its aging function.
- nature of reaction,
- ease of sampling and product analysis,

- degree of isothermality,
- effectiveness of contact between catalyst and reactant,
- handling of catalyst decay,
- equipment cost and ease of construction,
- residence-contact time distribution,
- meaningful data analysis, and
- flow maldistribution and extraneous mass and heat transfer effects.

For the kinetic studies of the condensation polymerisation reactions, involving three phases the following laboratory reactors were considered:

(a) Stirred Slurry Batch Reactor
(b) Stirred Basket-Type Reactor
(c) Integral (Fixed-Bed) Reactor
(d) Continuous-Stirred Tank Reactor

The stirred basket-type (semi-batch) reactor as illustrated in Figure 2.1 was selected for the following reasons:

(a) It was considered to be the most suitable and straightforward to use for the evaluation of kinetic data.
(b) It may be possible to follow the progress of multiple reactions since the batch reactor gives cumulative effects.
(c) Ease of construction and sampling.
(d) External mass transfer may be minimised by increasing the spinning rate of the basket stirrer.

(e) It may be possible to slow down the progress of reactions in a batch reactor, using a large batch of the fluid and less catalyst.

(f) Accurate residence time measurement may be possible.

(g) Good catalyst-feed contact and good isothermal condition may be achieved since the reactor is well mixed.

(h) The condensation polymerisation reaction produces water which may be removed as water vapour in the purge gas stream.

2.3 THEORETICAL ANALYSIS

In order to calculate kinetic data from the experimental results the following assumptions were made:

(a) isothermal conditions were maintained in the reactor,

(b) good mixing was achieved in the reactor,

(c) external mass transfer limitations were minimised,

(d) the reaction took place on the catalytic surface,

(e) the density of liquid was constant during the reaction, and

(f) the reaction was assumed to be irreversible.

The reaction studied was the condensation polymerisation of linear polydimethylsiloxanes to form a high molecular weight polymer of stable viscosity and low silonal content (SiOH). The mechanism of the condensation polymerisation reaction (described in Chapter 1, section 1.2) was classified as step polymerisation. One of the steps in this complex reaction scheme may be represented by

$$aA + bB \rightarrow cC + dD \qquad (2.1)$$

where:

A is $(CH_3)_3SiO[Si(CH_3)_2O]_xH$

B is $HO[Si(CH_3)_2\text{-}O]_yH$

C is $(CH_3)_3SiO[Si(CH_3)_2O]_zSi(CH_3)_3$

D is H_2O

and the stoichiometric coefficients can be a=2, b=3, c=1, d=4.

Expressing the reaction rate as a power law (Levenspiel, 1972) in terms of one of the reactants, A, gives

$$r_A = -\frac{dC_A}{dt} = k_s C_A^{\alpha} C_B^{\beta} \qquad (2.2)$$

where:

r_A	is the reaction rate,	mol m^{-3} s^{-1}
C_A	is the concentration of A,	mol m^{-3}
C_B	is the concentration of B,	mol m^{-3}
t	is the reaction time,	s
k_s	is the reaction rate constant,	in appropriate units

From the stoichiometric relationship C_B can be written as:

$$C_B = \left(\frac{\alpha}{\beta}\right) C_A \qquad (2.3)$$

Hence equation (2.2) becomes

$$r_A = -\frac{dC_A}{dt} = k_s C_A^{\alpha} \left(\frac{\alpha}{\beta}\right)^{\beta} C_A^{\beta} \qquad (2.4)$$

If overall order of reaction n, is expressed as "$n = \alpha + \beta$" then, equation (2.4) can be rewritten as:

$$r_A = -\frac{dC_A}{dt} = kC_A^n \qquad (2.5a)$$

where k is a reaction rate constant.

Recognising that condensation polymerisation mechanisms are complex (see Chapter 1, Section 2.1) the rate may be followed by monitoring the disappearance of one of the functional groups, *e.g.* hydroxyl groups (-OH). Therefore, the rate of disappearance of the reactant A may be expressed by the disappearance of hydroxyl groups as follows:

$$r_{OH} = -\frac{dC_{OH}}{dt} = kC_{OH}^n \qquad (2.5b)$$

where C_{OH} is the concentration of hydroxyl groups, mol m^{-3}

If the concentration of hydroxyl groups is expressed in terms of the number of moles of hydroxyl groups, for a first order reaction the rate equation becomes

$$r_{OH} = -\frac{dC_{OH}}{dt} = -\frac{d(N_{OH}/V_l)}{dt}$$

where V_l is the volume of the liquid, m^3. Differentiating equation (2.6) gives

$$r_{OH} = -\frac{dC_{OH}}{dt} + \frac{C_{OH}}{V_l}\frac{d(V_l)}{dt} \qquad (2.7)$$

In equation (2.7) the second term accounts for the volume change of the liquid which occurs during the reaction. However if it is assumed that the density of the liquid is constant then the volume change term may be neglected. In reality, the volume of the liquid in the semi-batch reactor changes as a result of sampling and volatilization of some by-products at the beginning of the reaction. However for the time interval between the taking of samples, the volume of the liquid is assumed to be constant and equation (2.7) is applied as

$$r_{OH} = -\frac{1}{(V_l)_i}\frac{dN_{OH}}{dt} \qquad (2.8a)$$

where i=1,2,3...m (m is the total number of samples taken). Most of the volatiles were emitted at the start of the reaction. It was assumed that all of the volatiles trapped in the condenser had been released before the first sample of fluid had been taken, $(V_l)_i$ is therefore calculated from

$$(V_l)_i = (V_l) - (V_v + n_s(s_v)_i) \qquad (2.8b)$$

where:

V_v is the volume of volatile fluids trapped in the condenser and measured at the end of the reaction, m^3

s_v is the volume of sample, m^3

n_s is the sampling number.

Expressing equation (2.8a) as a reaction rate based on unit geometric external surface area of the catalytic bed gives

$$(r_{OH})_e = -\frac{1}{S_e}\frac{(dN_{OH})_i}{dt} \qquad (2.9)$$

where:

$(r_{OH})_e$ is the rate of reaction in terms of the geometric external catalytic surface area, mol m_e^{-2} s^{-1}

S_e is the geometric external catalytic surface area, m_e^2

The rate of reaction, equation (2.8), may also be expressed per unit mass of catalyst.

$$(r_{OH})_c = -\frac{1}{W_c}\frac{dN_{OH}}{dt} \qquad (2.10)$$

where:

$(r_{OH})_c$ is the rate of reaction in terms of mass of catalyst, mol g^{-1} s^{-1}

W_c is the mass of catalyst, g

Combining equations (2.9) and (2.5a) gives

$$(r_{OH})_e = -\frac{1}{S_e}\frac{dN_{OH}}{dt} = k_r C_{OH}^n \qquad (2.11)$$

where k_r is the reaction rate constant in terms of external catalytic surface area, $m_l^3\ m_e^2\ s^{-1}$

Taking the natural logarithm of both sides of equation (2.11) gives

$$\ln\left[-\frac{1}{S_e}\frac{dN_{OH}}{dt}\right] = \ln k_r + n \ln C_{OH} \qquad (2.12)$$

For an irreversible reaction it may be possible to determine the reaction order n and the reaction rate constant k_r by a differential method of analysis or an integral method of analysis. In the differential method of analysis the values of n and k_r may be determined from a plot of $\ln\left[-\frac{1}{S_e}\frac{dN_{OH}}{dt}\right]$ versus $\ln[C_{OH}]$. From Arrhenius' law, the reaction rate constant k_r may be represented by

$$k_r = A \exp\left(-\frac{E}{RT}\right) \qquad (2.13)$$

where:

A	is the pre-exponential factor	$m_l^3\ m_e^{-2}\ s^{-1}$
E	is the activation energy,	$J\ mol^{-1}$
R	is the gas constant (8.314),	$J\ mol^{-1}\ K^{-1}$
T	is the absolute temperature,	K

From a plot of $(ln\ k_r)$ versus $(1/T)$ the activation energy and pre-exponential factor can be determined.

2.4 EXPERIMENTAL STUDIES

2.4.1 DESCRIPTION OF THE EXPERIMENTAL APPARATUS

The experiments were performed in a spinning basket semi-batch reactor with a capacity of 2 litres (see Figures 2.1 and Plate 2.1). The apparatus was specially designed and constructed for this work. A schematic flow diagram of the apparatus is illustrated in Figure 2.2. Since the fluid is colourless and the reactor was constructed of glass, the process could be observed readily. The basket which contained the catalyst was constructed of brass and stainless steel. Preliminary experiments were performed in which it was confirmed that these materials did not exhibit catalytic activity.

The reactor was externally heated and the temperature was controlled by means of a proportional differential controller (PDC). The maximum operating temperature was 413 K so as to minimise the occurrence of undesirable side reactions.

The catalyst used was tripotassium phosphate (K_3PO_4) and the feedstock consisted of linear (61.2 % w/w) and endblocked (38.8 % w/w) polydimethylsiloxanes, supplied by Dow Corning Ltd. Basic physical and chemical properties of the feedstock as provided by Dow Corning Ltd. are presented in Table 2.1.

A nitrogen gas purge stream was fed into the base of the reactor to facilitate removal of water which was a by-product of the reaction. Some of the volatile by-products formed in the reaction (i.e., cyclicpolysiloxanes) were also removed in the purge stream. These were then trapped in the two condensers to prevent them from entering the vacuum pump. The condensers were constructed from glass and were placed in thermos flasks containing dry ice. A mercury manometer was used to measure vacuum in the system.

The nitrogen flowrate was regulated by needle valves on two rotameters upstream of the reactor. Actual purge gas flowrates were measured at the exit of the vacuum pump.

Table 2.1 The properties of the polydimethylsiloxane feedstock.
(The properties and feedstock supplied by Dow Corning Ltd., 1989).

Boiling point (K)	>503
Vapour pressure (N m^{-2}, 293 K)	<700
Solubility in water (% w/w, 293 K)	<0.1
Specific gravity	0.97
Volatile content (% v/v) (Water and cyclicsiloxane)	15
Viscosity at 298 K (m^2 s^{-1}) x 10^4	1.5
Viscosity temperature coefficient	0.6
Coefficient of volume expansion (J K^{-1})	0.00096
Refractive index at 298 K	1.403
Surface tension at 298 K (N m^{-1})	21.0
Thermal conductivity at 323 K (W m^{-1} K^{-1})	0.155

2.4.2 CATALYST/SUPPORT SYSTEMS STUDIED

The following three different types of catalyst support systems were studied in the stirred basket batch reactor.

(a) Catalyst in pellet form: The catalyst was supplied by Dow Corning Ltd., (manufactured by Benckiser-Knapsack GMBH Ladenburg) as pellets of an irregular form. The properties of the pellets are summarised in Table 2.2. Heterogeneous reaction kinetics were determined for this material in order to act as a reference base with which to compare the performance of monolith support systems.

(b) Multi-channel monolith support: To test the feasibility of coating a multi-channel monolith support and in order to estimate the possible enhancement in reaction rate, a monolith was cut into sections to suit the basket and then coated with the catalyst. The properties of the monolith are summarised in Table 2.2. A number of coating techniques were tried, of which the following proved to be the most successful.

Monolith pieces were washed with pure water, dried in an oven at 393 K for 2 hours and then weighed. 10 g of catalyst pellets were then ground to a fine powder and mixed with ethanol (87 % w/w, pure) until a smooth slurry was formed. The monolith pieces were then dipped in the slurry and slowly dried in a nitrogen atmosphere at room temperature and then in an oven at 393 K and then weighed. The nitrogen atmosphere was maintained to prevent the catalyst from reacting with carbon dioxide in the atmosphere. Plate 2.2 shows the photograph of the coated and uncoated monolith pieces.

(c) Single channel ring elements: Single channel ring elements were selected since in subsequent trials it was intended to perform reaction experiments in a single channel

flow reactor. The heterogeneous kinetic data was determined for coated sections of the ceramic tube that were cut into rings to suit the basket. These ceramic rings were coated with catalyst using the same procedure as described for the multichannel monolith support system. The properties of the ceramic tube are described in Table 2.2. Plate 2.3 shows scanning electron micrographs of the surface of the coated and uncoated ceramic rings.

2.4.3 EXPERIMENTAL PROCEDURE

2.4.3.1 START-UP

(a) Ensure that all tubing is correctly fitted.

(b) Check the vacuum in the system and ensure that there are no leaks.

(c) Place one litre of feedstock into the reactor.

(d) Switch on the heating and thermocouple temperature indication systems.

(e) When the reactor temperature reaches 413 K, lower the spinning basket into the feedstock, switch on the stirrer, vacuum pump and the nitrogen purge.

(f) Read the gas flowrate and system pressure.

2.4.3.2 OPERATION

(a) During the course of the reaction it may be necessary to take samples for analysis. This may be done by switching off the vacuum pump and using a pipette to draw a sample for analysis.

2.4.3.3 SHUT-DOWN

(a) Turn off the heating system and the stirrer.

(b) Switch off the vacuum pump and then close the nitrogen purge valve.

(c) Allow the system to cool before handling.

(d) Switch off the temperature indicator.

2.4.4 ANALYTICAL TECHNIQUES

The progress of the reaction was followed by measuring the hydroxyl concentration. This was determined by titration with aluminium dibutylamide, using 4-phenylazodiphnylamine as an indicator. Kinematic viscosity was also measured using a U-tube, reverse flow viscometer. Details of the titration method are provided in Appendix B, section B.1.

Since the method of assessing the end-point in the titration is prone to experimental error a calibration curve was prepared of the concentration of hydroxyl versus viscosity, enabling in subsequent experiments the viscosity measurements to be used to determine the concentration of hydroxyl groups. The error analysis and calibration curve are presented in Appendix B, sections B.2 and B.3.

Table 2.2 Properties of the catalyst/support systems.

	Irregular pellets	Single channel ring elements	Multi-channel monolith
Support	-	Alumina silicate	Alumina silicate
Bed void fraction	0.50*	0.56**	0.64***
Hydraulic diameter of the cell (or average pellet diameter), m x 10^3	3.0	15	2.0
Wall thickness, m x 10^3	-	2.5	0.5
Geometric surface area per unit bed volume,(1) $m_e^2\ m_{bed}^{-3}$	1000	266.7***	1280
Total surface area per mass of catalyst,(2) $m_t^2\ g^{-1}$	14	2.0	1.4
Cell density,(3) cell cm^{-2}	-	57.73	1600

(1) Calculated value of external geometric surface area per unit bed volume, (see Appendix A, section A.2).

(2) Measured by means of Surface Area Analyzer as total catalytic surface area per unit mass of bed.

(3) Calculated value (see Appendix A, section A.4).

(*) Estimated experimentally (see Appendix A, section A.1a).

(**) Calculated value (see Appendix A, section A.1b and A.1c).

(***) Only the inside surface area of the channel is considered.

Subscripts

t represents the total surface area

e represents the geometric external surface area

bed represents the catalytic bed

2.4.5 PRELIMINARY EXPERIMENTAL TRIALS

In order to establish experimental conditions for the acquisition of kinetic data a number of preliminary experiments were performed and the following was determined:

- the extent of homogeneous reaction,
- mass of catalyst required,
- speed of rotation, and
- purge gas flowrate.

2.4.5.1 TESTING ANY NON-CATALYTIC REACTION

The absence of any significant non-catalytic reaction was confirmed by carrying out the experiments in the absence of a catalyst. As can be seen in Figure 2.3 there was 46% increase in viscosity when the non-catalytic experiments were performed. However, the results of the concentration analysis (see Figure 2.4) reveal that the concentration of hydroxyl groups in the liquid increased during the non-catalytic reaction. This resulted from a loss of volatiles and water during the course of the experiment. The increase in concentration of hydroxyl groups suggests that the increase in viscosity occurred as a result of the loss of volatile cyclicsiloxanes and water. The non-catalytic reaction was considered to be insignificant.

2.4.5.2 MASS OF CATALYST REQUIRED

A series of experiments was undertaken to select the quantity of catalyst required to achieve a measurable rate of reaction. These showed that 2 g of the pellet form of

catalyst in 1 litre liquid volume was adequate to evaluate the reaction kinetics using an integral method of analysis. Figure 2.5 shows the change in concentration of hydroxyl groups during preliminary experiments with different quantities of catalyst.

2.4.5.3 THE EFFECT OF VOLATILES ON THE OVERALL RATE

As the condensation polymerisation reaction proceed the molecular weight of the polymer and the viscosity of the liquid increases. However, the increase in viscosity is not only due to the chemical reaction but also due to volatilisation of water and cyclicsiloxanes both of which are present in the feedstock at a level of 15 % v/v, see Table 2.1, and formed during the reaction. Since the reaction is reversible the removal of the water vapour and volatile materials from the system may result in an increase in reaction rate. In order to observe the effect of volatilisation on the overall rate, an experiment was performed with 1.4 g of the pellet form of catalyst in a 1 litre liquid volume which was maintained at a temperature of 413 K and stirred for a period of 30 minutes. The reaction was then started and it was observed that the foaming which had previously been observed in the proximity of the catalyst was substantially reduced. In Figure 2.6 concentration changes as a function of time are compared for the crude feedstock and preheated feedstock. From this it is evident that a high conversion is achieved as a result of preheating. This confirms that the volatilisation of water and cyclicsiloxanes affects the overall reaction rate. It is also interesting to note that for the pretreated feedstock the initial rate of change in hydroxyl groups is low. This suggests that the initial changes observed in the untreated feedstock occur as a result of both the reaction and the removal of water/volatiles. This pretreatment was not applied in subsequent experiments.

2.4.5.4 THE EFFECT OF MIXING ON THE OVERALL RATE

A series of experiments was performed with each of the support systems in order to assess the effect of the speed of basket rotation on reaction rate. A rotational speed was then selected at which further increases did not significantly affect conversion and hence external mass transfer was not the rate limiting step. The results of these experiments are presented in Figures 2.7, 2.8 and 2.9 for the pellet, multi-channel and single channel ring elements respectively. Above a rotational speed of 220 rpm conversion was not significantly affected, hence all subsequent experiments were performed at a spinning rate of 220 revolutions per minute.

From Figures 2.7 to 2.9 it is interesting to note that the initial rate is affected by the speed of rotation and therefore it is likely that the reaction is initially chemical reaction rate-limited. However, as the polymerisation reaction proceeds the molecular weight of the polymer increases considerably and the reaction may become external mass transfer limited at low stirrer speed.

2.4.5.5 THE EFFECT OF GAS FLOWRATE AND PRESSURE ON THE OVERALL RATE

Experiments were also performed to explore the effect of varying the nitrogen purge gas flowrate. Unfortunately because of the limitations in the experimental apparatus it was not possible to maintain the system pressure constant whilst these changes were made, as an increase in gas flowrate resulted in a concomitant increase in system pressure. A low pressure is desirable since it aids the removal of water which in turn increases the rate of reaction. From the results in Figure 2.10 it is evident that purge

gas flowrate has a major effect on the overall reaction rate. Since the gas was bubbled through the reaction mixture the reaction rate has most probably been enhanced by the stripping of volatiles and water from the fluid.

2.5 EXPERIMENTAL RESULTS

2.5.1 DETERMINING THE ORDER OF THE REACTION

The experimental data may be analysed either by the differential method or by the integral method of analysis (Levenspiel, 1972). In ascertaining the order of reaction both methods were used.

2.5.1.1 DIFFERENTIAL METHOD ANALYSIS

The method has already been described in Section 2.3. The following is a worked example of the method used. Further details of the calculation steps are presented in Appendix C, Sections C.1 and C.2. In this example the catalyst is in pellet form, and the reaction experiment was performed at 413 K.

From a plot of N_{OH}/S_e as a function of time, as shown in Figure 2.11, the slope of the curve, $\frac{d(N_{OH}/S_e)}{dt}$, was determined at a number of time intervals. From a plot of $\ln\left(\frac{d(N_{OH}/S_e)}{dt}\right)$ versus $\ln(C_{OH})$ (see Figure 2.12) the slope of the line gives the reaction order, (*i.e.* n=1.02), while the intercept gives (not shown on Figure 2.12) the reaction rate constant (*i.e.* k_r=2.3x10^{-5}m$_l^3$m$_e^2$s^{-1}). At a fixed operation temperature of 413 K the following reaction rate equation was obtained:

$$(r_{OH})_e = (2.3\times 10^{-5})C_{OH}^{1.02} \qquad (2.14)$$

2.5.1.2 INTEGRAL METHOD ANALYSIS

In the integral method of analysis it is necessary to assume an order for the reaction and then test the fit. Assuming an expression of the following form for first order,

$$(r_{OH})_e = -\frac{1}{S_e}\frac{d(N_{OH})}{dt} = k_r C_{OH} \qquad (2.15)$$

The fractional conversion of hydroxyl groups, X_{OH}, which have been consumed during the reaction may be expressed as:

$$X_{OH} = \frac{(N_{OH})_0 - (N_{OH})}{(N_{OH})_0} \qquad (2.16)$$

where $(N_{OH})_o$ is the number of moles of hydroxyl groups at the beginning of the reaction.

Equation (2.16) may also be written as:

$$N_{OH} = (N_{OH})_o(1 - X_{OH}) \qquad (2.17)$$

Differentiation of equation (2.17) gives

$$-dN_{OH} = (N_{OH})_o dX_{OH} \qquad (2.18)$$

Since at ten minute intervals, a known volume of liquid was taken from the reactor for analysis, the liquid volume in the reactor was known at each of the sampling intervals. Hence C_{OH} is calculated on the basis of the number of moles of hydroxyl groups and the liquid volume in the reactor. Equation (2.15) therefore becomes

$$(r_{OH})_e = \frac{(N_{OH})_o}{S_e}\frac{dX_{OH}}{dt} = k_r\frac{(N_{OH})_o(1-X_{OH})}{(V_l)_i} \qquad (2.19)$$

Rearranging of equation (2.19) gives

$$\frac{dX_{OH}}{(1-X_{OH})} = \frac{k_r S_e dt}{(V_l)_i} \qquad (2.20)$$

Integrating equation (2.20) from $X_{OH}=0$ to $X_{OH}=X_{OH}$ and $t=0$ to $t=t$ gives the reaction rate constant based on external geometric surface area as follows:

$$k_r = -\frac{\ln(1-X_{OH})}{tS_e}(V_l)_i \qquad (2.21)$$

From equation (2.21), if the first order assumption is valid, then a straight line plot would be expected. For the same example that had been previously considered (by the differential method) this was observed as is illustrated in Figure 2.13.

2.5.2 EVALUATING AN EXPRESSION FOR THE REACTION RATE CONSTANT

The integral method of analysis was used to determine the reaction rate constant at different temperatures. Details of the experimental measurements and calculated parameters are available in Appendix D.

2.5.2.1 THE PELLET FORM OF CATALYST

A number of reaction experiments were performed at different temperatures. The experimental conditions are given in Table 2.3. The results of these experiments are presented in Table 2.4 and in Figure 2.14 in accordance with Arrhenius' Law as a plot of (ln k_r) versus (1/T). Applying the method of least square regression the activation energy E and pre-exponential factor A were obtained and values are shown in Table 2.11.

Table 2.3 Summary of the experimental conditions for the pellet form of catalyst in the spinning basket, semi-batch reactor.

$(C_{OH})_{feed}$	171 mol m^{-3}
Viscosity of feed	1.5 x 10^{-4} m^2 s^{-1}
Spinning Rate	200 to 220 rpm
Gas flowrate (STP)	9.16 x 10^{-5} m^3 s^{-1}
Absolute pressure	0.213 bar
Catalyst mass	2.0 g
Geometric external surface area of the bed in the basket(*)	3.14 x 10^{-3} m^2
Total surface area per unit mass of the bed	14 x 10^{-5} m^2 g^{-1}
Reaction time	50 min

(*) the details of this calculation are given in Appendix A (see section A.3).

Table 2.4 Calculated reaction rate constant values for the pellet form of catalyst.

Experiment Number	T (K)	k_r ($m_l^3\ m_e^2\ s^{-1}$) x 10^4
1	373	0.73
2	383	0.76
3	393	0.98
4	403	1.07
5	408	1.23
6	413	1.47
7	423	1.49

2.5.2.2 THE MULTI-CHANNEL MONOLITH

Another series of reaction experiments were undertaken at different temperatures for the experimental conditions summarised in Table 2.5. The results of the these experiments are presented in Table 2.6 and in Figure 2.15 in accordance with Arrhenius' Law as a plot of ($\ln k_r$) versus (1/T). Applying the method of the least square regression the activation energy and pre-exponential factor were obtained and values are shown in Table 2.11.

2.5.2.3 THE SINGLE CHANNEL RING ELEMENTS

Reaction experiments were performed for the experimental conditions summarized in Table 2.7. The results of the these experiments are presented in Table 2.8 and in Figure 2.16 in accordance with Arrhenious' Law as a plot of ($\ln k_r$) versus (1/T). Applying the method of the least square regression the activation energy and pre-exponential factor were obtained and values are shown in Table 2.11.

Table 2.5 Summary of the experimental conditions for the multi-channel monolith support system in the spinning basket batch reactor.

$(C_{OH})_{feed}$	171 mol m^{-3}
Viscosity of feed	1.5 x 10^{-4} m^2 s^{-1}
Spinning Rate	200 to 220 rpm
Gas flowrate (STP)	9.16 x 10^{-5} m^3 s^{-1}
Absolute pressure	0.213 bar
Catalyst mass	3.0 g
Geometric external surface area of the bed in the basket(*)	19.3 x 10^3 m^2
Total surface area per unit mass of the bed	1.4 m^2 g^{-1}
Reaction time	50 min

(*) the details of this calculation are given in Appendix A (see section A.3).

Table 2.6 Calculated reaction rate constant values for the multi-channel monolith support system.

Experiment Number	T (K)	k_r ($m_l^3\ m_e^2\ s^{-1}$) x 10^4
8	368	0.17
9	373	0.18
10	398	0.19
11	403	0.21
12	408	0.25
13	413	0.29
14	423	0.34

Table 2.7 Summary of the experimental conditions for the single channel ring elements in the spinning basket batch reactor.

$(C_{OH})_{feed}$	171 mol m^{-3}
Viscosity of feed	1.5×10^{-4} m^2 s^{-1}
Spinning Rate	200 to 220 rpm
Gas flowrate (STP)	9.16×10^{-5} m^3 s^{-1}
Absolute pressure	0.213 bar
Catalyst mass	1.5 g
Geometric external surface area of the bed in the basket(*)	4.46×10^3 m^2
Total surface area per unit mass of the bed	2.00 m^2 g^{-1}
Reaction time	50 min

(*) the details of this calculation are given in Appendix A (see section A.3)

Table 2.8 Calculated reaction rate constant values for the single channel ring elements.

Experiment Number	T (K)	k_r $(m_l^3\ m_e^2\ s^{-1}) \times 10^4$
15	368	0.46
16	373	0.69
17	383	0.91
18	393	0.94
19	408	0.95
20	413	1.13
21	423	1.18

2.6 DISCUSSION OF THE RESULTS

For the experimental conditions presented in Table 2.9 the values of the reaction rate constant calculated on the basis of external geometric surface area, total surface area, and mass of catalyst on the support are compared in Table 2.10. The geometric external surface area was calculated for the monolith supports assuming that the catalytic surface is smooth (i.e. a flat surface for the square shapped cells). The total surface area was measured using a 2100D Model, ORR Surface Area Analyzer (minimum measurable pore size 100 Angstrom) and included the internal surface area of the catalyst/support. Reaction rate constants are compared on the basis of the initial rate of reaction over a 10 minute period, since it was considered that the effects of any transport resistances would be lower in the early phases of the reaction.

The calculated low value of the reaction rate constant, k_t in terms of total surface area for the pellet form of catalyst shows that the reaction occurs mostly on the external liquid-solid contact area.

As can be seen in Table 2.10 comparing the values of the reaction rate constant, k_r, (in terms of the geometric external surface area) the value for the multi-channel monolith support is very low. This may have arose as a result of not having achieved a uniform coating for this particular support system. During the coating process it was difficult to ensure that the high concentrate catalyst slurry coated all of the small channels in the multi-channel monolith in a uniform manner. In order to achieve a uniform coating a variety of alternative coating procedures and different solvents were tried. Ethanol was found to be a more suitable solvent than water. The value for the larger diameter single channel ring elements compares more closely with the pellet form of catalyst, see Table 2.10. The single channel rings had been coated using ethanol as a solvent and hence better adhesion of the catalyst to the surface had been

achieved. Results of reaction experiments were similar to the water based coating system indicating that the use of ethanol had not affected the catalytic properties of the system. In Table 2.11 values are presented for the activation energy and pre-exponential factor (calculated by least square regression) for the three catalyst support systems. The values of the activation energy for the pellets and for the single channel ring elements are found to be similar.

In order to explore opportunities for using monolith supports the geometric surface area of packed pellet beds and monolith catalyst supports was plotted as a function of pellet diameter and monolith cell density respectively. Details of the calculation steps are presented in Appendix A, section A.2. The diameter of commercial pellets generally varies from 3 to 5 mm whereas the cell density of monoliths varies from 30 to 60 cells cm^{-2} (DeLuca and Campbell, 1977). The void fraction of packed pellet beds generally varies from 0.3 to 0.5, whereas the void fraction of a monolith may vary from 0.5 to 0.7. Typical operating ranges are shaded in Figure 2.17, from which it is evident that the square cell monolith support offers a relatively high surface to volume ratio to be exploited.

Making use of Figure 2.17, and the results of the reaction experiments, the viability of using a monolith support *versus* a packed bed system was explored. For the sake of this comparison, a void fraction of 0.5 is assumed for both the monolith and pellet form of support. In performing this comparison no allowance was made for additional transport resistances that may prevail in the flow reactors. Reaction rates were calculated for a point in the bed represented by a fixed value of $C_{OH} = 119$ mol m^{-3}, which equated to a fractional conversion of $X_{OH} = 0.3$. The details of calculation are given in Appendix A, section A.5. The results are illustrated in Figure 2.18, where the reaction rate is compared on the basis of unit bed volume. Since the diameter of the pellets used in a packed bed is likely to range from 3 to 5 mm, and the cell density of the monolith

could range from 30 to 60 cells cm^{-2}, it is evident that there is considerable potential to achieve higher reaction rates with the use of square cell monoliths as catalyst support systems.

Table 2.9 The experimental data over which the values of the reaction rate constant were compared (T= 413 K ; S.R.= 210 rpm ; V_l=1 l ; $(C_{OH})_{feed}$= 171 mol m^{-3} ; P= 0.213 bar).

	Catalyst form		
Experimental conditions	Pellets	Multi-channel monolith	Single channel ring elements
Initial viscosity of the feedstock ($m^2\ s^{-1}$) x 10^4	1.5	1.5	1.5
Gas flowrate ($m^3\ s^{-1}$) x 10^5 (@ STP)	9.16	9.16	9.16
Mass of the catalyst (g)	2.00	3.00	1.50
Mass of the bed (g)	2.00	10.8	8.00
External surface area (m^2) x 10^3	3.14	19.27	4.46
Total surface area per unit mass of the bed($m^2\ g^{-1}$)	14.10	1.40	2.00
Experimental data for the first 10 minutes of the reaction			
Concentration of hydroxyl groups (mol m^{-3})	137	127	124
Viscosity of the liquid ($m^2\ s^{-1}$) x 10^4	1.77	1.89	1.94
Fractional conversion	0.28	0.34	0.35

Table 2.10 Comparing the values of the reaction rate constant calculated on the basis of: external surface area, total surface area and mass of the catalyst, for the first 10 minutes of the reaction.

	Catalyst form		
Reaction rate constant	Pellets	Multi-channel monolith	Single channel ring elements
k_r (1) $(m_l^3\ m_e^2\ s^{-1}) \times 10^4$	1.62	0.32	1.46
k_t (2) $(m_l^3\ m_t^2\ s^{-1}) \times 10^6$	0.26	4.72	2.62
k_c (3) $(m_l^3\ g^{-1}\ s^{-1}) \times 10^7$	0.73	2.05	3.28

(1) $$k_r = -\frac{\ln(1 - X_{OH})V_l}{tS_e}$$

(2) $$k_t = -\frac{\ln(1 - X_{OH})V_l}{tS_pW_{bed}}$$

(3) $$k_c = -\frac{\ln(1 - X_{OH})V_l}{tW_c}$$

where:

S_p is the total surface area per mass of the bed, $m_t^2\ kg^{-1}$

W_{bed} is the mass of the bed, kg

W_c is the mass of the catalyst, kg

subscripts

l represents the liquid,

c represents the catalyst, and

t represents the total surface area.

Table 2.11 Values of activation energy and pre-exponential factor determined for the three catalyst system studies.

	Catalyst form		
	Pellets	Multi-channel monolith	Single channel ring elements
Activation Energy ($J\ mol^{-1}$)	2.1×10^4	1.5×10^4	1.9×10^4
Pre-exponential factor ($m_l^3\ m_e^2\ s^{-1}$)	0.058	0.0023	0.033

2.7 CONCLUSIONS

(a) A new method of coating the monolith pieces with a K_3PO_4 catalyst was developed. The catalyst dispersed in an alcohol slurry was dried on the support in an inert atmosphere.

(b) The results of the kinetic experiments in the spinning basket semi-batch reactor demonstrate that in simplified form the condensation polymerisation reaction is overall first order with respect to C_{OH}, and may be represented by

$$r_{OH} = A\exp(-E/RT)C_{OH}$$

for C_{OH}= 20 to 169 mol m^{-3}

(c) The dramatic effect of the purge gas flowrate on the reaction rate confirms that the polymerisation reaction is very complicated. Although the reaction rate expression was shown to be well represented by a first order irreversible rate expression in terms of the hydroxyl groups, the removal of water/volatile components (by higher purge gas rates) from the reaction mixtures was also shown to influence the overall rate. A fixed purge gas flow rate and hence pressure was therefore selected for the comparative study.

(d) The heterogeneous kinetics based on the external surface area of the pellet, multi-channel and single channel ring elements were determined to be

for the pellet form of catalyst,

$$(r_{OH})_e = 0.0580 \exp\left(-\frac{2.10 \times 10^4}{RT}\right) C_{OH}$$

for the multi-channel monolith catalyst,

$$(r_{OH})_e = 0.0023 \exp\left(-\frac{1.50 \times 10^4}{RT}\right) C_{OH}$$

for the single-channel monolith catalyst,

$$(r_{OH})_e = 0.03 \exp\left(-\frac{1.90 \times 10^4}{RT}\right) C_{OH}$$

for C_{OH} = 20 to 169 mol m^{-3} and T = 373 to 418 K

(e) Calculated values of the reaction rate constant based on unit external surface area for the pellets and the single channel ring elements are similar. However, when reaction rates are calculated and compared based on unit volume for a packed bed reactor, then at high cell densities (> 20 cell cm^{-2}) the monolith support should achieve higher reaction rates per unit bed volume. The monolith support system therefore shows potential as a catalyst support to be used in a three-phase reactor.

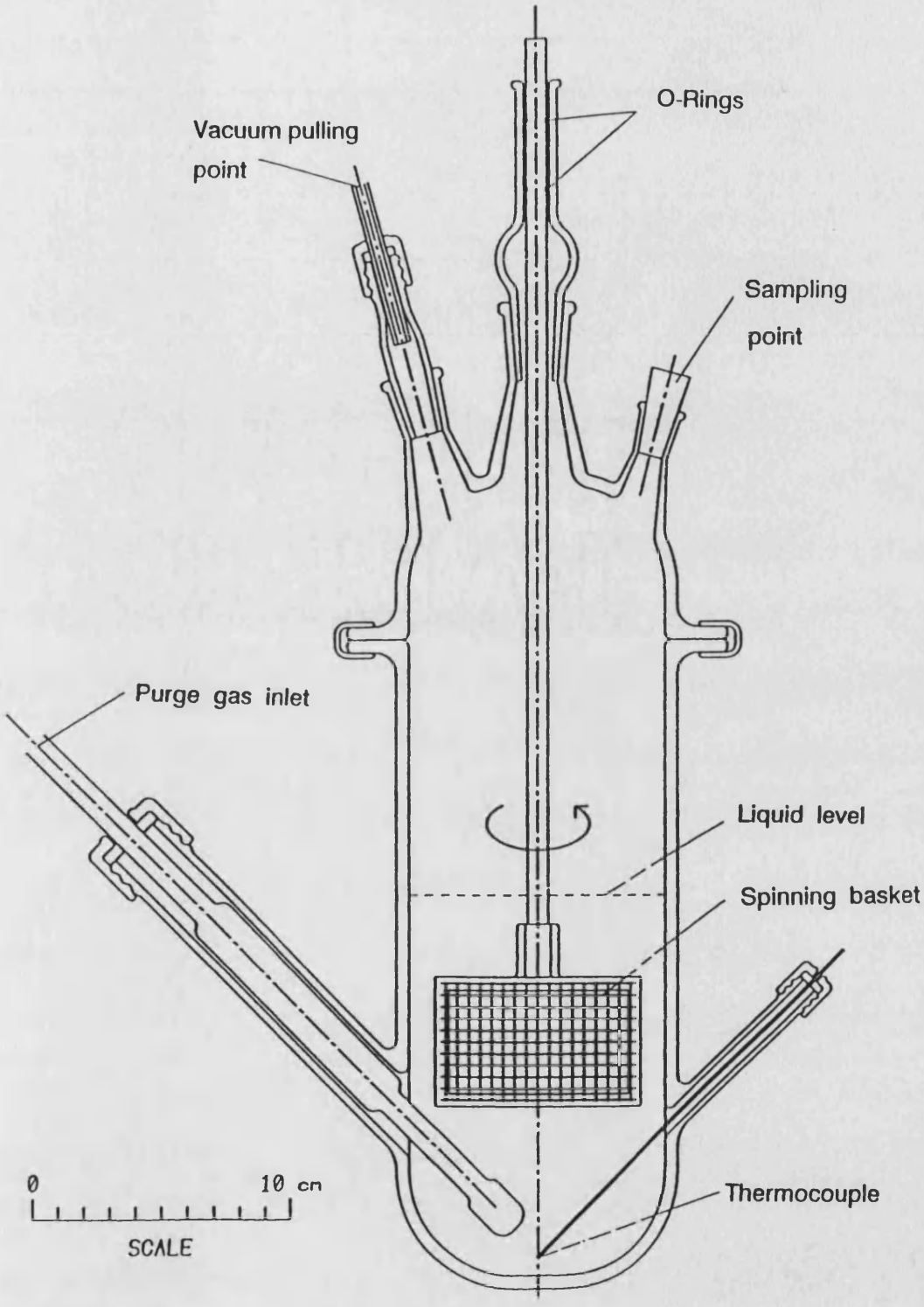

Figure 2.1 The spinning basket, semi-batch reactor.

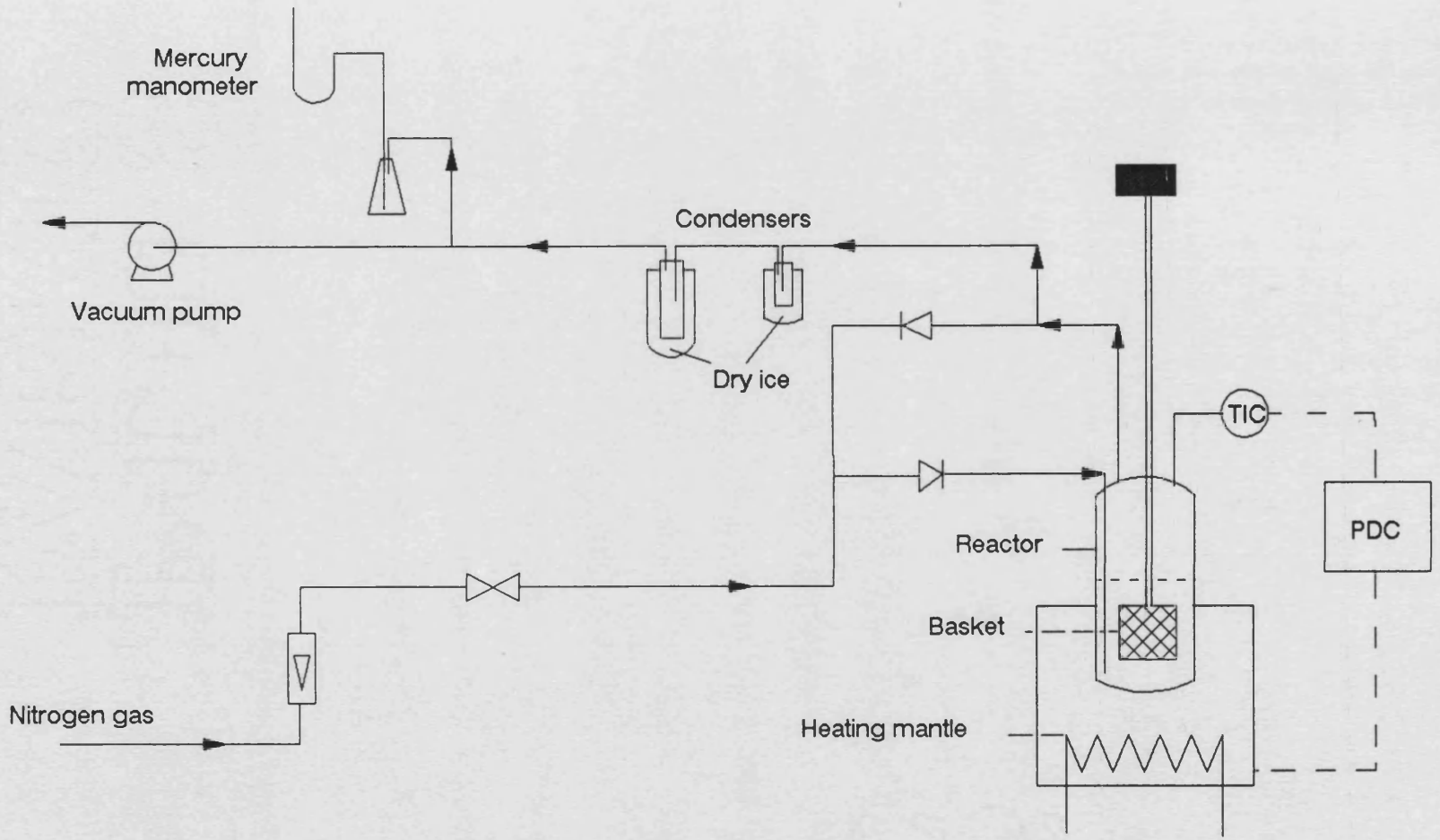

Figure 2.3 Schematic flow diagram of the apparatus.

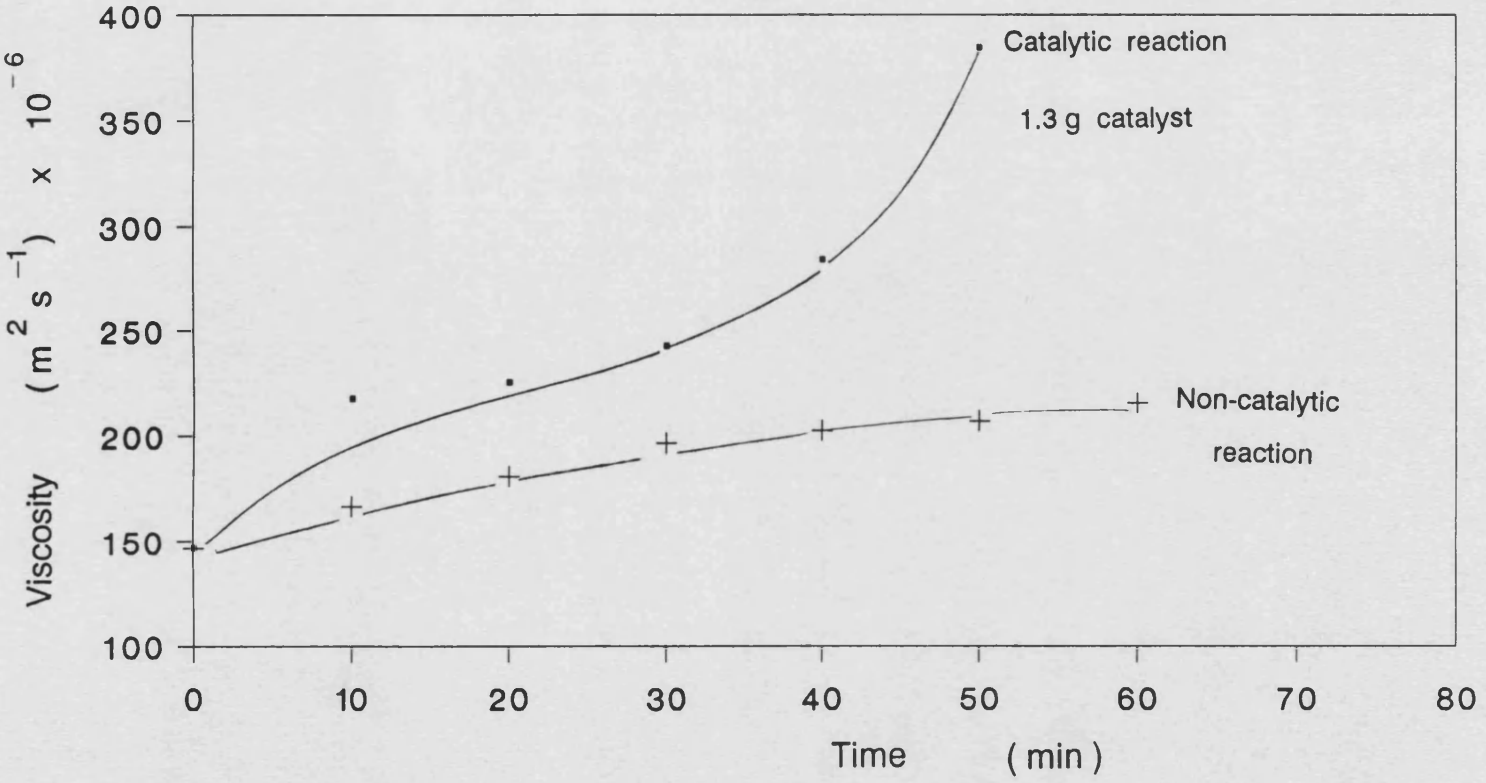

Figure 2.3 Viscosity changes as a function of time for the pellet form of catalyst (T = 413 K ; S.R = 220 rpm ; V_l = 1 litre ; ^{V_g} =9.2x10^{-5} m^3 s^{-1}; P = 0.213 bar)

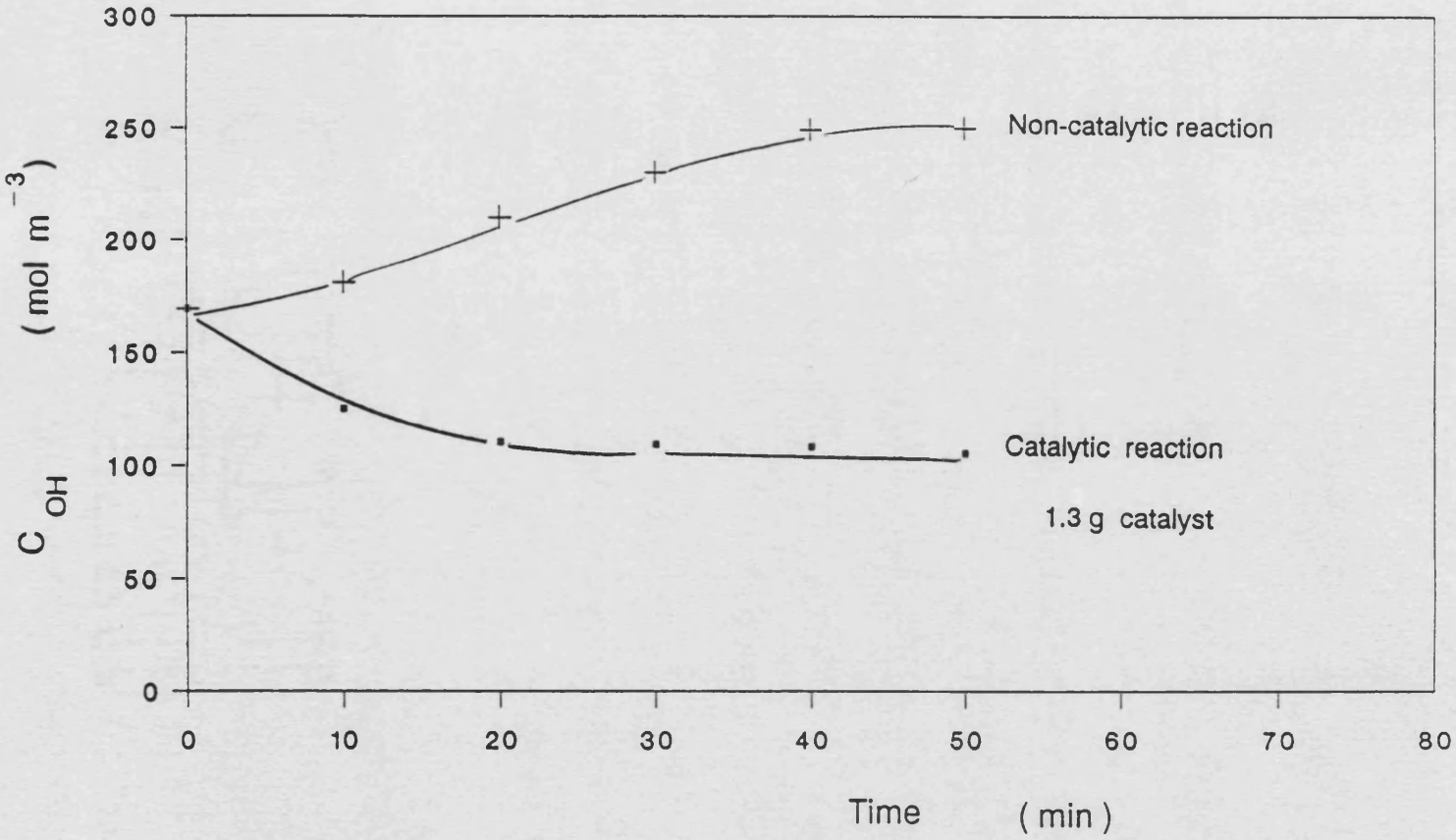

Figure 2.4 Concentration changes as a function of time for the pellet form of catalyst

(T = 413 K ; S.R = 220 rpm ; V_l = 1 litre ; v_g = 9.2x10^{-5} m^3 s^{-1}; P =0.213 bar)

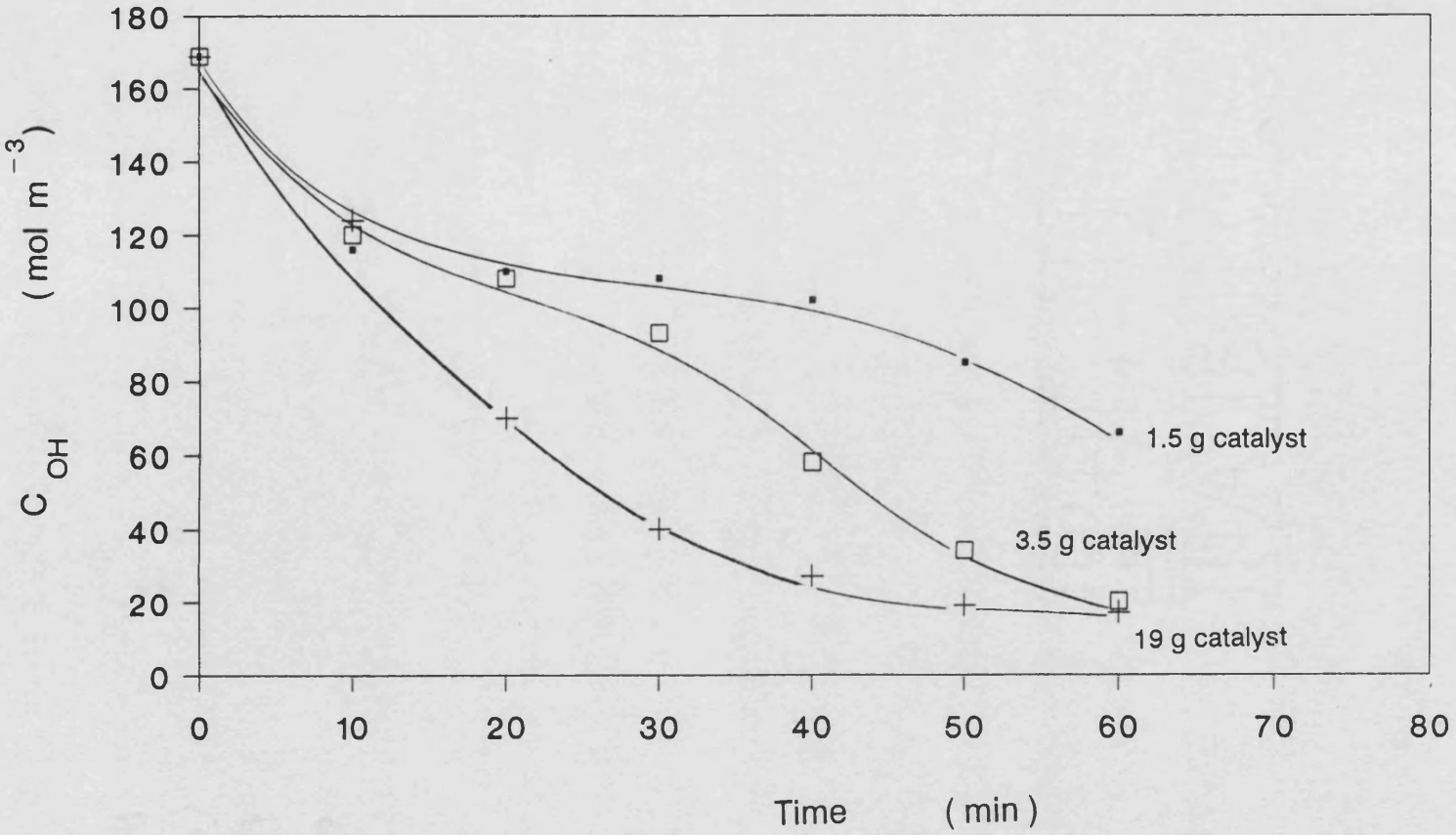

Figure 2.5 Comparison of concentration changes as a function of time for different loading of the pellet form catalyst (T = 413 K ; S.R. = 220 rpm ; V_l = 1 litre ; v_g = 9.2x10^{-5} m^3 s^{-1}; P =0.213 bar)

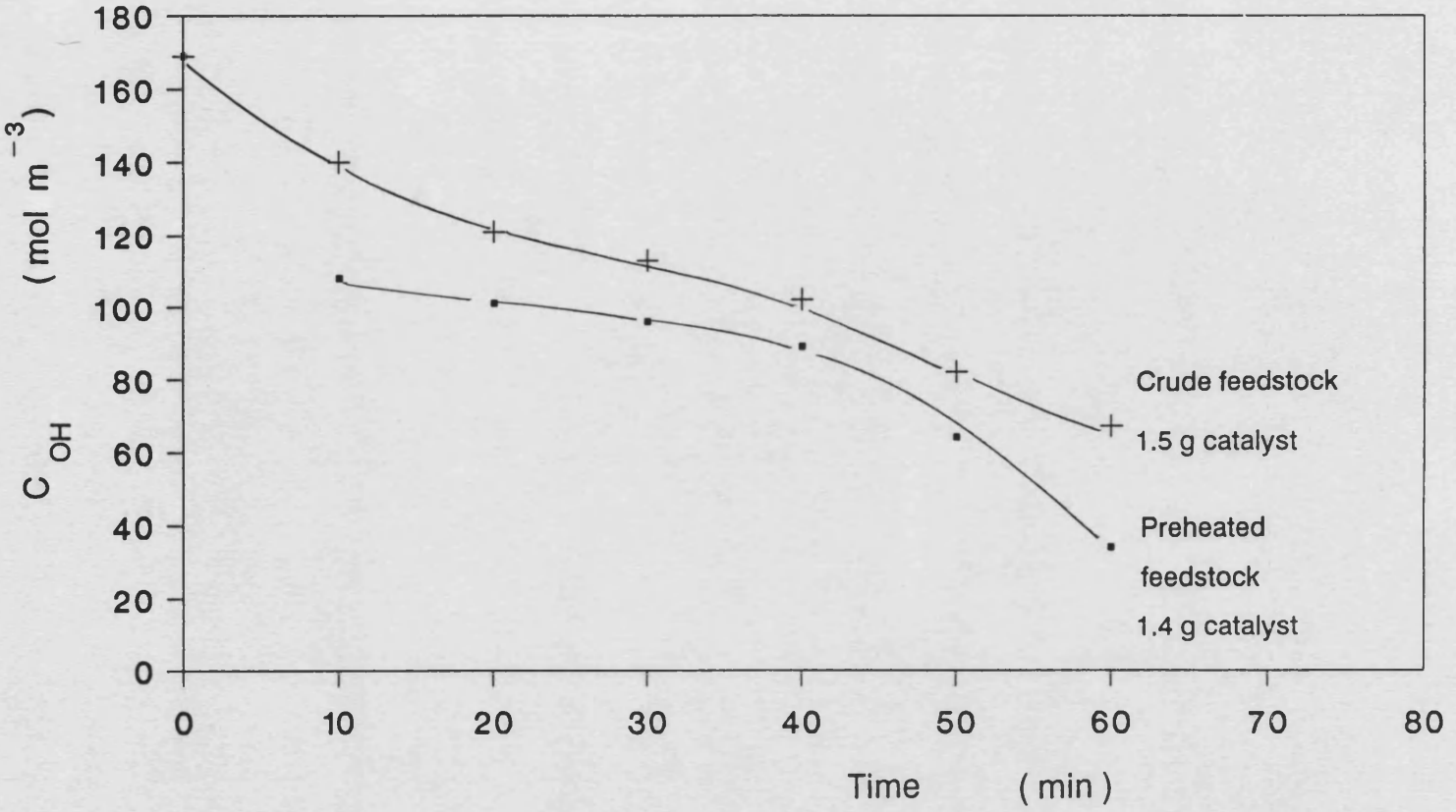

Figure 2.6 Effect of feedstock pretreatment on concentration of hydroxyl groups
(T = 413 K ; S.R = 220 rpm ; V_l = 1 litre ; v_g = 9.2x10^{-5} m^3 s^{-1}; P = 0.213 bar)

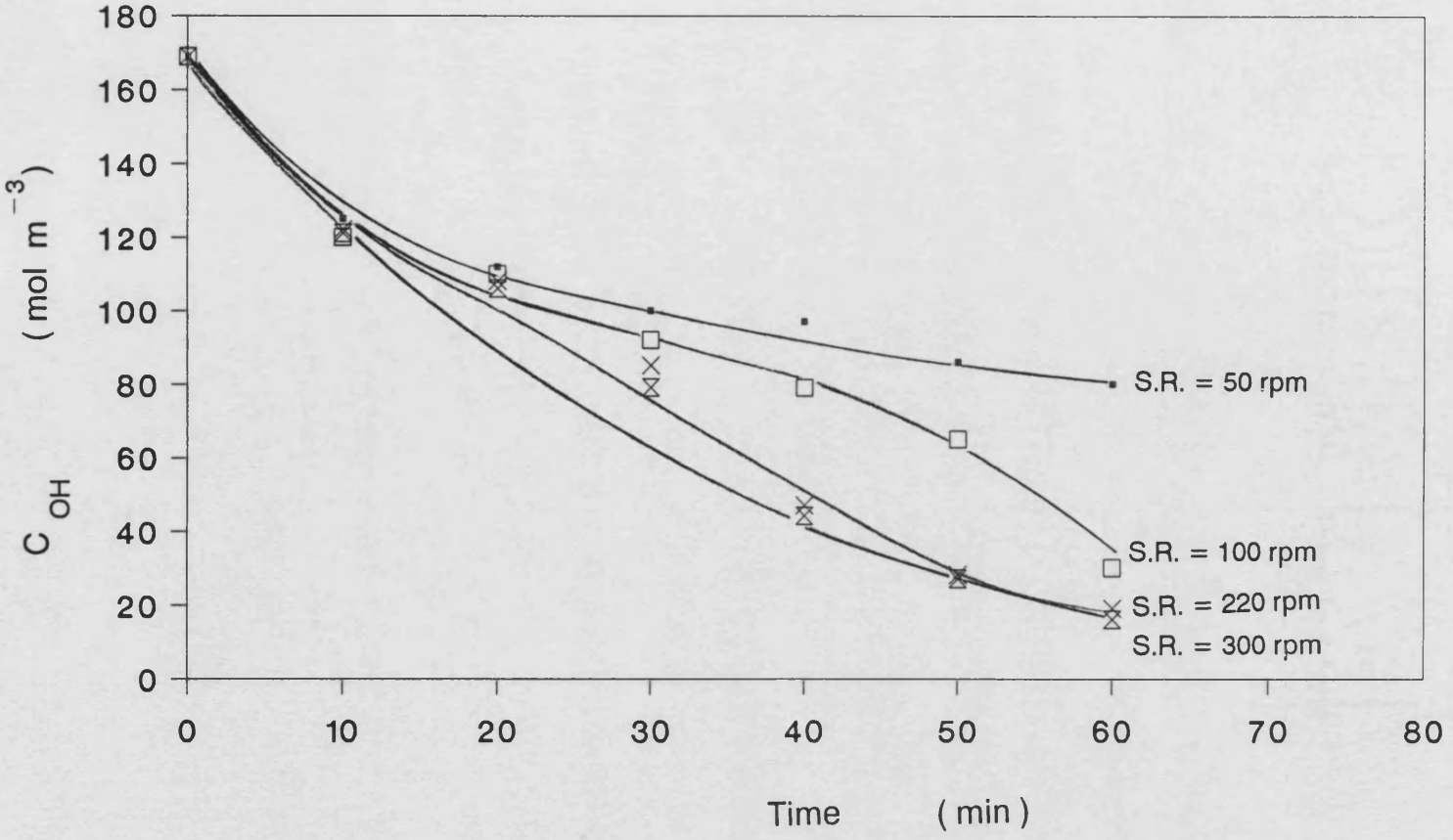

Figure 2.7 Effect of rotational speed of basket on the concentration of hydroxyl groups for the pellet form of catalyst (T= 413 K ; W_c = 3.5 g ; V_l = 1 litre ; $v_g = 9.2 \times 10^{-5}$ m^3 s^{-1}; P = 0.213 bar)

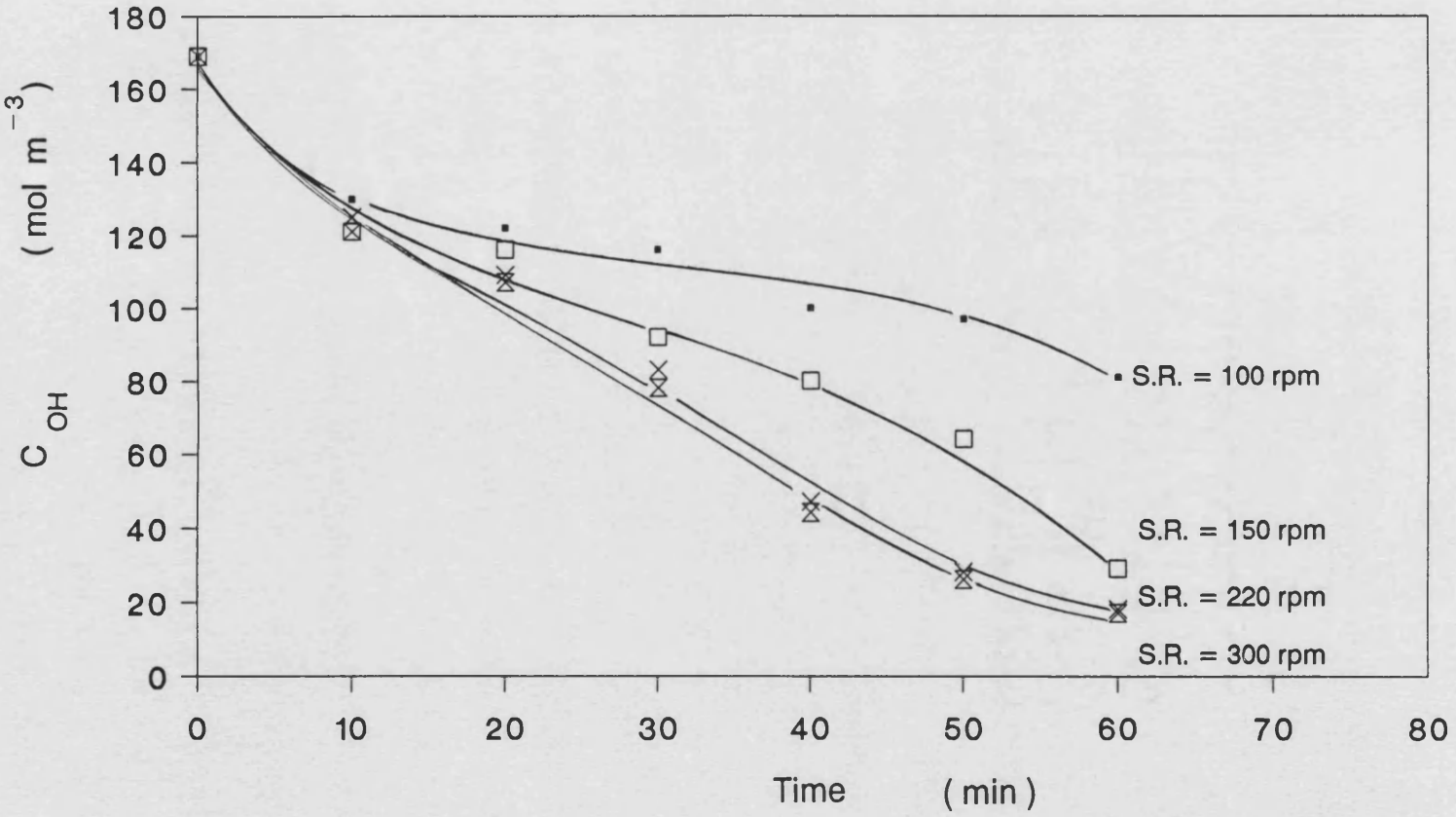

Figure 2.8 Effect of rotational speed of basket on the concentration of hydroxyl groups for the multi-channel monolith support system (T= 413 K ; W_c = 3.5 g ; V_l = 1 litre ; v_g = 9.2x10^{-5} m^3 s^{-1}; P = 0.213 bar)

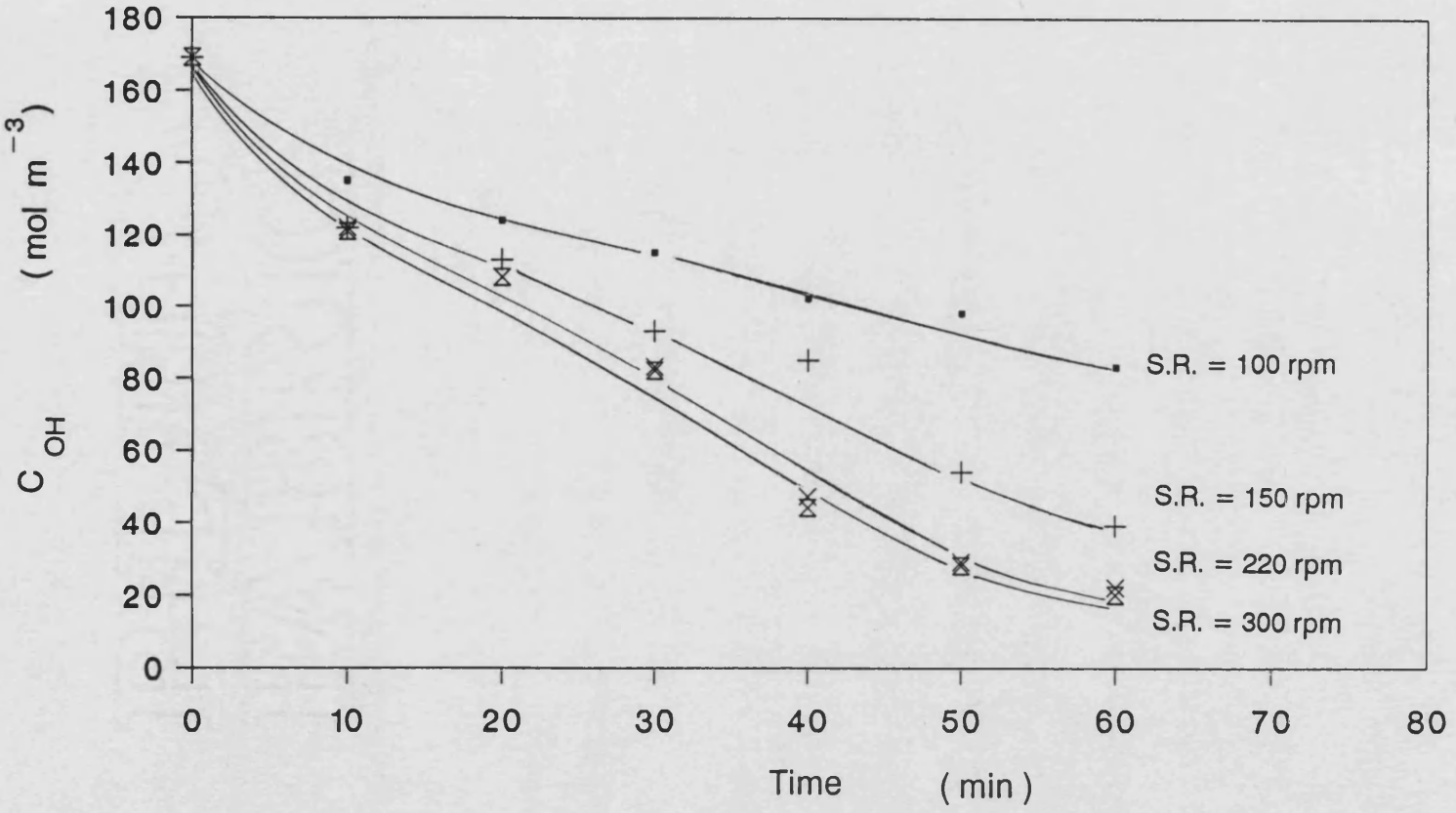

Figure 2.9 Effect of rotational speed of basket on the concentration of hydroxyl groups for the single channel ring elements (T= 413 K ; W_c = 3.5 g ; V_l = 1 litre ; v_g = 9.2x10^{-5} m^3 s^{-1}; P =0.213 bar)

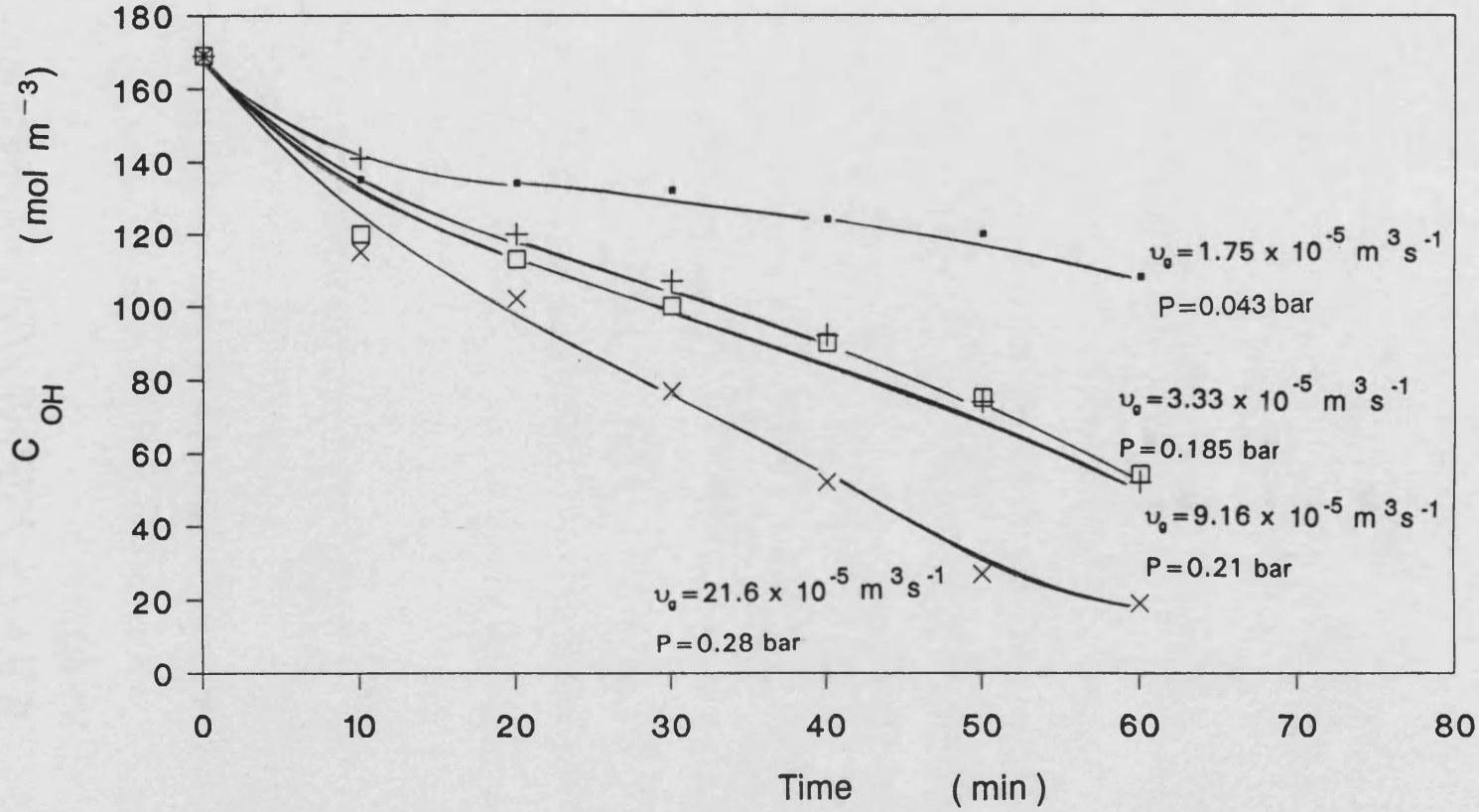

Figure 2.10 Effect of purge gas flowrate and system pressure on the concentration hydroxyl groups (T= 413 K ; W_c = 3.5 g ; V_l = 1 litre)

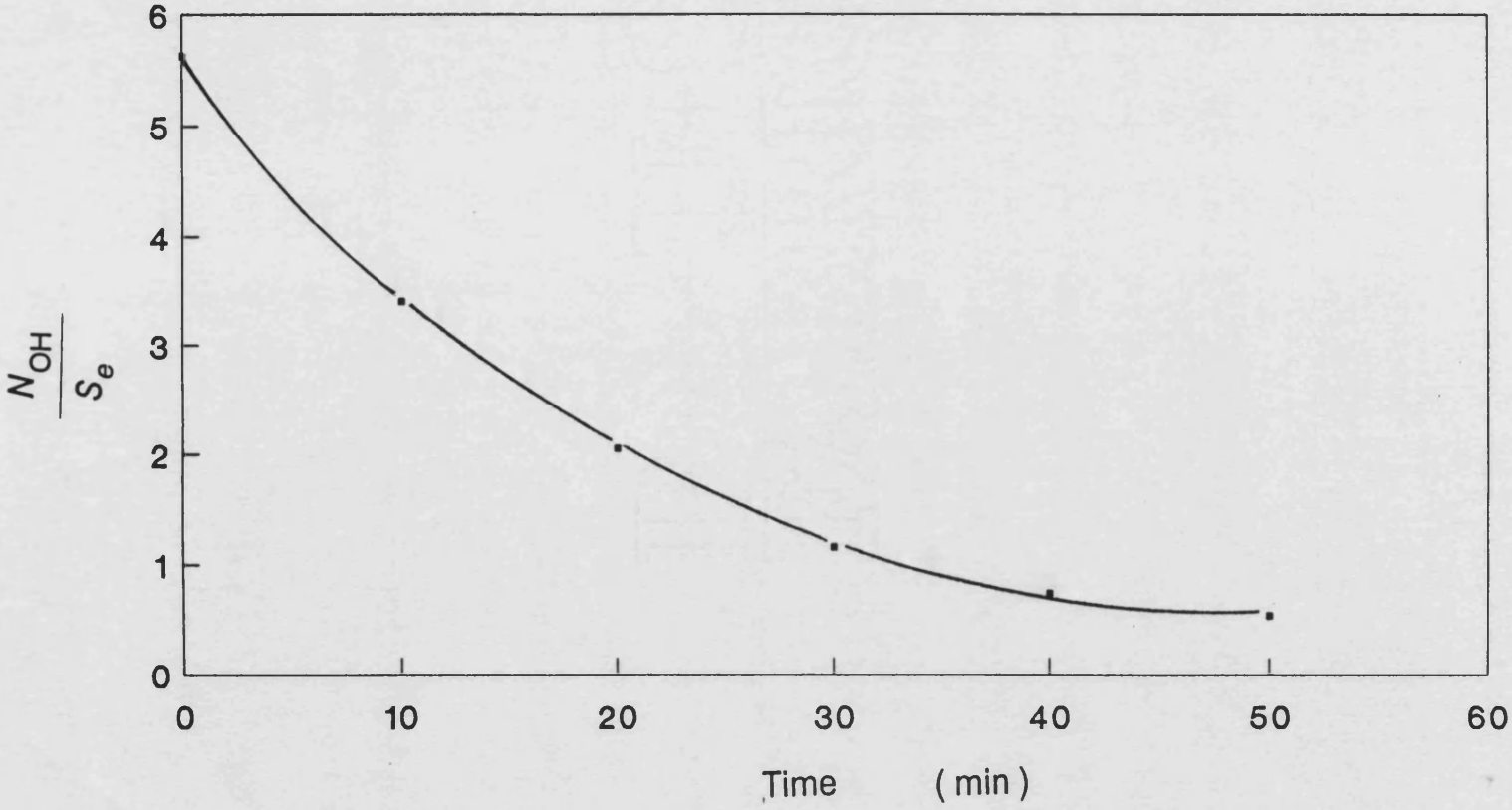

Figure 2.11 Applying the differential method of analysis for the pellet form of catalyst

(T= 413 K ; W_c = 19 g ; V_l = 1 litre ; v_g = 9.2x10^{-5} m^{3}s^{-1} ; P = 0.213 bar)

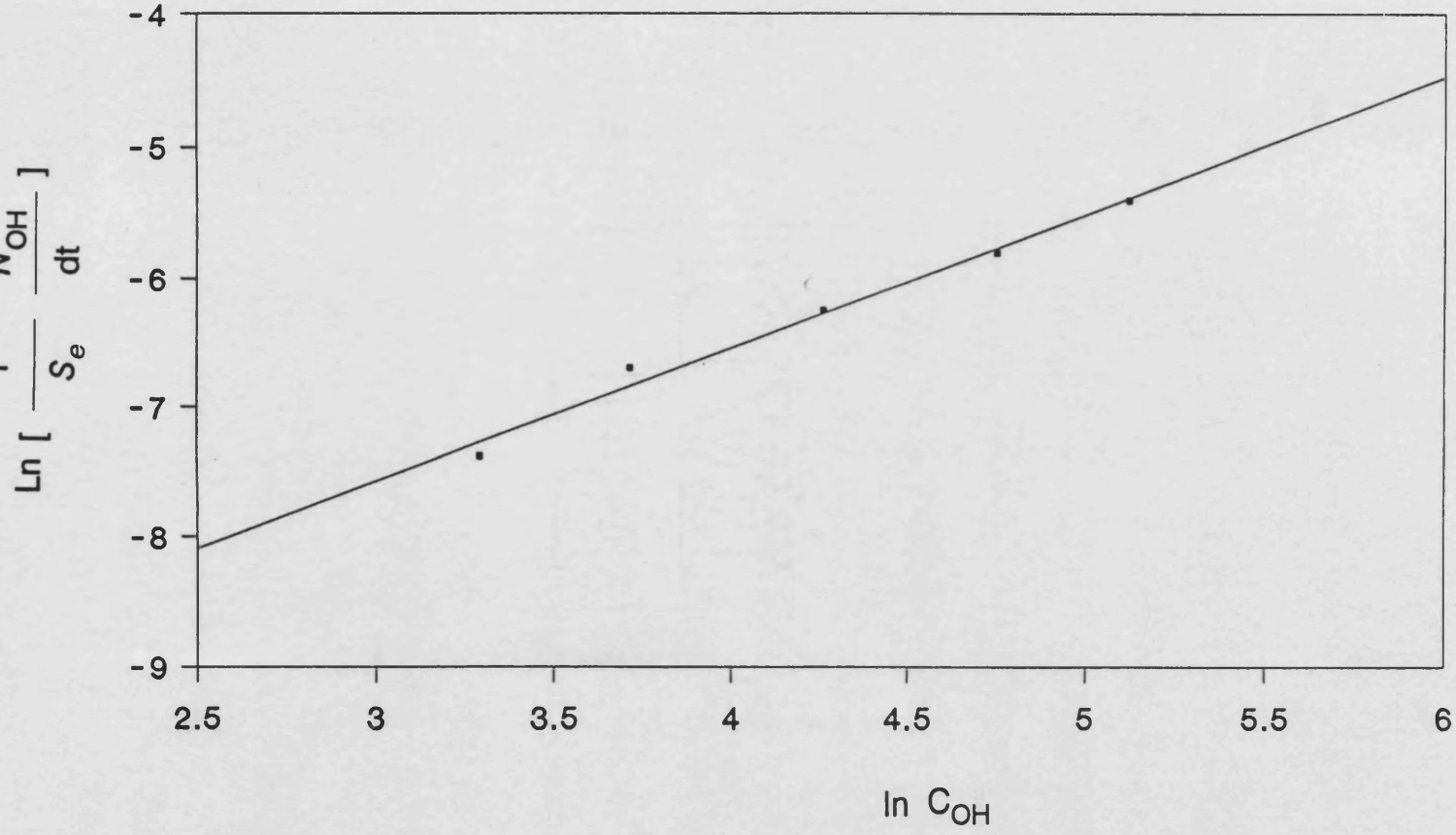

Figure 2.12 Determining the order of the reaction applying the differential method of analysis for the pellet form of catalyst. (W_c = 19 g ; V_l = 1 litre ; T = 413 K ; S.R. = 220 rpm)

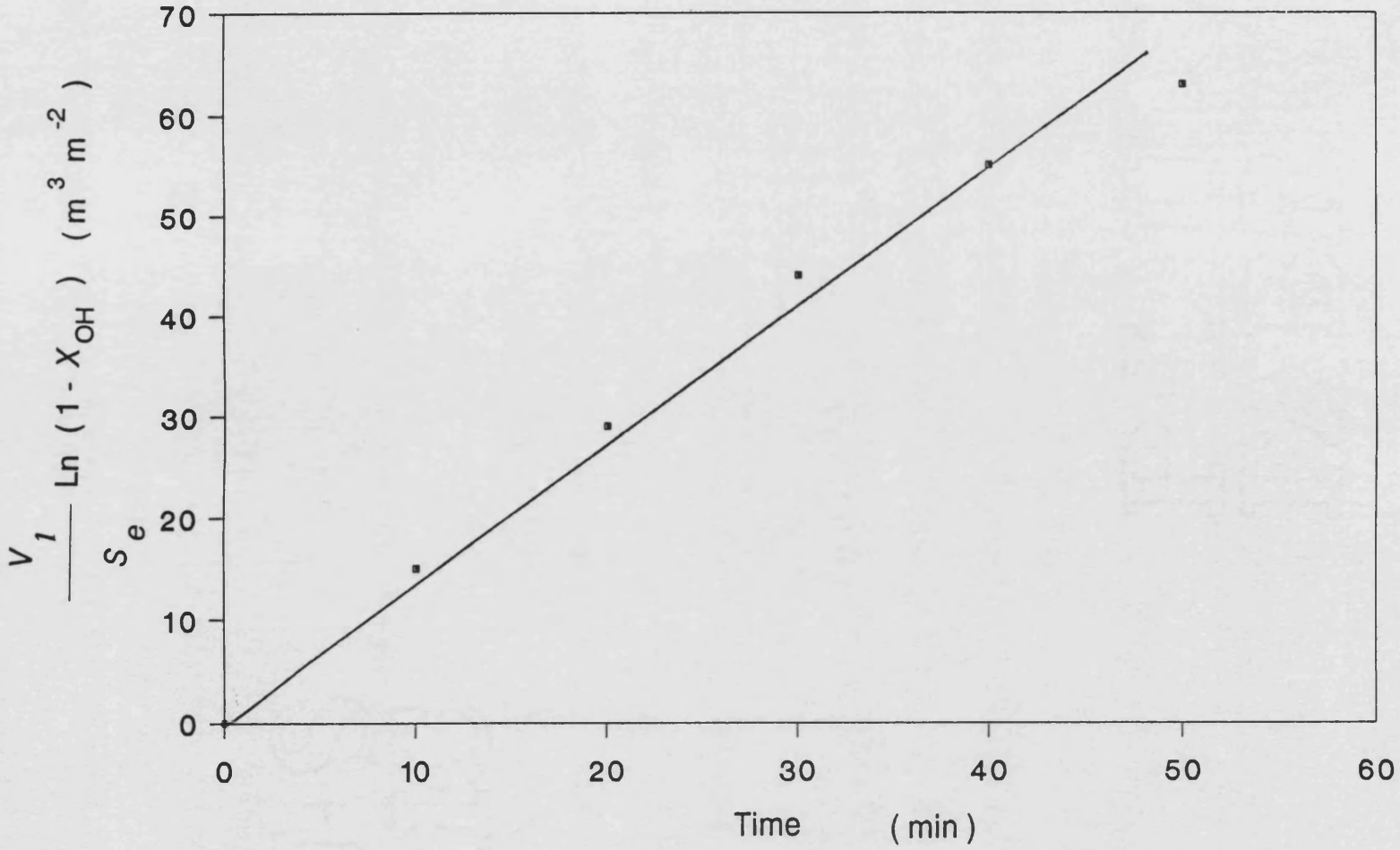

Figure 2.13 Result of the integral method of the analysis for the pellet form of catalyst (W_c = 19 g ; V_l = 1 litre ; T = 413 K ; S.R. = 220 rpm)

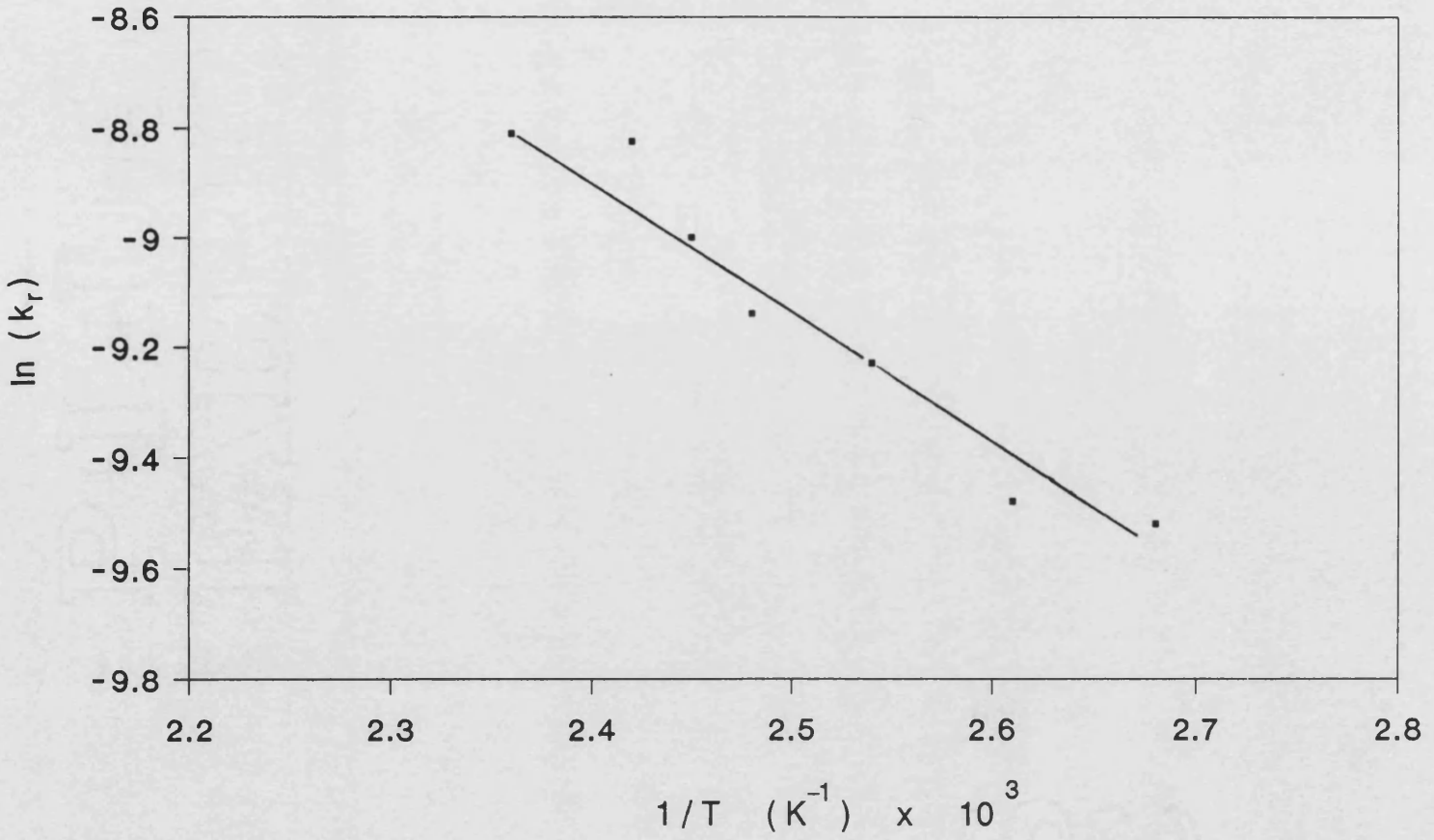

Figure 2.14 Results of kinetic experiments with the pellet form of catalyst.

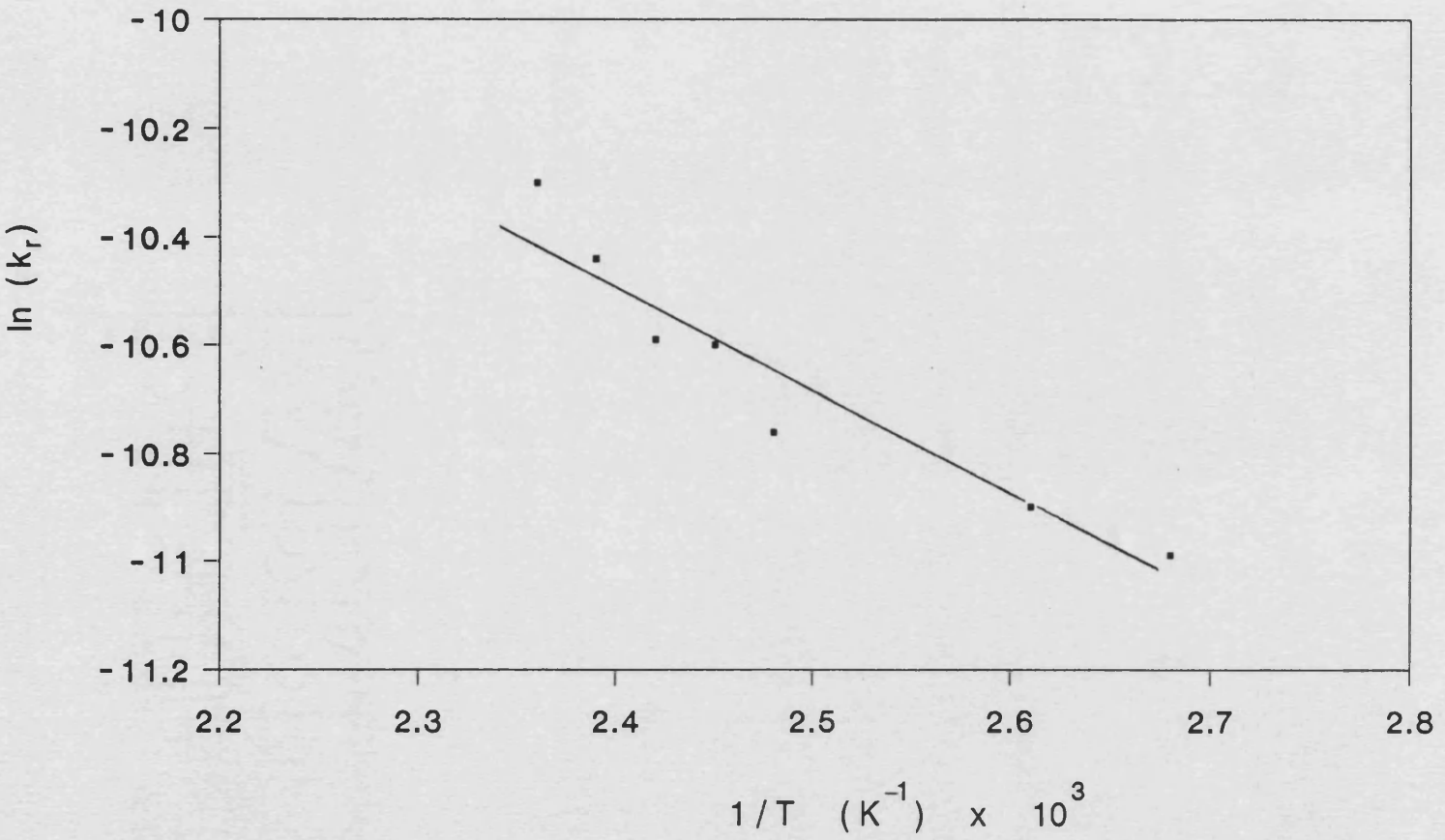

Figure 2.15 Results of kinetic experiments for the multi-channel monolith

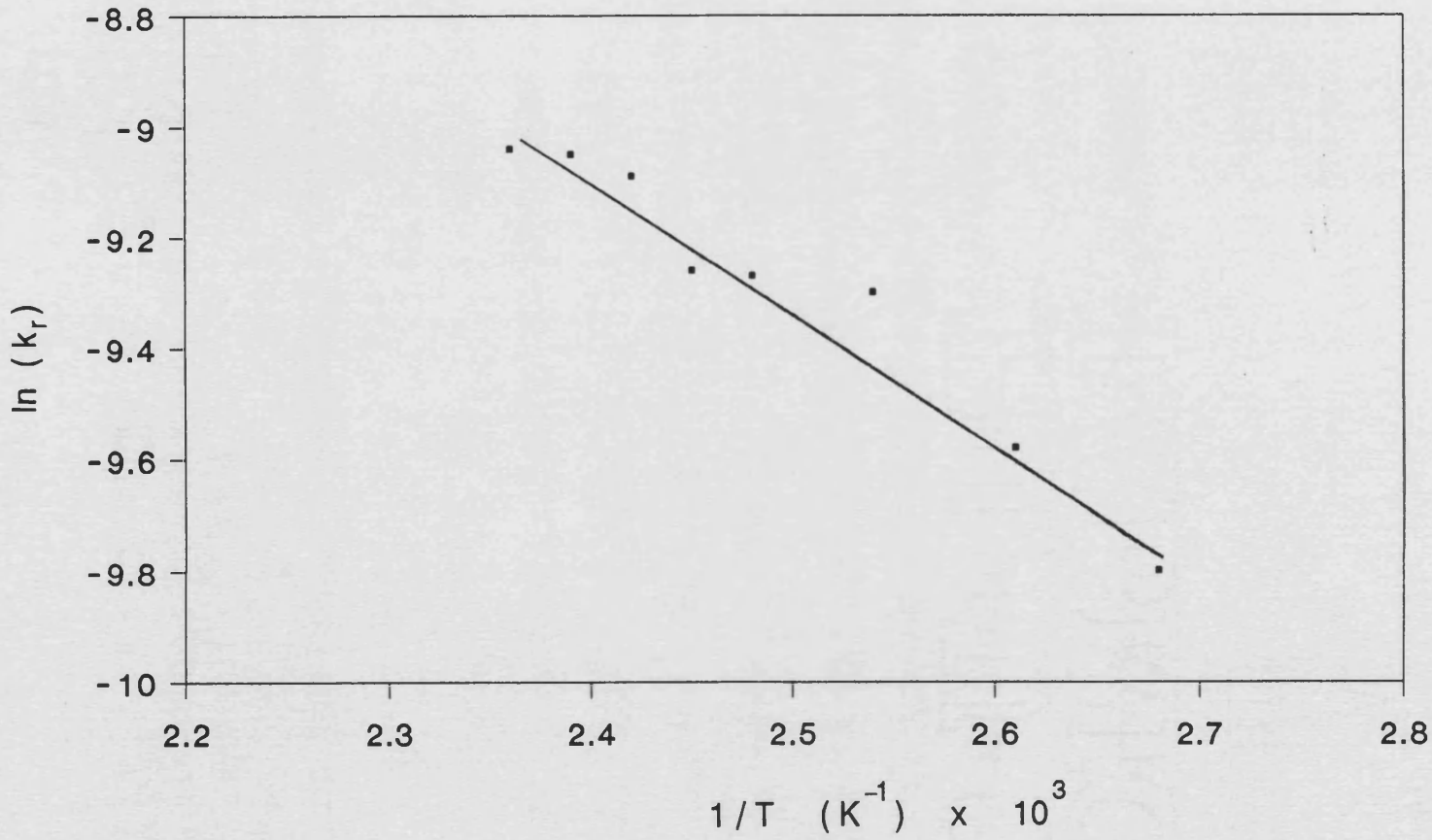

Figure 2.16 Results of the kinetic experiments for the single channel ring elements.

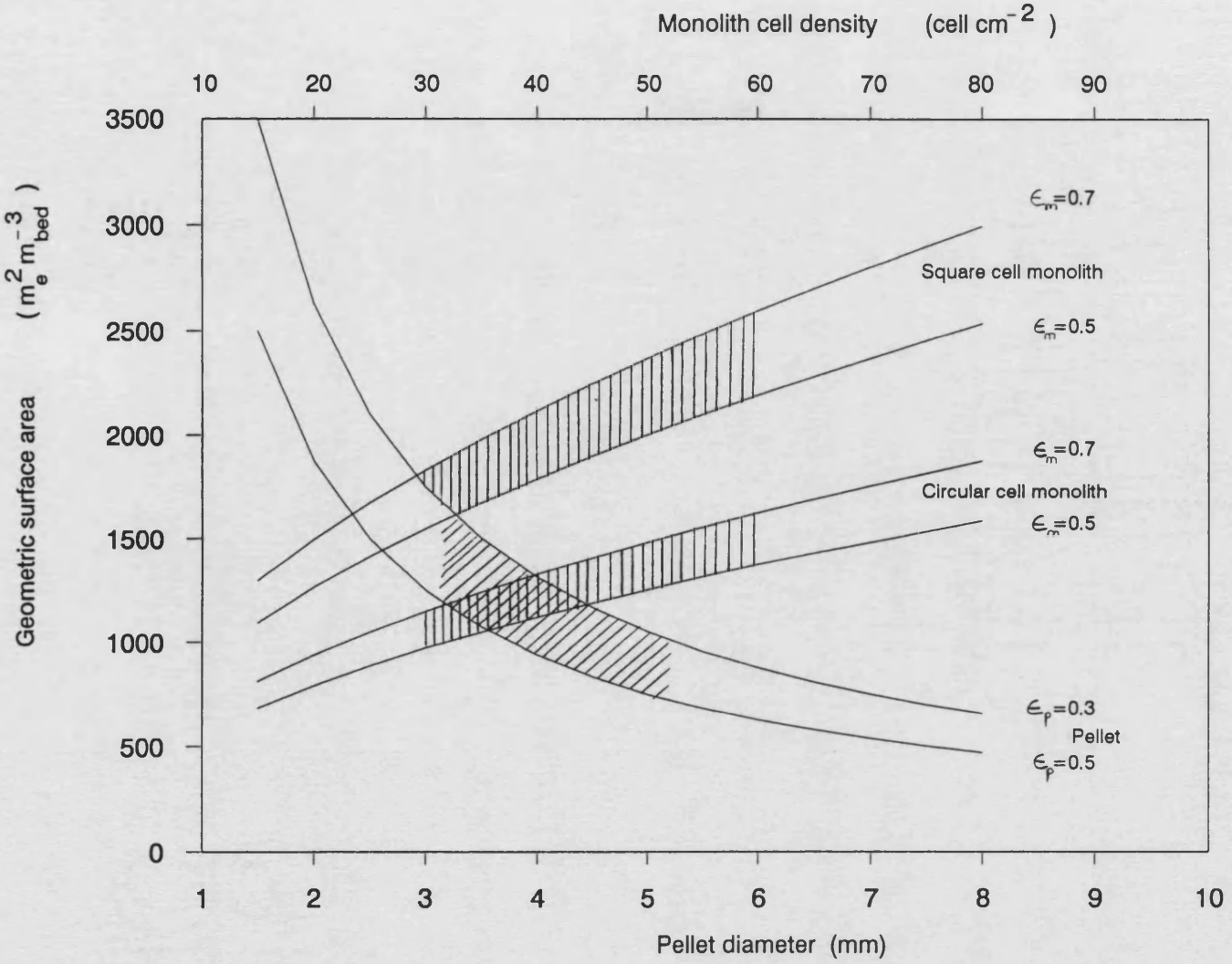

Figure 2.17 Comparing the geometric surface area per unit bed volume for a packed bed versus monolith supports

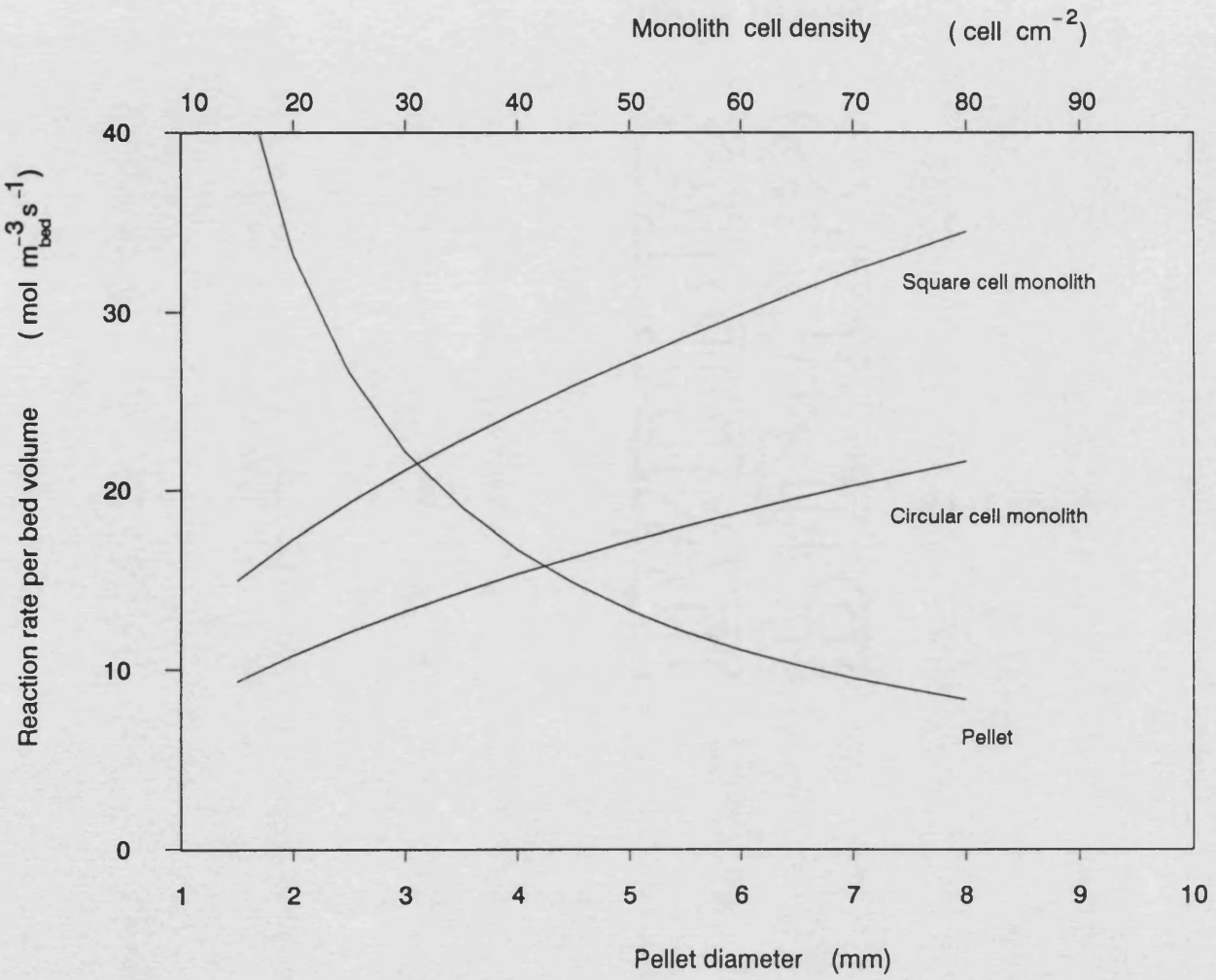

Figure 2.18 Comparing the reaction rate per unit bed volume for a packed bed versus monolith supports ($\epsilon = 0.5$)

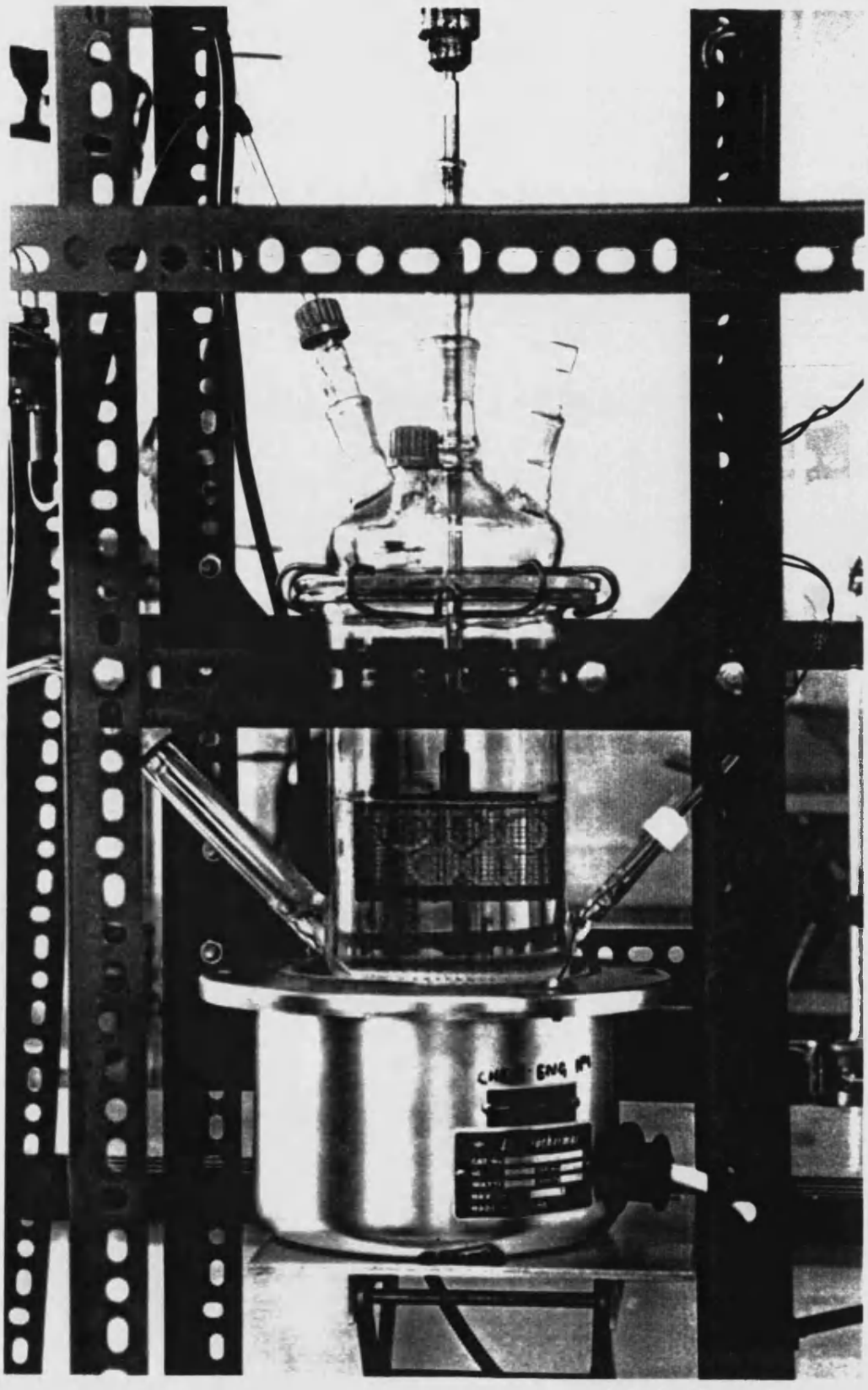

Plate 2.1 Photograph of the spinning basket, semi-batch reactor

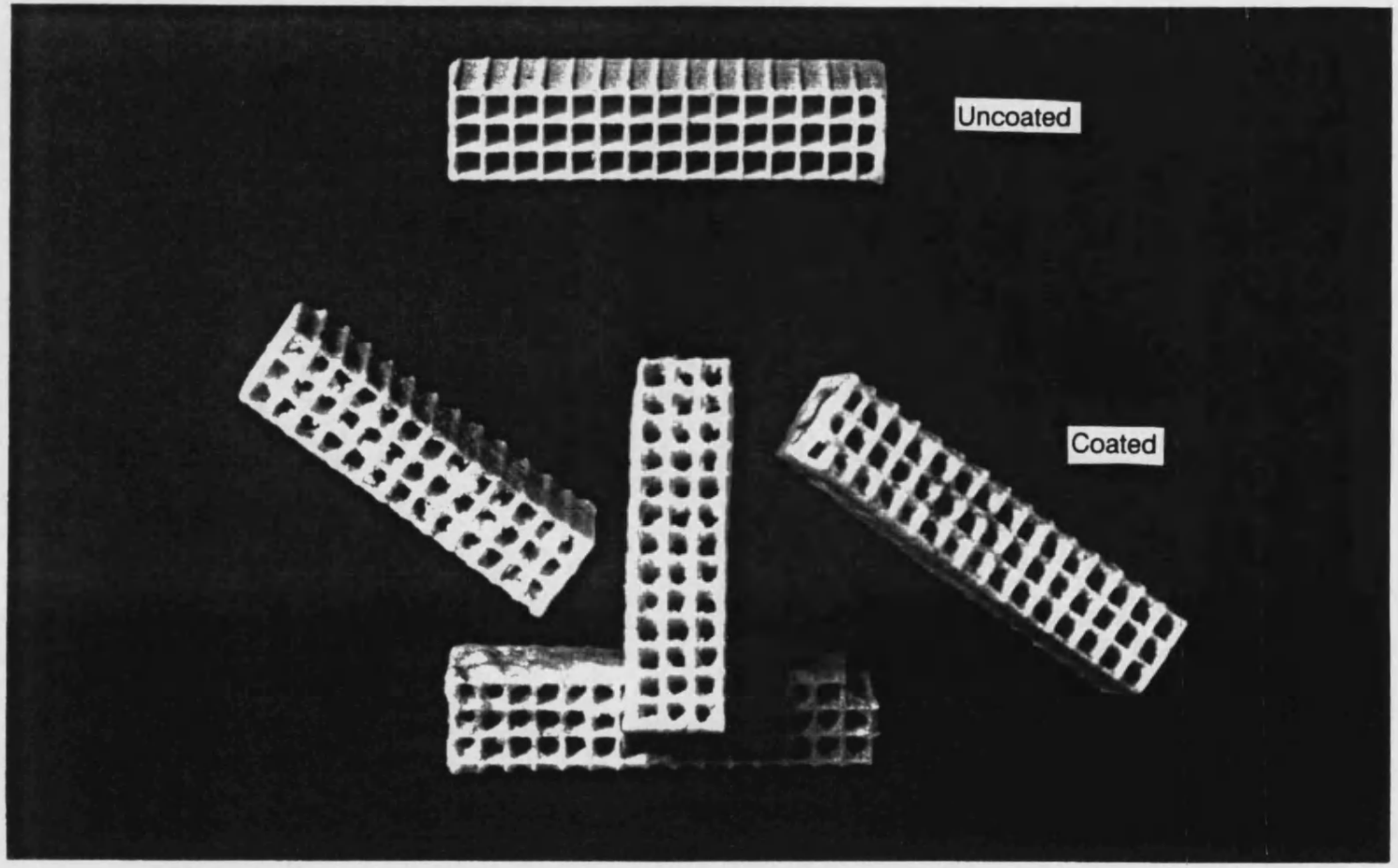

Plate 2.2 Photograph of the coated and uncoated monoliths

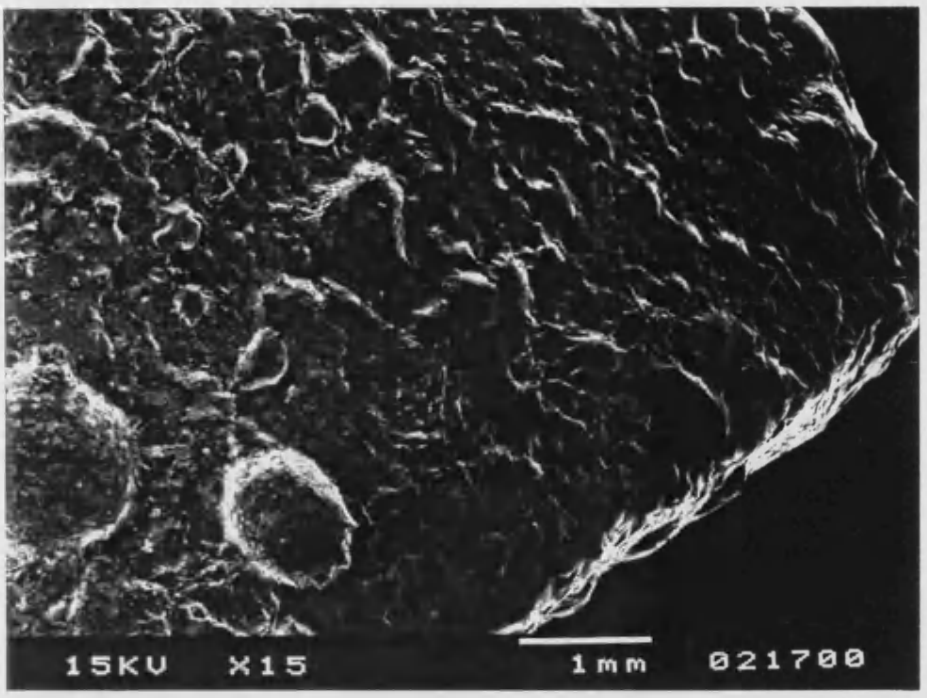

(a)

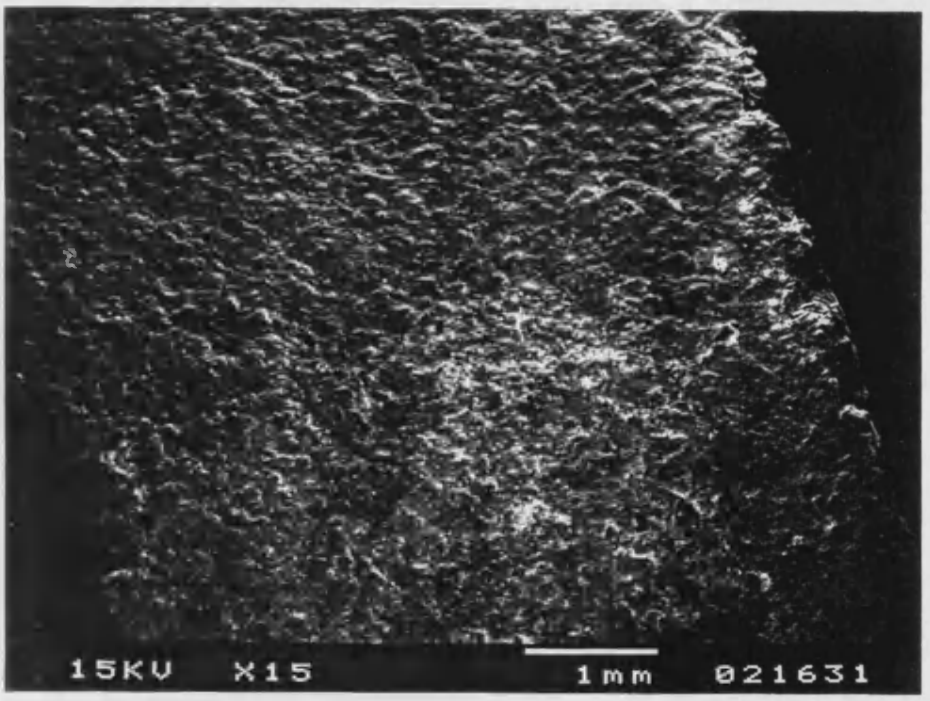

(b)

Plate 2.3 Scanning electron micrographs of

(a) coated (b) uncoated ceramic rings

CHAPTER 3

THE SINGLE CHANNEL TRICKLE FLOW CATALYTIC REACTOR

INTRODUCTION

Having identified in Chapter 2 that considerable potential exists for the use of a monolith as a catalyst support system, experiments are performed in a single channel monolith reactor.

A single channel monolith trickle flow reactor was selected for the following reasons:

(a) to avoid the potential problems of feed maldistribution, which can occur in a multi-channel monolith system,

(b) to achieve a uniform and known gas and liquid distribution, and

(c) to investigate the performance of a single channel that represents one of the channels in a multi-channel system.

A 15 mm *i.d.* ceramic tube was coated with catalyst and selected to represent a single channel of a multi-channel reactor. The effect on reaction rate of a number of important variables was studied. These included gas and liquid flowrates, temperature and pressure. The length of the reactor and catalyst loading were however maintained the same for each run.

The tube was mounted vertically and liquid was fed at the top and directed onto the inside surface of the tube. The nitrogen purge gas stream was fed in cocurrent mode, see Figure 3.1. For a limited number of experiments the gas was fed in at the bottom of the reactor and flowed countercurrent to the liquid.

This chapter is presented under the following headings:

3.1 THE DEVELOPMENT OF A ONE DIMENSIONAL MODEL

A one dimensional model describing the simultaneous process of mass transfer and chemical reaction is developed for a trickle flow single channel monolith reactor. Reaction kinetics are then evaluated in the single channel system. Mass transfer coefficients are determined under reaction conditions and an empirical correlation is developed. The results are compared with a theoretical correlation for flow down an inclined surface.

In developing the equations to model the reactions in the single channel flow reactor the following assumptions were made:

(a) The polymerisation reaction is modelled as an irreversible reaction of first order with respect to the concentration of hydroxyl groups (see Chapter 2, Section 2.5).

(b) The condensation polymerisation reaction occurs on the external surface of the catalyst, and therefore there are no internal mass transfer limitations in the catalyst system (see Chapter 2, Section 2.6).

(c) The single channel flow reactor would be considered to operate under isothermal conditions. The reactor was housed in an electrically heated fluid jacket, and measurements confirmed that isothermal conditions could be achieved (see Appendix E).

(d) Both the liquid and gas flows may be described by plug flow.

(e) Steady state conditions apply.

(f) The pressure drop per unit length is constant throughout the channel.

(g) The thickness of the liquid film is uniform around the circumference and along the axis of the reactor.

(h) The reactor has been coated with the catalyst in a uniform manner.

(k) All surfaces of the catalyst wall are wetted.

(l) There are no axial and radial dispersions.

In the thin liquid flow zone a mole balance for the hydroxyl groups in the reactor segment between z and z+Δz in Figure 3.1 may be represented by

$$F_l x_{OH}|_z - F_l x_{OH}|_{z+\Delta z} - (r_{OH})_o a(S_o \Delta z) = 0 \qquad (3.1)$$

where:

F_l is the molar flowrate of the liquid phase, mol s^{-1}

x_{OH} is the mole fraction of hydroxyl groups in the liquid phase

z axial direction, m

a is the surface area on the inside channel wall coated with the catalyst per unit free volume of the tube (m^{-1}) calculated from

$$a = \frac{S_e}{A_s L} \tag{3.2}$$

where:

L is the reactor length, m

S_e is the external catalytic surface area (on the inside channel wall), m^2

A_s is the free channel area, m^2

Values of S_e and A_s are determined from

$$S_e = \pi d_i L \tag{3.3}$$

and

$$A_s = \frac{\pi d_i^2}{4} \tag{3.3a}$$

respectively, where d_i is the inlet channel diameter, m. Dividing equation (3.1) by ($S_e \Delta z$) and taking the limit as Δz goes to zero, gives

$$-\frac{1}{S_e}\left(\frac{dF_l x_{OH}}{dz}\right)-(r_{OH})_e a = 0 \qquad (3.4)$$

The molar flowrate of hydroxyl groups can be described as:

$$F_l x_{OH} = F_l \frac{C_{OH}}{C_l} = \upsilon_l C_{OH} \qquad (3.5)$$

where υ_l is the volumetric flow rate of the liquid, $m^3\ s^{-1}$ and C_l is the liquid concentration, mol m^{-3}.

Substituting equation (3.5) into equation (3.4) gives

$$-\frac{\upsilon_l}{S_e}\frac{dC_{OH}}{dz}-(r_{OH})_e a = 0 \qquad (3.6)$$

Since the system is assumed to be at steady state the disappearance of hydroxyl groups can be expressed either in terms of the rate of transport of reactants from the bulk fluid to the external surface,

$$(r_{OH})_e = k_m(C_{OH_b} - C_{OH_s}) \qquad (3.7)$$

where:

k_m is the mass transfer coefficient, $m^3\ m^{-2}\ s^{-1}$

$(C_{OH})_b$ is the concentration of hydroxyl groups in the bulk liquid, mol m^{-3}

$(C_{OH})_s$ is the concentration of hydroxyl groups at the catalytic surface, mol m^{-3}

or in terms of the rate of the chemical reaction at the catalytic surface,

$$(r_{OH})_e = k_r(C_{OH})_s \qquad (3.8)$$

In both of these expressions the rate is expressed in terms of the concentration of hydroxyl groups at the surface, $(C_{OH})_s$, which is difficult to measure during the experiment. Therefore, it is eliminated by combining equations (3.7 and 3.8) as follows:

$$(C_{OH})_s = \frac{k_m}{k_r + k_m}(C_{OH})_b \qquad (3.9)$$

Equation (3.9) is then substituted into equation (3.7) or equation (3.8) to give

$$(r_{OH})_e = \frac{k_r k_m}{k_m + k_r}(C_{OH})_b = \frac{1}{1/k_r + 1/k_m}(C_{OH})_b \qquad (3.10)$$

Equation (3.10) is the expression for the global (overall) rate in terms of the concentration of hydroxyl groups in the liquid phase. Hence, the overall rate constant, k_o, may be expressed by

$$k_o = \frac{1}{1/k_m + 1/k_r} \qquad (3.11)$$

which shows that the effect of reaction and mass transfer are additive and they are resistances in series for this first order rate expression.

Since a positive concentration difference between bulk liquid and solid surface is necessary to transport the hydroxyl groups to the catalyst surface, the surface concentration will be less than the bulk liquid concentration. Figure 3.2 shows schematically how the concentration varies between bulk fluid and catalyst surface depending on whether the rate is chemical kinetically controlled or mass transfer controlled (Smith, 1981).

If the reaction rate is expressed as the rate of transport of hydroxyl groups from bulk phase to the catalyst surface, equation (3.6) can be rewritten as

$$-\frac{\upsilon_l}{S_e}\frac{d(C_{OH})_b}{dz} = k_m a(C_{OH_b} - C_{OH_s}) \qquad (3.12)$$

Substituting equaton (3.9) into equation (3.12) gives

$$-\frac{\upsilon_l}{S_e}\frac{d(C_{OH})_b}{dz} = k_m a(C_{OH})_b - k_m a\left(\frac{1}{k_r/k_m + 1}\right)(C_{OH})_b \qquad (3.13)$$

Rearranging then equation (3.13) becomes

$$-\frac{d(C_{OH})_b}{(C_{OH})_b} = \frac{aS_e}{\upsilon_l}\left(\frac{k_r k_m}{k_r + k_m}\right)dz \qquad (3.14)$$

If the reaction rate constant is very much greater than the mass transfer coefficient, the value of $\left(\frac{k_m}{k_r}+1\right)$ approaches 1. Equation (3.14) may then be integrated from $z=0$ to $z=L$ (see Figure 3.1) to yield

$$(C_{OH})_b|_{exit}=(C_{OH})_b|_{feed}\exp\left(-\frac{aS_e k_m}{v_l}L\right) \tag{3.15}$$

If the reaction rate constant is very much less than the mass transfer coefficient, the value of $\left(\frac{k_r}{k_m}+1\right)$ approaches 1. Equation (3.14) may then be integrated from $z=0$ to $z=L$ (see Figure 3.1) to give

$$(C_{OH})_b|_{exit}=(C_{OH})_b|_{feed}\exp\left(-\frac{aS_e k_r}{v_l}L\right) \tag{3.16}$$

This analysis will then be used in sections 3.3.3 and 3.4 to interpret the results of the experiments in the single channel system.

3.2 EXPERIMENTAL STUDIES

3.2.1 DESCRIPTION OF THE EXPERIMENTAL APPARATUS

A schematic of the experimental apparatus is shown in Figure 3.3 and a photograph of the equipment is presented in Plate 3.1. The nitrogen purge gas stream was fed into the centre of the ceramic tube. The flow of the liquid from the heated reservoir to the distributor was controlled with a needle valve. The inlet gas and liquid temperatures were measured with thermocouples. A cross-sectional view of the reactor is illustrated in Figure 3.4.

In order to ensure an even distribution of liquid, a fine mesh, stainless steel gauze (42 mm *o.d.*) was positioned between the ceramic and the Pyrex tubes to provide a uniform circumferential distribution of liquid around the ceramic tube. Figure 3.5 and Plate 3.2 show a cross-sectional view and a photograph of the liquid distributor. The ceramic tube was sealed with an O ring and held in position with a pin, see Figure 3.5a. In the distributor the liquid flowed into the reactor through small holes (1 mm *i.d.* at 2 mm intervals) drilled in the side of the ceramic tube (see Figure 3.5b). The section of ceramic tube in the distributor had not been coated with catalyst. Prior to performing reaction experiments preliminary trials were performed in a similar design of distributor that was partly constructed of glass and ceramic in which it was confirmed that a uniform liquid distribution could be achieved. The distributor was constructed from a ceramic tube that had been cut along its axis and bonded to a glass tube to form a half-glass half-ceramic tube (see Plate 3.3). The glass part of the tube enabled visual observation of the liquid distribution inside the test tube. A uniform liquid distribution was observed on the ceramic side of the tube.

The catalytic part of the ceramic tube was positioned inside a stainless steel tube (20 mm *i.d.*, 780 mm long) that was housed in a Pyrex tube (74.2 mm *i.d.*, 600 mm long) that acted as a heating jacket. The jacket consisted of an electrical heating coil and silicone heat transfer fluid. Thermocouples were installed at the bottom and top of the heated jacket. The bottom one was connected to a proportional differential controller (PDC). The temperature in the jacket was maintained uniform by introducing a purge of nitrogen which mixed the silicon heat transfer fluid. Expansion bellows (made from PTFE) were positioned between the flange and the Pyrex tube in order to accommodate any differential thermal expansion that may arise.

The outlet temperature of the liquid was measured at the end of the stainless steel tube where the liquid flowed over a weir. The exit gas temperature was measured with a thermocouple positioned in the centre of the stainless steel tube. From preliminary experiments it was evident that the liquid and gas temperatures approached each other at the reactor outlet, so the exit temperature of the liquid and gas could be deduced from a single measurement at the end of the tube (see Appendix E). The fluid product from the reactor could be directed (*via* a two way valve) to one of the two reservoirs. One was used during start-up and shut-down operations whilst the other was dedicated to collecting the products for a controlled experiment once steady state has been achieved. The reservoirs were graduated so that the quantity of liquid could be determined over a period of time and hence the flowrate could be calculated.

A nitrogen purge gas stream was fed into the top of the reactor to facilitate the removal of water and any volatile by-products formed during the reaction. These substances were subsequently trapped in two condensers. The pressure in the system was reduced

with the aid of a vacuum pump, in order to aid the removal of the volatile substances and water from the system. A mercury manometer was used to measure the pressure in the system.

3.2.2 COATING OF THE SINGLE CHANNEL MONOLITH

A ceramic tube 740 mm in length with a 15 mm *i.d.*, was used as the reactor. A short section of the tube, 240 mm in length was left uncoated and used as the liquid distributor. This section of tube had 1 mm holes drilled 2 mm apart and arranged as shown in Figures 3.5b and Plate 3.3. The remainder of the tube was coated with catalyst in the form of an ethanol slurry. The catalyst-ethanol (approximately 70% w/w catalyst) slurry was prepared as previously described in Chapter 2, Section 2.4.2. The slurry was poured into the 500 mm long section of tube and the uniformity and thickness of the catalyst layer were adjusted with a 12 mm *o.d.* glass tube that was positioned centrally inside the ceramic tube. The coated tube was then dried for one hour in an oven at 373 K in a nitrogen atmosphere. The weight of the tube both before and after coating was measured from which the weight of the catalyst was deduced.

3.2.3 EXPERIMENTAL PROCEDURE

3.2.3.1 START-UP AND OPERATION

(i) Check all auxiliary equipment

(ii) Ensure that all tubing and fittings are correctly positioned.

(iii) Check the vacuum in the system and ensure that there are no leaks.

(iv) Switch on the heating system for the heated jacket and the upper reservoir.

(v) Switch on the temperature indicator and ensure that operating temperatures are achieved.

(vi) Switch on the vacuum pump.

(vii) Switch on the gas system and set the gas flow rate.

(viii) Turn the liquid valve on and adjust the flow rate.

(ix) Read the liquid inlet and outlet temperatures.

(x) Read gas and liquid inlet and outlet temperatures.

(xi) Ensure the system reaches steady state.

(xii) Take a sample of the fluid product for analysis.

3.2.3.2 SHUT-DOWN

(i) Turn the vacuum pump off.

(ii) Turn the gas system off.

(iii) Turn the liquid valve off.

(iv) Allow the system to cool before handling.

(v) Switch off the temperature indicators.

3.2.4 ANALYTICAL TECHNIQUES

The progress of the reaction was followed by measuring the concentration of hydroxyl groups. In order to determine the concentration of the hydroxyl groups in solution a

small quantity of sample was titrated with lithium aluminium dibutylamide using 4-phenylazodiphenylamine as an indicator. Details of the titration method are provided in Appendix B, Section B.1.

3.3 EXPERIMENTAL RESULTS

The absence of any significant non-catalytic reaction was confirmed by performing the experiments in the absence of a catalyst.

3.3.1 INVESTIGATING THE EFFECT OF LIQUID FLOWRATE ON THE OVERALL RATE

For the range of operating conditions summarised in Table 3.1, column (a), preliminary experiments were conducted at a temperature of 413 K, in which the effect of liquid flowrate was investigated. The results of these experiments are presented in Figures 3.6 and 3.7 where the fractional conversion and the overall reaction rate were calculated from

$$X_{OH} = \frac{(N_{OH})_o - (N_{OH})}{(N_{OH})_o} \qquad (2.16)$$

and

$$\Re_{OH} = \frac{F_{OH}|_{feed} - F_{OH}|_{exit}}{S_e} \qquad (3.17)$$

respectively. Where $\Re$ is the overall rate, mol m^{-2} s^{-1}.

From Figure 3.7, at liquid flowrates less than 7.7×10^{-7} m^3 s^{-1} it is evident that flowrate and hence mass transfer affects reaction rate. However, since fractional conversion can range from $0.1 < X_{OH} < 0.35$ (see Figure 3.6), then in accordance with equation (3.10) the depletion of hydroxyl groups in the bulk liquid would also affect the rate.

It is, however, interesting to note that above a flowrate of 7.7×10^{-7} m^3 s^{-1}, a change in liquid flowrate has a very small effect on reaction rate. This also indicates the point at which external mass transfer may become much faster than the intrinsic reaction rate at the catalyst surface. Therefore, mass transfer resistance may be minimised by operating at liquid flowrates $> 7.7 \times 10^{-7}$ m^3 s^{-1} and reaction experiments could be performed to determine the reaction rate constant.

3.3.2 INVESTIGATING THE EFFECT OF GAS FLOWRATE AND PRESSURE ON THE OVERALL RATE

A number of experiments were performed to investigate how the overall reaction rate was influenced by purge gas flowrate. Unfortunately because of the limitations in the experimental apparatus it was not possible to maintain system pressure constant whilst these changes were made, as an increase in gas flowrate resulted in a concomitant increase in system pressure. The results are presented in Figure 3.8 as a plot of the fractional conversions of hydroxyl groups *versus* gas flowrates. As can be seen in Figure 3.8 the fractional conversion increases with purge gas flowrate. This effect

was also clearly observed in the experiments with the spinning basket reactor (see Chapter 2, Section 2.4.5.5). Operating pressure is also likely to affect reaction rates. These two effects may occur as follows:

(a) As the condensation polymerisation reaction proceeds the molecular weight of the polymer increases. The water molecules produced as by products during the reaction should be removed in order to help the reaction proceed further. The high viscosity of the polymer makes it difficult to remove the water molecule from the system. Introducing a low pressure to the system aids the removal of water molecule and consequently increases the reaction rate.

(b) Since the removal of water affects the reaction rate, a high purge gas flowrate increases the mass transfer of the volatiles from the liquid to the gas phase and hence increases the reaction rate.

Reaction kinetic experiments were therefore performed at a fixed value of pressure and purge gas flowrate.

Table 3.1 Experimental conditions for reaction experiments in the single channel flow reactor, (a) effect of flowrate on rate controlling process; (b) chemical kinetics; (c) mass transfer.

	(a)	(b)	(c)
Liquid flow rate ($m^3 s^{-1}$) x 10^7	0.13-13	>7.7	<7.7
Inlet concentration of OH (mol m^{-3})	172	172	172,153,139
Reaction temperature (K)	413	373-418	413
Gas flowrate(STP) ($m^3 s^{-1}$) x 10^5	3.33	3.33	<3.33
Catalyst coated tube length (m)	0.5	0.5	0.5
Initial viscosity ($m^2 s^{-1}$) x 10^4	1.5	1.5	1.5,1.6,1.7
Absolute pressure (bar)	0.0789 bar		
Tube diameter (m)	0.015		
Coated catalyst amount on the inside channel wall (g)	15		
Catalytic surface area of the inside channel wall (m^2)	0.0235		
Geometric surface area on the inside channel wall per unit free volume of the tube ($m^2 m^{-3}$)	266.7		

3.3.3 DETERMINING THE REACTION KINETICS IN THE FLOW SYSTEM

The method of integral analysis was used to determine the chemical kinetics and is described as follows:

(a) A series of experiments was performed in the chemical kinetically controlled region, *i.e.* $\upsilon_l > 7.7 \times 10^{-7}$ $m^3 s^{-1}$, for the range of conditions summarised in Table 3.1, see column (b). At each temperature a concentration *versus* flowrate plot was obtained to which a non-linear regression was applied. An example of one of these plots is illustrated in Appendix F.

(b) Making use of the regressed fit and considering only data when $\upsilon_l > 7.7 \times 10^{-7}$ $m^3 s^{-1}$, the results are plotted in Figure 3.9 in accordance with the following equation:

$$\ln(1 - X_{OH}) = \alpha k_r L \frac{S_e}{\upsilon_l} \qquad (3.18)$$

as a plot of $\ln(1 - X_{OH})$ *versus* S_e/υ_l. As seen in Figure 3.9 a straight line is obtained as expected for a first order assumption. From the slope of the straight line the reaction rate constant was determined to be 3.8×10^{-6} $m_l^3 m_e^{-2} s^{-1}$.

(c) The results of these experiments at different temperatures are presented in Figure 3.10 in accordance with Arrhenius' law as a plot of $\ln k_r$ *versus* 1/T. Applying linear regression, the following rate constant was determined:

$$k_r = 4.2x10^{-4}\exp\left(-\frac{1.6x10^4}{RT}\right) \qquad (3.19)$$

It is encouraging to find that the value of the activation energy is of a similiar order of magnitude to that determined in the spinning basket reactor experiments. However, it is slightly lower than the value for the single channel rings. This may have occurred as a result of differences in the way of the catalyst had been coated onto the ceramic surface. The coating of a long tube was more difficult than the coating of the ceramic rings.

3.4 ESTIMATING THE MASS TRANSFER COEFFICIENT

From equation (3.14) the overall rate constant may be expressed as:

$$k_o = -\ln\left(\frac{C_{OH\,b\,|\,exit}}{C_{OH\,b\,|\,feed}}\right)\frac{\upsilon_l}{\alpha S_e L} \qquad (3.20)$$

By performing experiments for the range of conditions described in Table 3.1, see column (c), k_o may be determined and as the value of k_r as a function of temperature is now known, the mass transfer coefficient k_m may be calculated from

$$1/k_m = 1/k_o - 1/k_r \qquad (3.21)$$

Calculated values of k_o and k_m are summarised in Table 3.2. It should be noted that for experimental runs 2, 3, and 4, the initial concentration of hydroxyl groups was lower, since the feed stock had already been previously processed in the reactor and was being reused for this series of experiments. In order to select a form of equation for the mass transfer correlation, a relation between a modified Sherwood number and Reynolds and Schmidt numbers was developed through dimensional analysis. For a thin liquid film flowing down a vertical cylindrical surface, the following equation was derived:

$$Sh = \theta(Re)^{\alpha}(Sc)^{\gamma}\left(\frac{d_i}{\delta}\right)^{\beta}\left(\frac{L}{\delta}\right)^{\sigma} \qquad (3.22)$$

Equation (3.22) is of a similar form to that developed by Cussler (1984) for mass transfer in a tube, except that the unit length is the film thickness, δ, instead of the diameter of the tube.

Making use of the physical properties and transport data summarised in Table 4.1 the dimensionless groups Re, Sc and Sh were evaluated. Assuming laminar flow and no rippling, the film thickness, δ, was calculated from the well known theoretical expression (*e.g.* Danckwerts, 1970)

$$\delta = \left(\frac{3\mu\upsilon_l}{g\rho\pi d_i}\right)^{1/3} \qquad (3.23)$$

and the dimensionless groups calculated from

$$Sh = \frac{k_m \delta}{D} \tag{3.24}$$

$$Re = \frac{\upsilon \delta}{\nu} \tag{3.25}$$

$$Sc = \frac{\nu}{D} \tag{3.26}$$

where:

D	is diffusivity constant	$m^2\ s^{-1}$
υ	is the velocity of the liquid	$m\ s^{-1}$
ν	is kinematic viscosity	$m^2\ s^{-1}$
ρ	is the density,	$kg\ m^{-3}$
μ	is the viscosity,	$kg\ m^{-2}\ s^{-1}$

Making use of the experimental data obtained in the series of experiments identified as runs 1, 2 and 3 in Table 3.2, and applying the method of non-linear regression analysis, the following empirical expression was determined:

$$Sh = 0.00178(Re)^{1.37}(Sc)^{1.27}\left(\frac{d_i L}{\delta^2}\right)^{-0.32} \tag{3.27}$$

Figure 3.11 shows the result of the non-linear regression as a plot of Sherwood number calculated from the experimental results *versus* estimated Sherwood number from the correlation. In Figure 3.12 the experimental results (for the series of

experiments in runs 1, 2 and 3) and correlation are presented and compared with predictions from the use of a theoretical correlation described in Skelland (1974), for laminar flow down an inclined flat plate, of the following form

$$Sh = 0.783 Re^{(1/9)} Sc^{(1/3)} \left(\frac{(L_p)^3 \rho^2 g \sin\alpha}{\mu^2} \right)^{(2/9)} \qquad (3.28a)$$

where L_p is the length of the inclined plate. The dimensionless numbers are described as follows:

$$Sh = \frac{k_m L_p}{D} \qquad (3.28b)$$

$$Re = \frac{4 \upsilon_l}{a S_e \nu} \qquad (3.28c)$$

$$Sc = \frac{\nu}{D} \qquad (3.28d)$$

According to Tallmadge and Gutfinger (1967), thin-film flow down a vertical cylindrical surface is hydrodynamically equivalent to that down a vertical flat plate when the Goucher number Go, is greater than 3. In this study the Goucher number was calculated to be 3.58 as follows:

$$Go = \frac{d}{2} \left(\frac{\rho g}{2\sigma} \right)^{0.5} = 3.58 \qquad (3.29)$$

where σ is the surface tension (21 N m^{-1}, see Table 2.1).

It may therefore be assumed that the thin film flow of the siloxane polymer down the inner wall of the ceramic tube is equivalent to that on a vertical flat plate. However, from the comparison in Figure 3.12, it is evident that calculated experimental values are substantially higher. Skelland (1974) recognized that experimental results frequently show mass transfer rates that are substantially higher than predicted by those relationships based on laminar parabolic velocity distribution. Under the experimental conditions higher rates arise as a result of eddying and turbulence within the film. Since the surface of the catalyst is rough after coating, and bubbles of vapour are likely to be formed on the surface of the catalyst as the reaction proceeds, mass transfer rates would be substantially enhanced above the laminar flow case.

It is however interesting to compare the coefficients with predictions from the use of the correlation developed by Hatziantoniou and Andersson (1982). They studied the mass transfer of benzoic acid in two phase slug flow down a coated cylindrical tube (0.17 m long, 2.35 mm and 3.094 mm id.) and determined mass transfer coefficients in the approximate range of 3.0×10^{-5} to 8.0×10^{-5} m s^{-1}. These values are close to those found in this study. Although the flow pattern is different, it is not surprising that mass transfer rates had been enhanced as a result of the nature of turbulence within the film.

3.5 THE EFFECT OF COUNTERCURRENT GAS-LIQUID FLOW ON THE OVERALL RATE

The results of a limited number of experiments, with countercurrent gas-liquid flow are illustrated and compared with co-current flow in Figure 3.13. From this it is evident that co-current flow gives higher conversion than countercurrent flow. The

differences in conversion between the different modes of flow are 7.7 % at high liquid flowrates and 27 % at low liquid flowrates. This may have occured as a result of the countercurrent gas flow affecting the form of the falling liquid film. Also, at the entrance of the tube the driving force for the removal of water from the liquid to the purge gas is less than that obtained in co-current flow. This in turn would have reduced the reaction rate in the entrance section of the reactor.

Table 3.2 Experimental measurement and mass transfer calculations.

$(C_{OH})_{initial}$(mol m^{-3})	υ_l (m^3 s^{-1}) x 10^7	k_o (m s^{-1}) x 10^6	k_m (m^3 m^{-2} s^{-1}) x 10^5	δ (m) x 10^4
Run 1				
172	5.5	3.41	2.87	8.23
172	5.3	3.29	2.18	8.13
172	5.0	3.24	2.00	7.98
172	4.5	3.05	1.44	7.74
172	4.2	2.97	1.27	7.52
172	3.9	2.87	1.11	7.37
172	3.3	2.62	0.816	6.97
172	3.1	2.56	0.813	6.87
172	3.0	2.47	0.659	6.80
172	2.5	2.21	0.516	6.39
172	1.3	1.47	0.238	5.70
172	0.81	1.05	0.144	4.46
172	0.47	0.71	0.0865	3.75
172	0.22	0.35	0.0385	2.94

Continuing of Table 3.2

$(C_{OH})_{initial}$(mol m^{-3})	υ_l (m^3 s^{-1}) x 10^7	k_o (m s^{-1}) x 10^6	k_m (m^3 m^{-2} s^{-1}) x 10^5	δ (m) x 10^4
Run 2				
153	7.10	3.25	2.02	9.08
149	4.50	2.92	1.19	7.92
146	3.80	2.59	0.79	7.51
135	1.60	1.30	0.19	5.66
Run 3				
139	7.10	3.40	2.76	9.08
127	4.50	3.04	1.41	7.92
125	3.80	2.67	0.86	7.51
118	1.60	1.47	0.247	5.66
Run 4				
123	7.10	3.50	3.20	9.43
107	4.50	3.22	1.90	8.41
105	3.80	2.91	1.10	8.00
90	1.6	1.70	0.30	6.31

3.6 CONCLUSIONS

(a) In the chemical kinetically controlled region the results of the kinetic experiments in the single channel flow reactor showed that the condensation polymerisation reaction is of a first order with respect to hydroxyl groups and the reaction rate based on the external catalytic surface area may be represented by

$$r_{OH} = 4.2x10^{-4}\exp\left(-\frac{1.6x10^{4}}{RT}\right)C_{OH}$$

for the range of:

C_{OH} = 153 mol m^{-3} to 172 mol m^{-3},

T = 373 K to 413 K, and

P = 0.0798 bar.

(b) To evaluate mass transfer coefficients in the single channel monolith flow reactor, at a fixed pressure and purge gas flowrate a semi-empirical correlation of the following form was developed:

$$Sh = 0.00178(Re)^{1.37}(Sc)^{1.27}\left(\frac{d_i}{\delta}\right)^{-0.32}\left(\frac{L}{\delta}\right)^{-0.32}$$

for the range of:

$(C_{OH})_{feed}$ = 139 mol m^{-3} to 172 mol m^{-3}

υ_l = 1.7 x 10^{-8} - 7.1 x 10^{-7} m^3 s^{-1},

δ $= 2.7 \times 10^{-4} - 9.2 \times 10^{-4}$ m,

L $= 0.5 - 1.5$ m,

Re $= 0.002 - 0.1$, and

Sc $= 5.4 \times 10^{5} - 9.5 \times 10^{5}$.

(c) Increasing purge gas flowrate and maintaining a low pressure in the system assist the removal of water and volatiles, and consequently increases the reaction rate.

(d) At a fixed pressure and purge gas flowrate, the co-current method of operating the single channel flow reactor provides a higher reaction rate than the countercurrent method of operation.

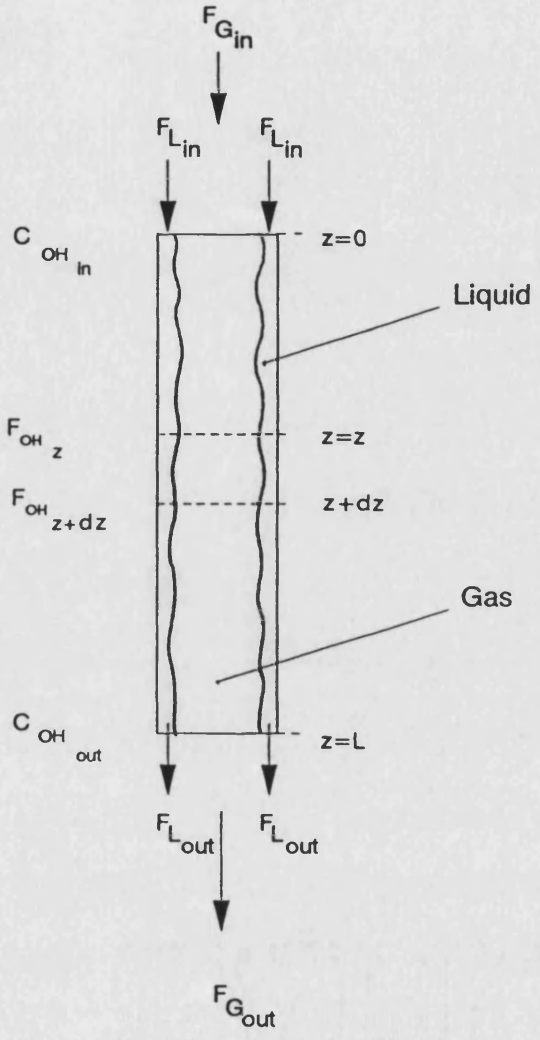

Figure 3.1 Axial section of the single channel monolith reactor with cocurrent flow.

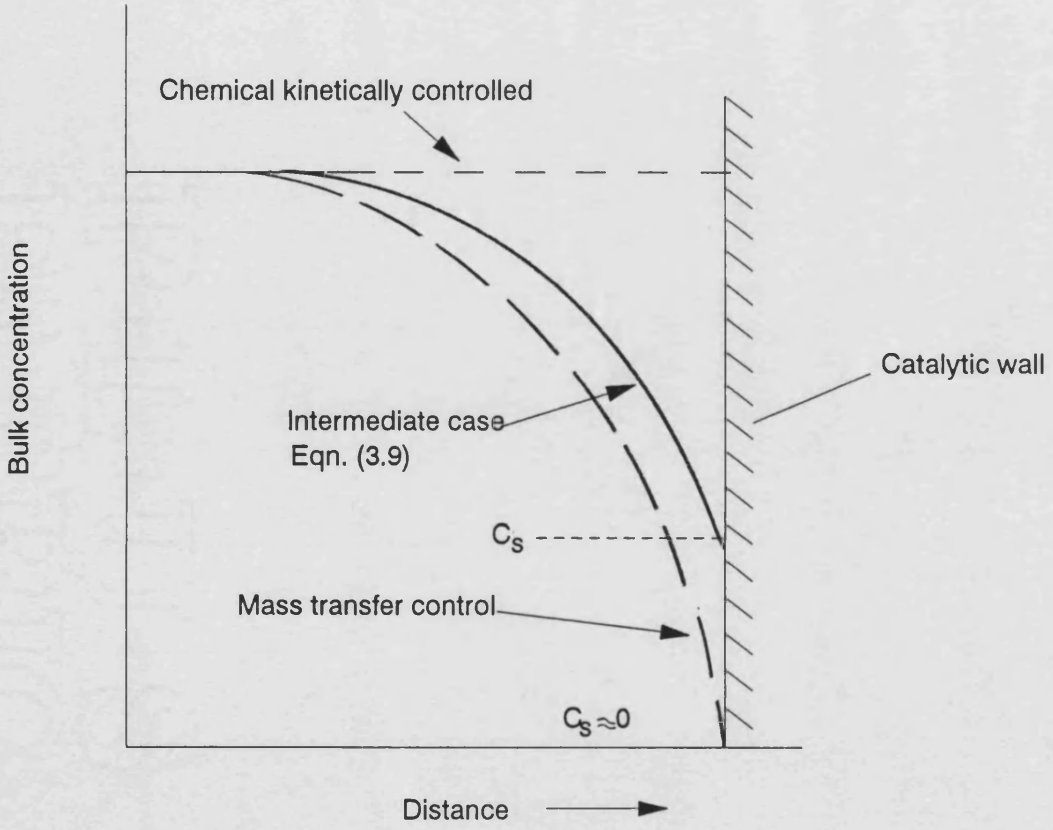

Figure 3.2 Concentration distribution under mass transfer and chemical kinetically controlled reaction (Smith, 1981)

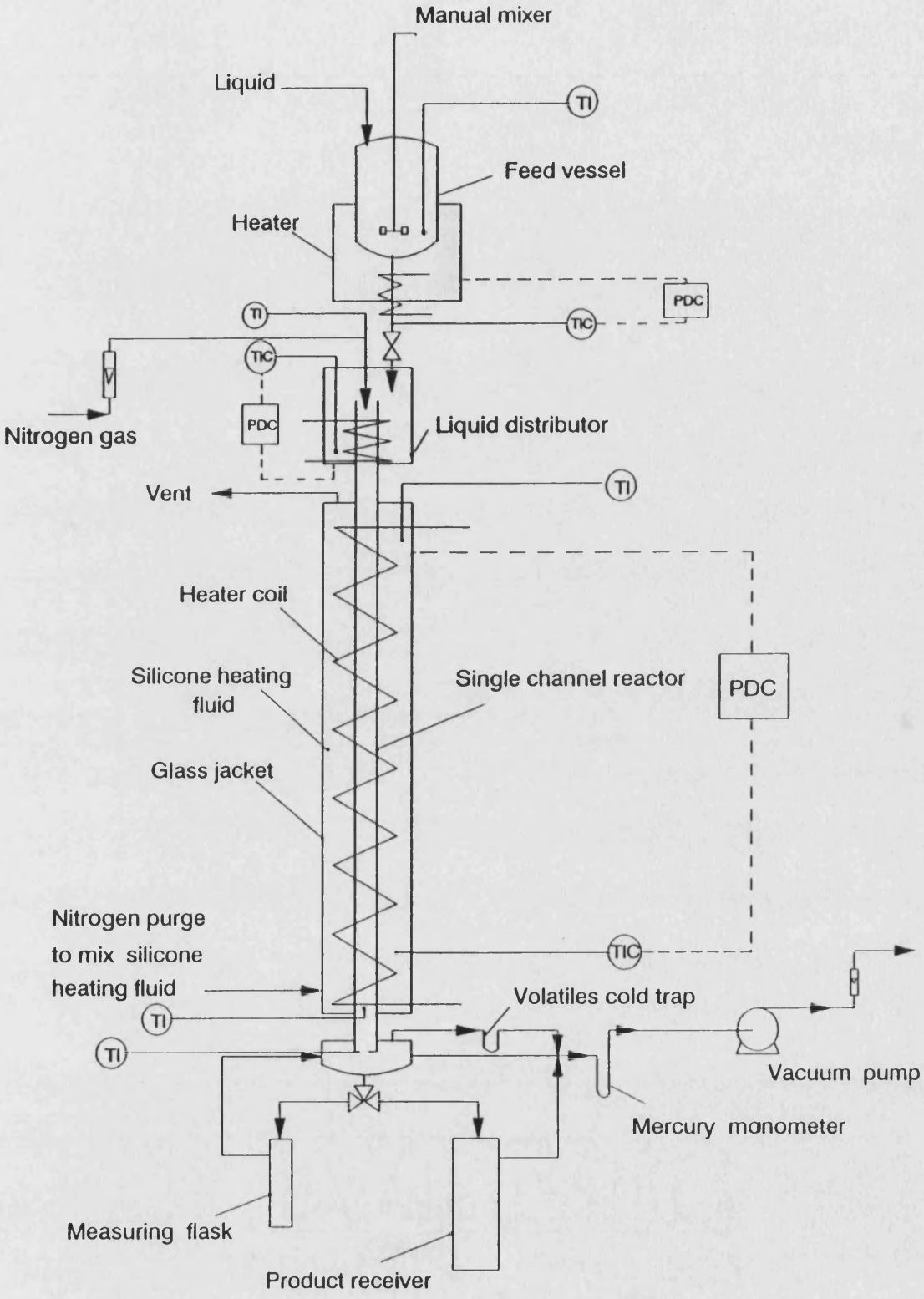

Figure 3.3 Schematic diagram of the single channel flow reactor system.

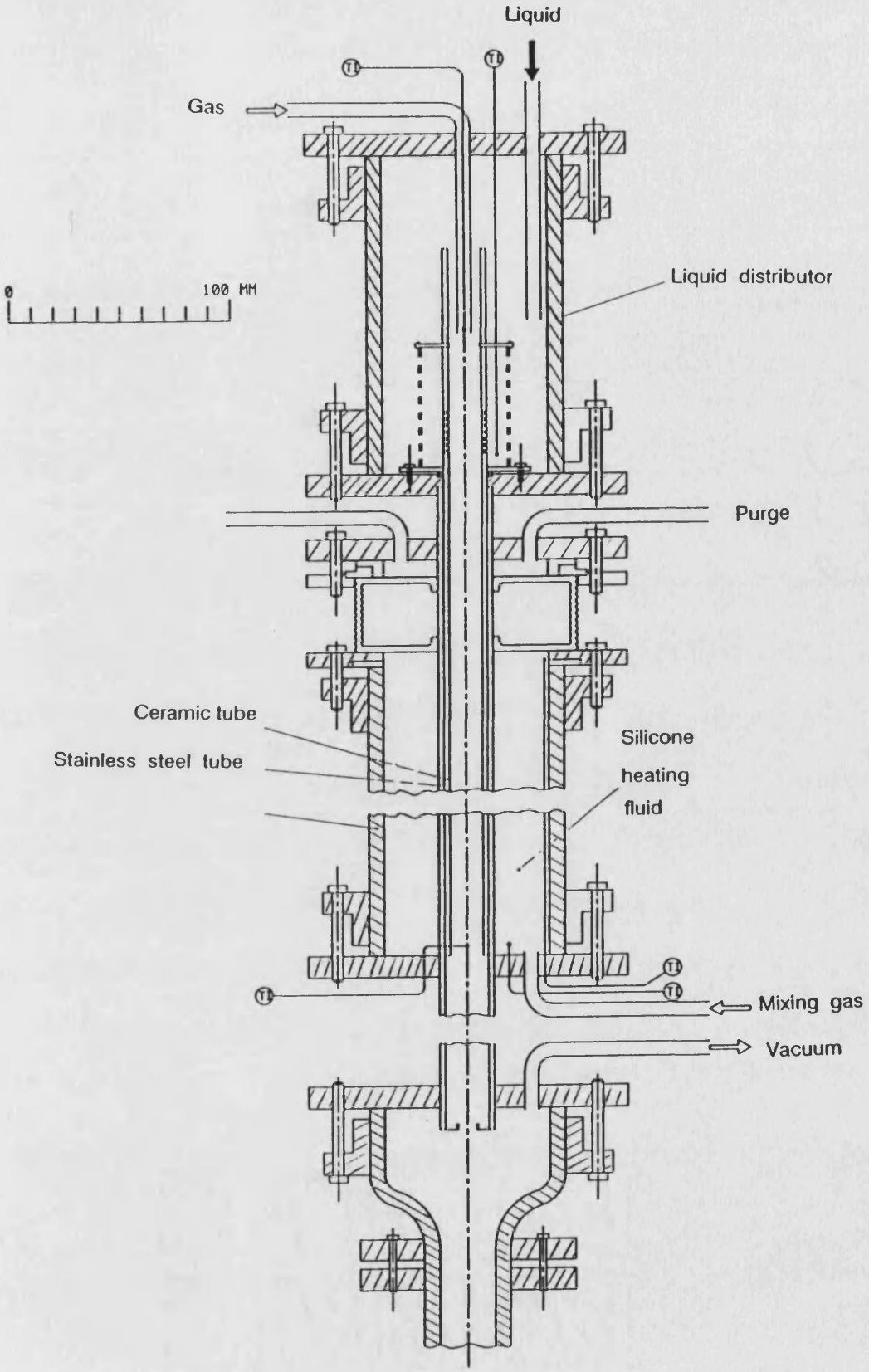

Figure 3.4 A detailed cross-sectional view of the single channel reactor

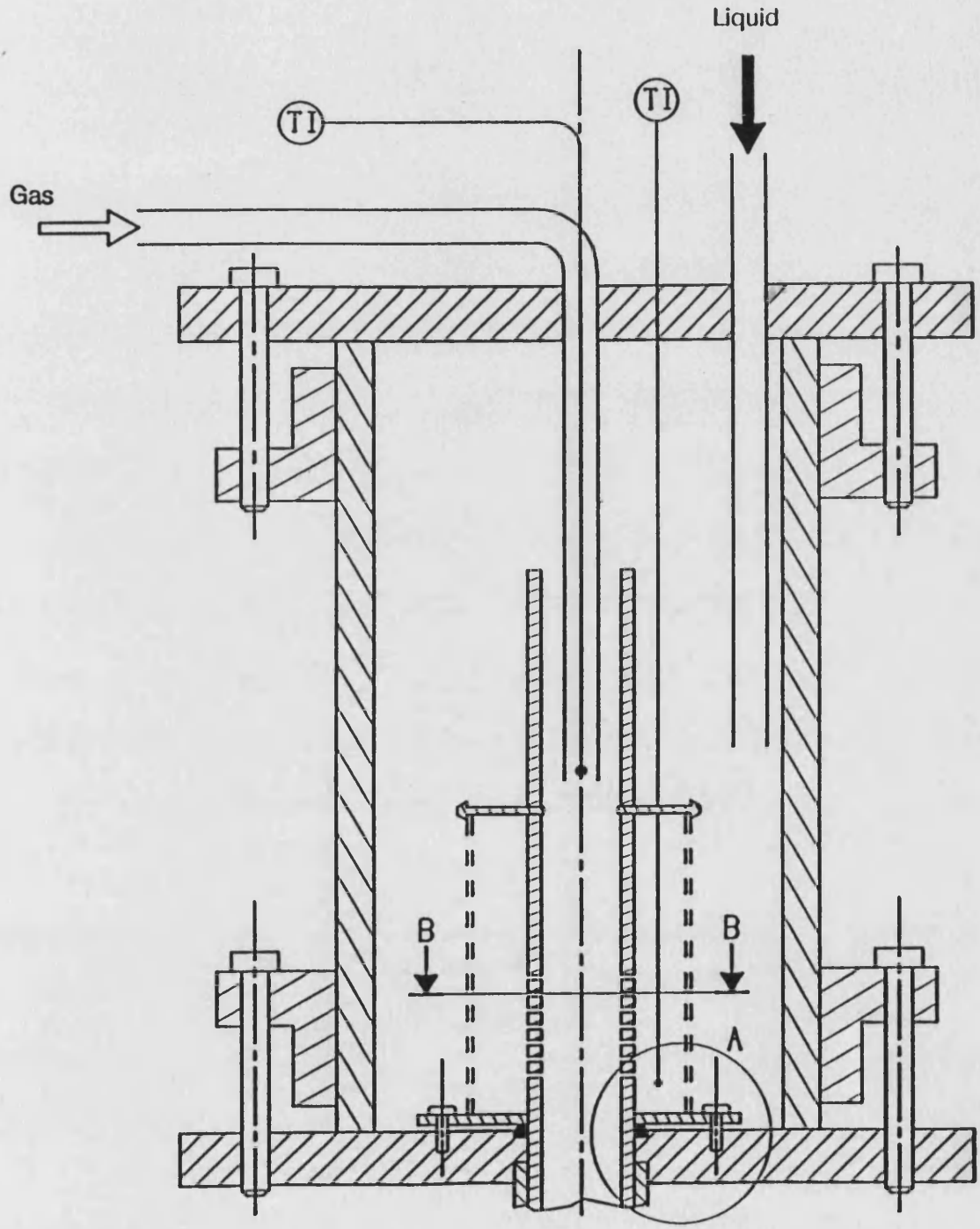

Figure 3.5 A cross-sectional view of the liquid distributor.

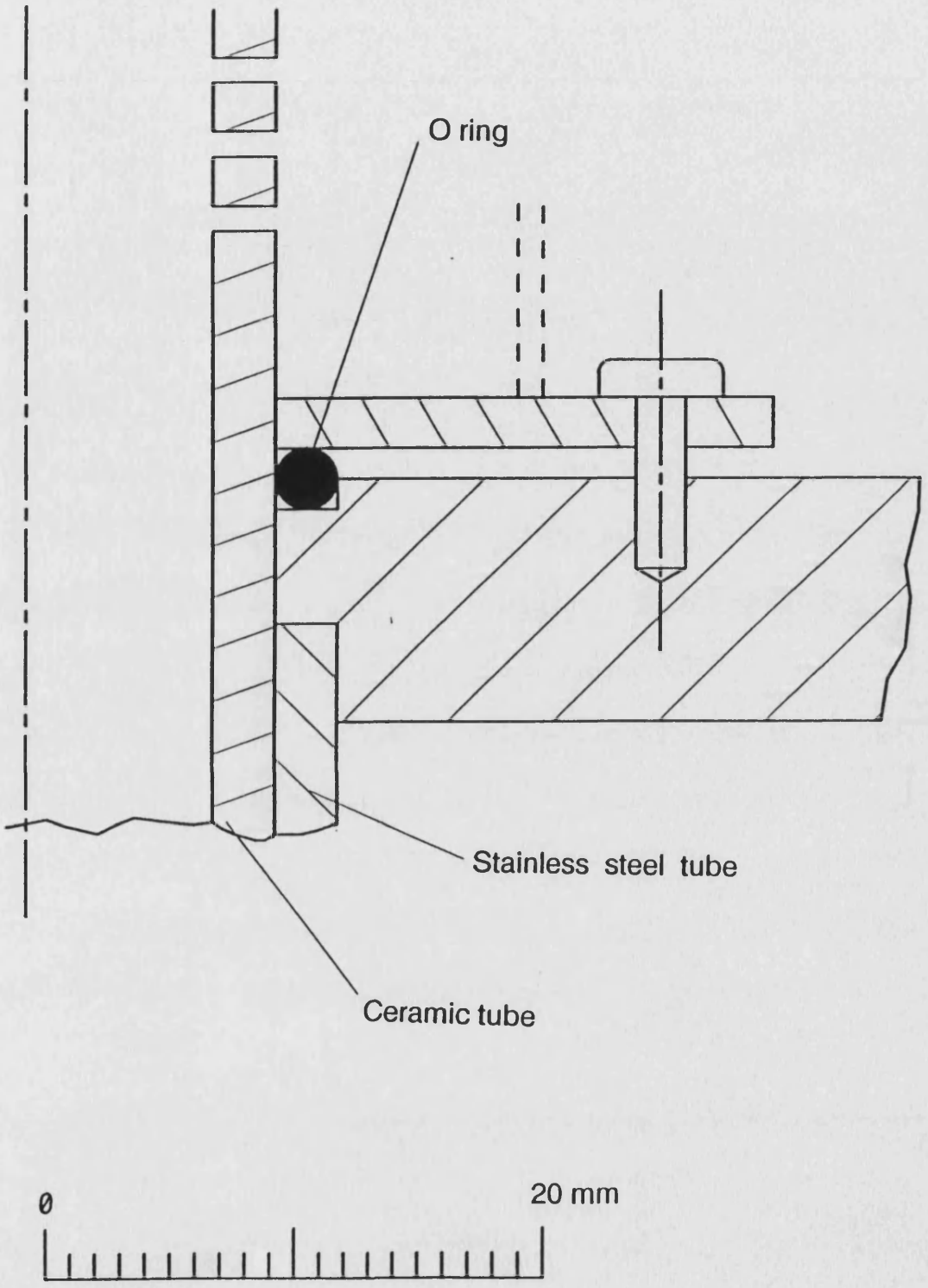

Figure 3.5a View A-A in Figure 3.5, illustrating the position of O ring.

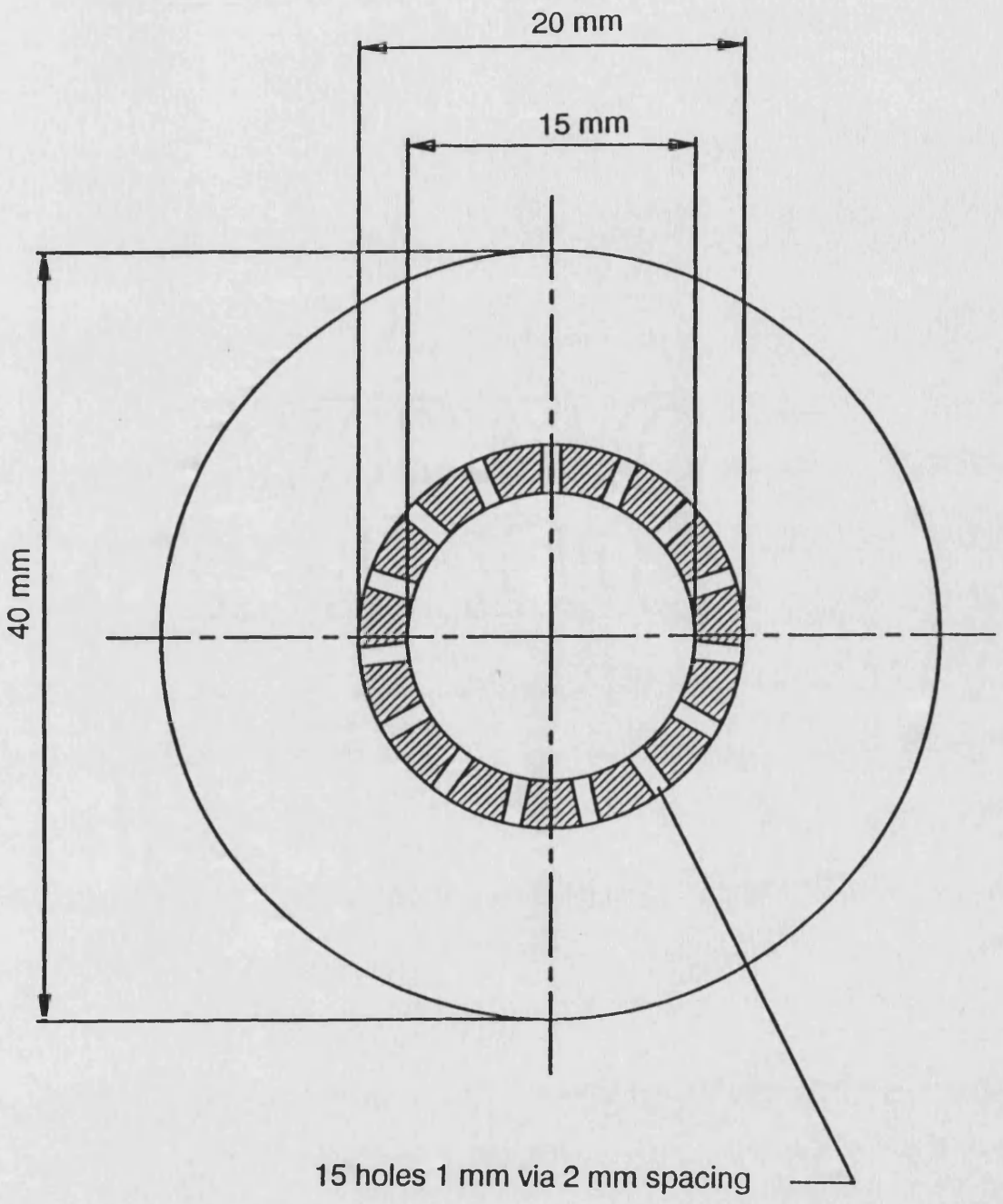

Figure 3.5b View B-B in Figure 3.5, illustrating the position of the holes

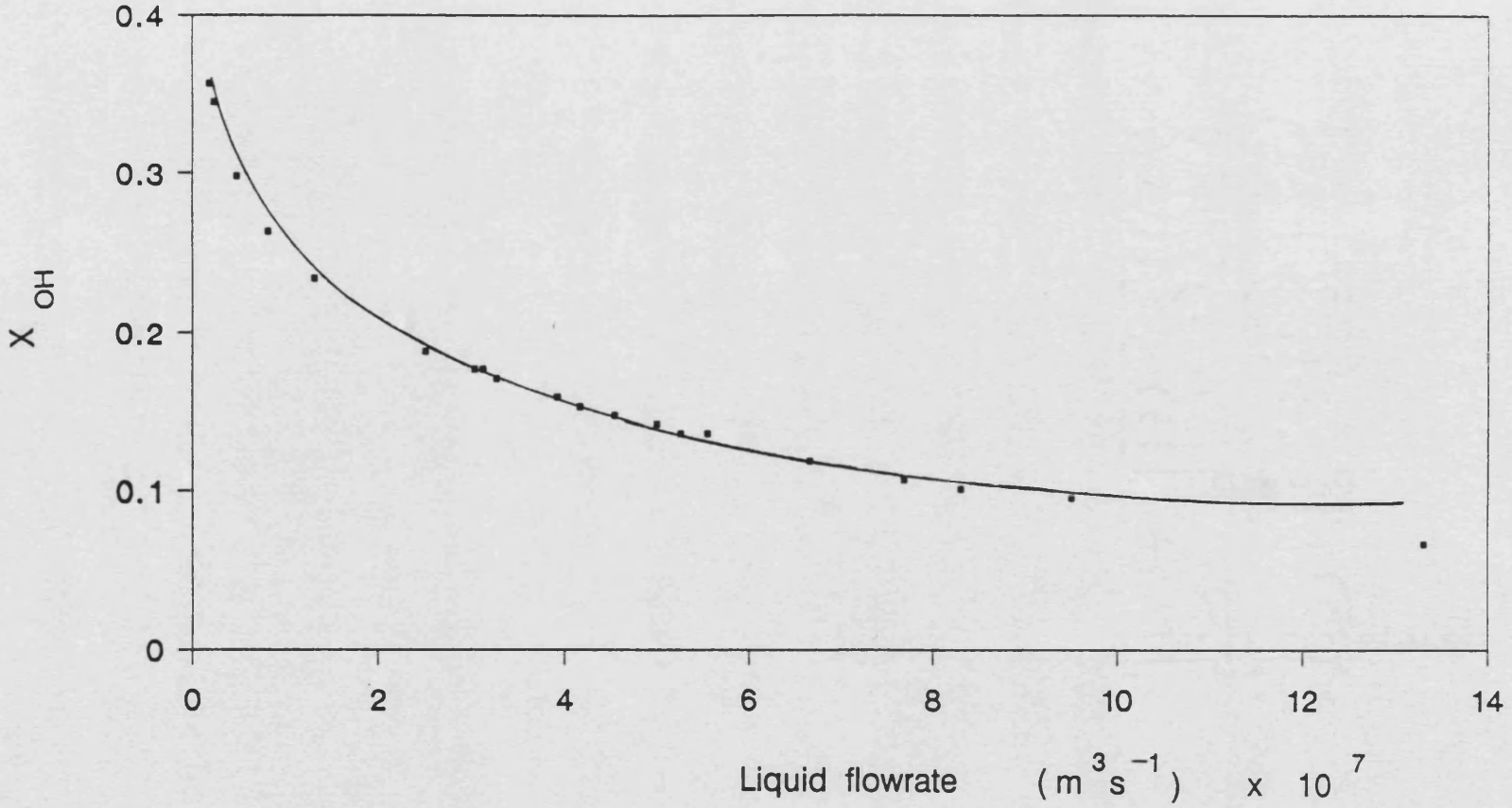

Figure 3.6 Reaction experiments in the single channel reactor: effect of flowrate on conversion.
(T = 413 K ; P = 0.079 bar ; $\upsilon_g = 3.34 \times 10^{-5}$ m^3 s^{-1})

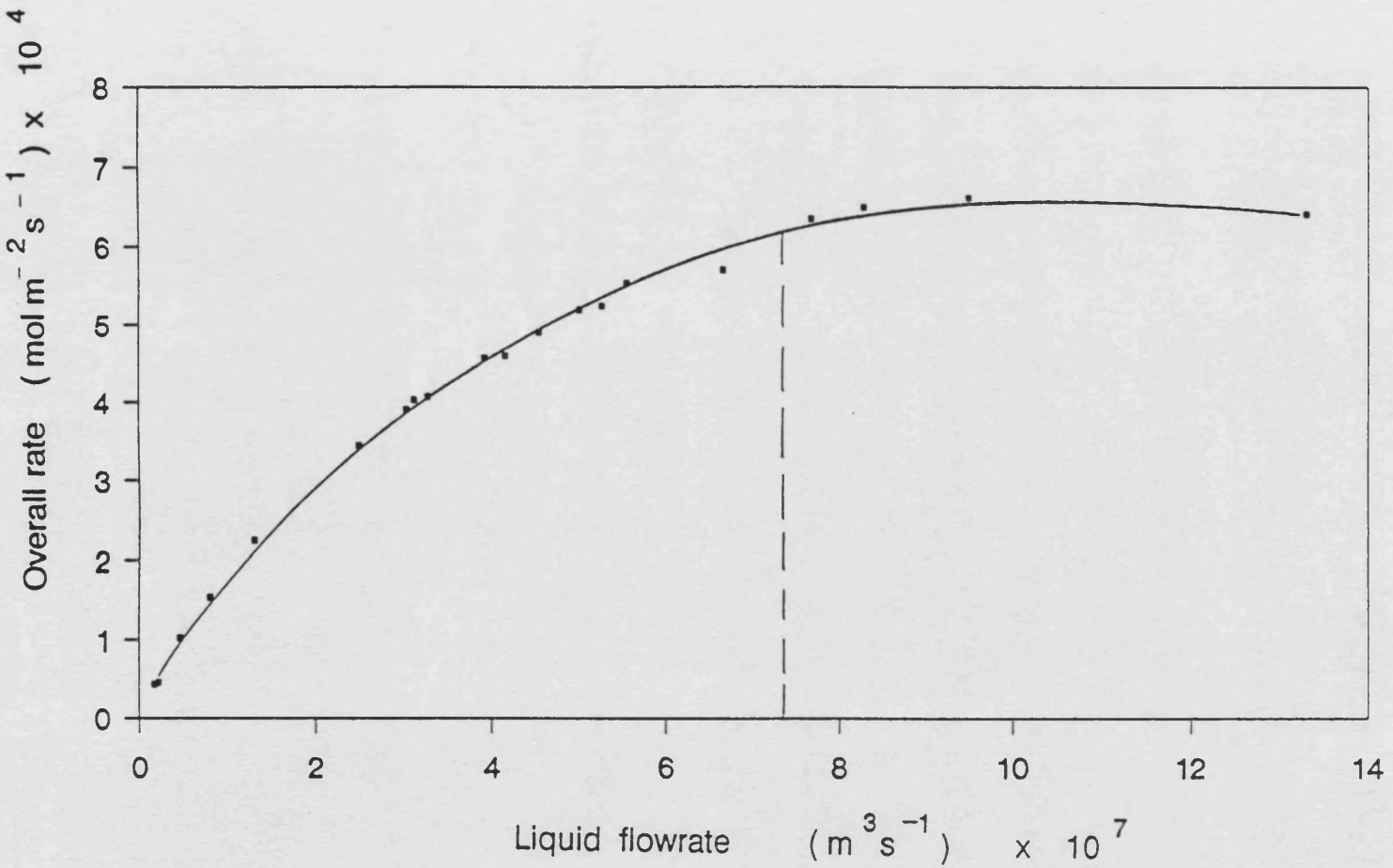

Figure 3.7 Reaction experiments in the single channel reactor :effect of flow rate on overall rate.
(the dotted lines represent the point at which external mass transfer effects were minimised, T=413 K; P=0.079 bar).

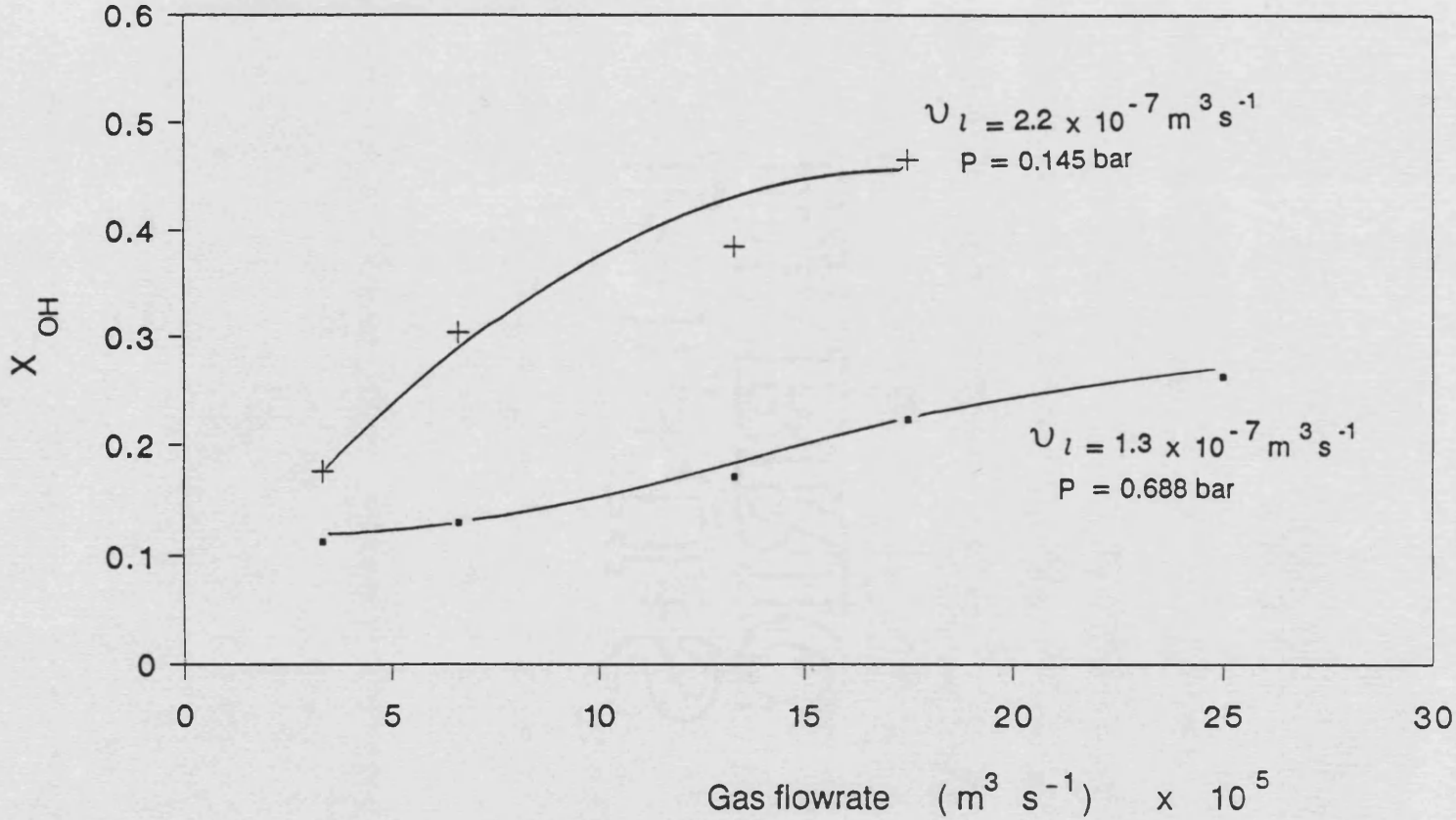

Figure 3.8 Investigating the effects of varying purge gas flowrate at T= 413 K.

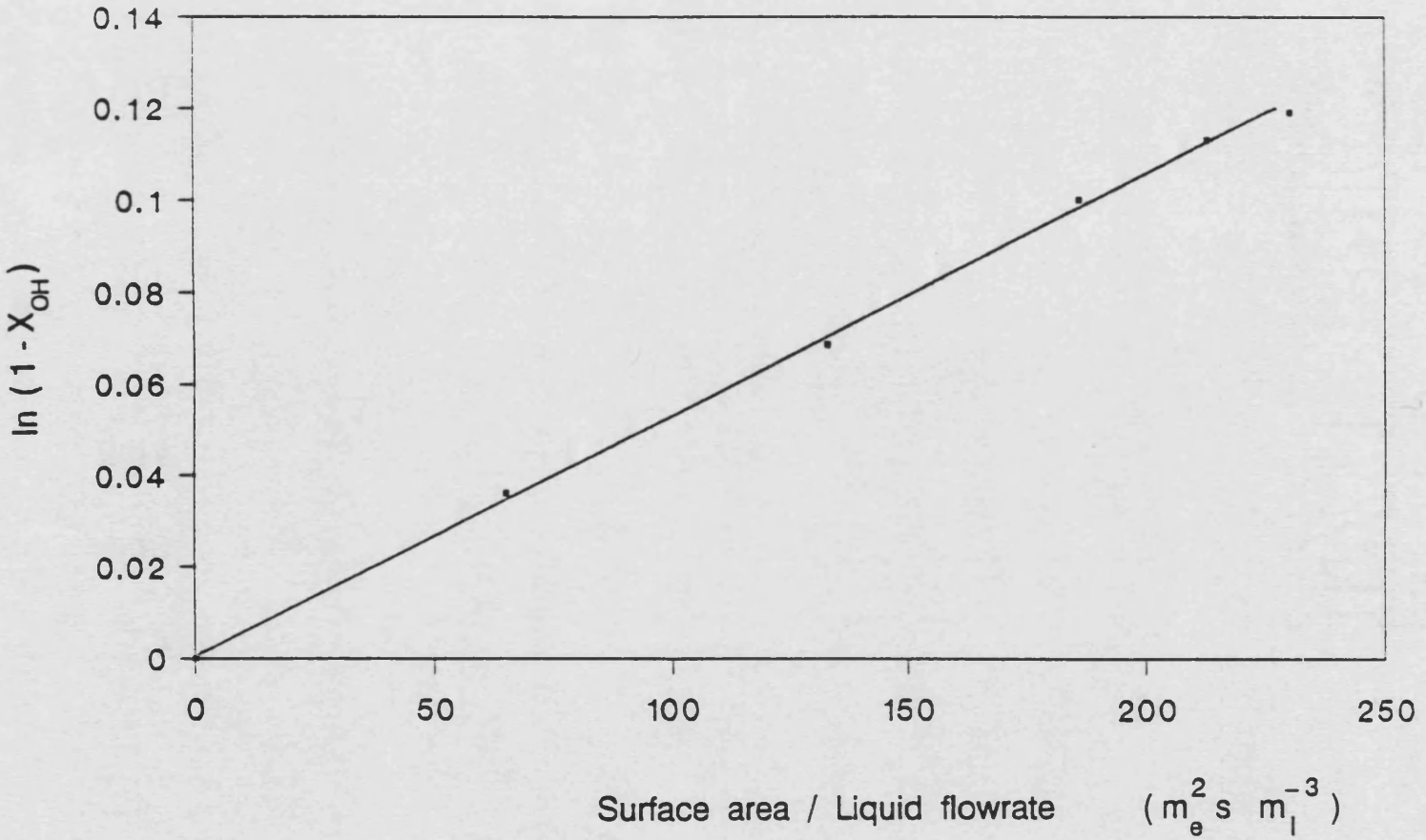

Figure 3.9 Results of the integral method of analysis assuming a first order reaction (T = 413 K).

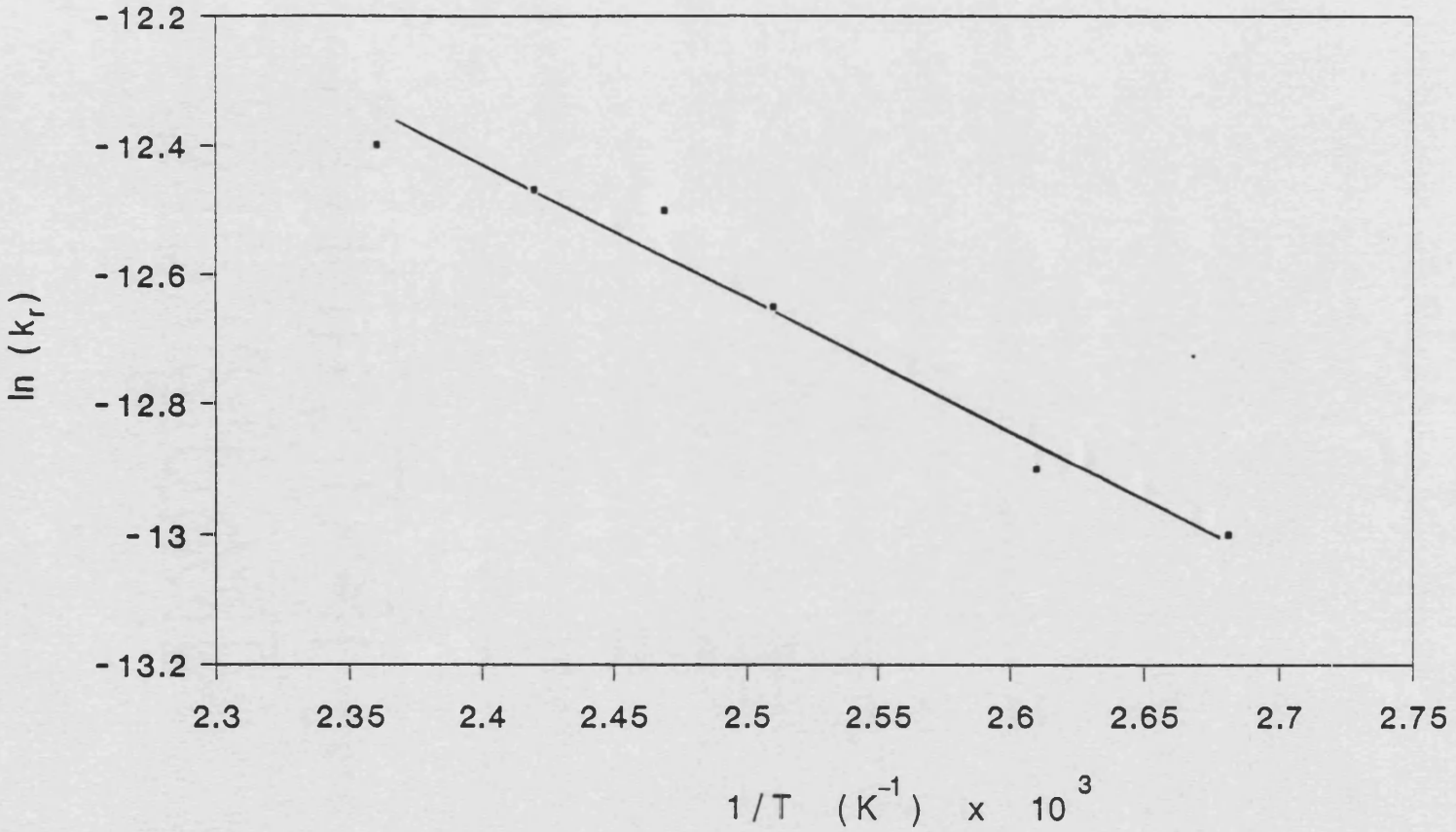

Figure 3.10 Results of the kinetic experiments ($\upsilon_l > 7.7 \times 10^{-7} m^3 s^{-1}$).

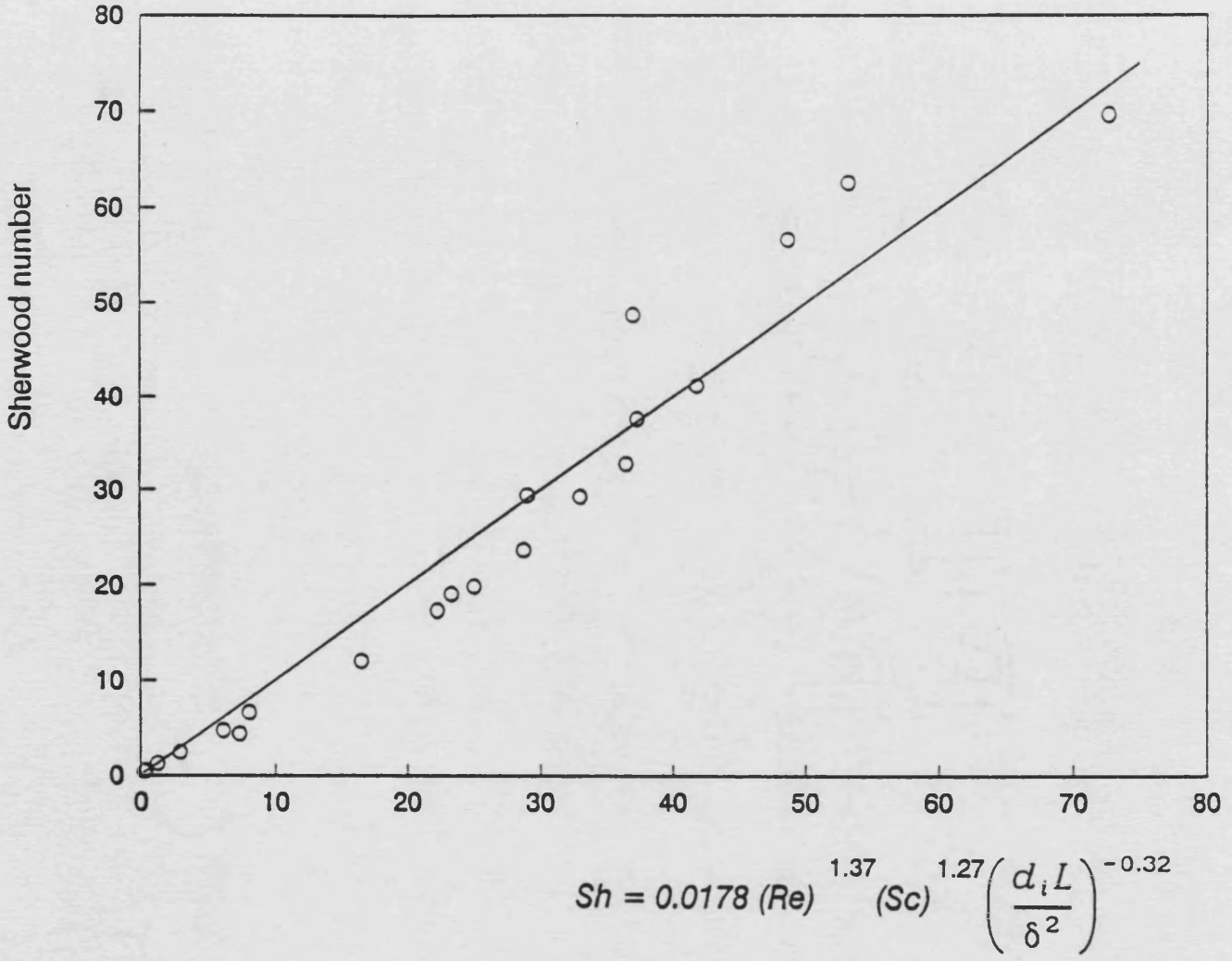

Figure 3.11 Correlating the experimental results of the mass transfer study. The continuous line represents the regressed data.

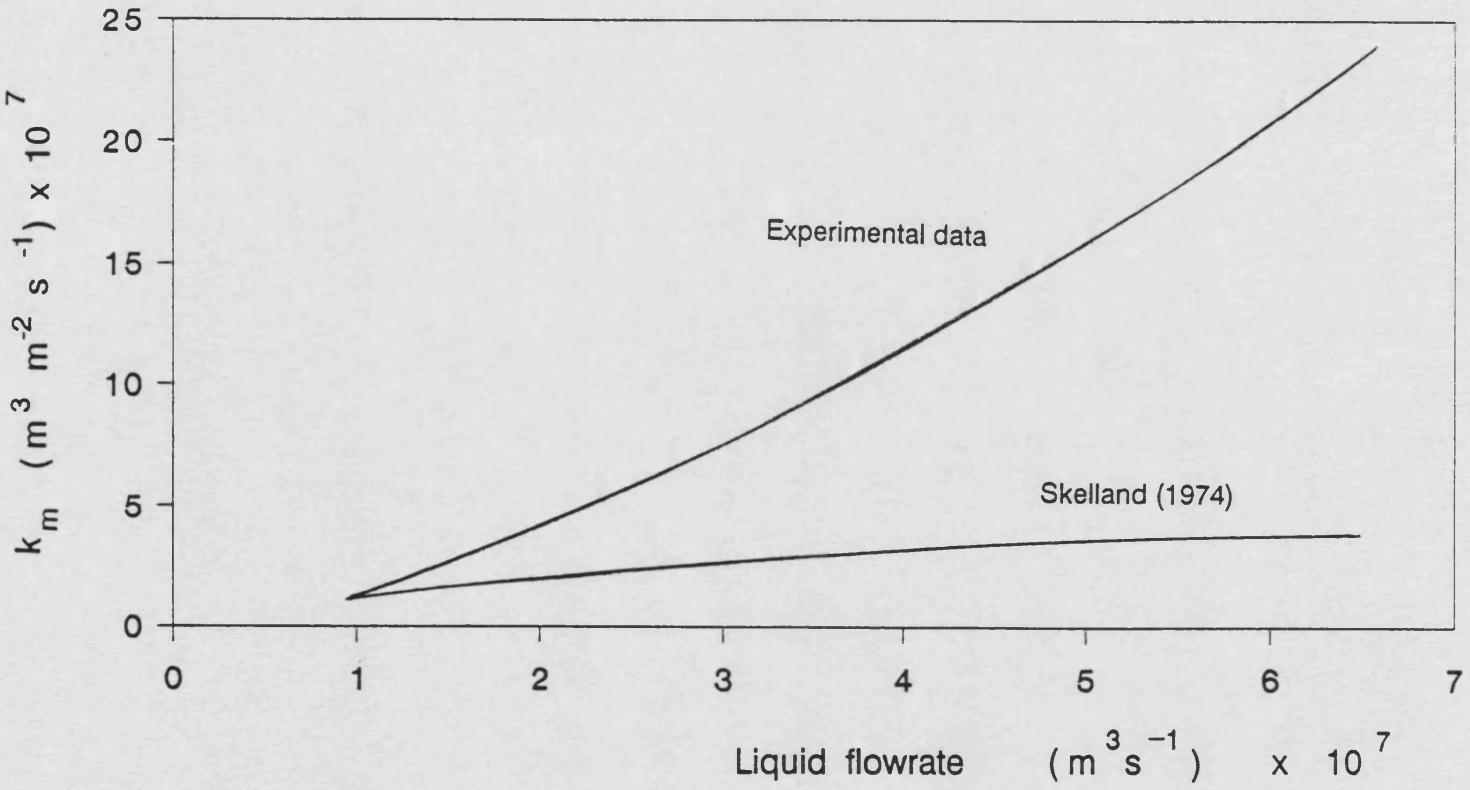

Figure 3.12 Correlated experimental results of the mass transfer study compared with a theoretical correlation for flow down an inclined plate.

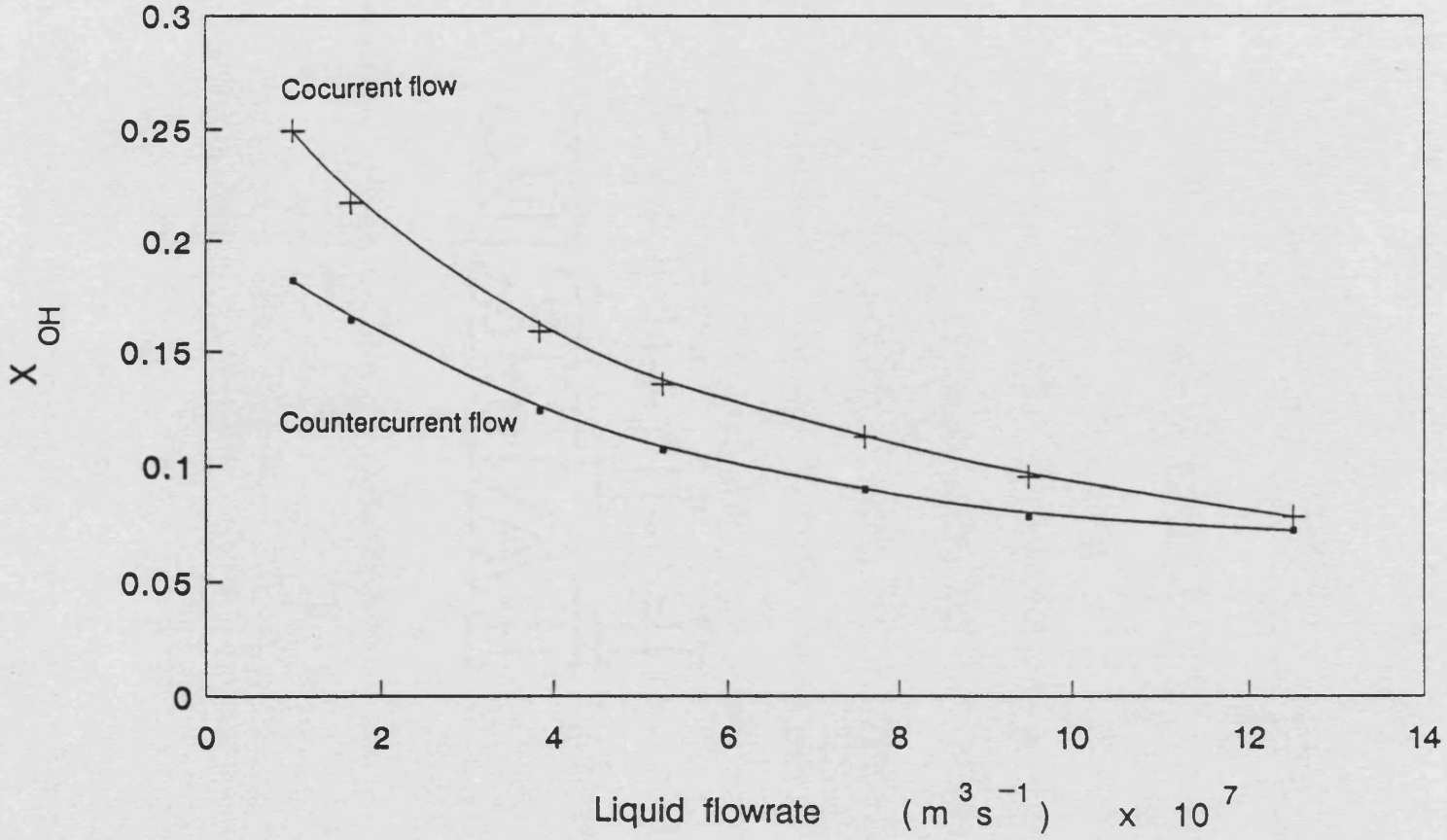

Figure 3.1.3 Comparison of countercurrent and cocurrent flow modes in the single channel reactor (T = 413 K ; P = 0.0789 bar ; $\upsilon_l = 3.34 \times 10^{-5} m^3 s^{-1}$)

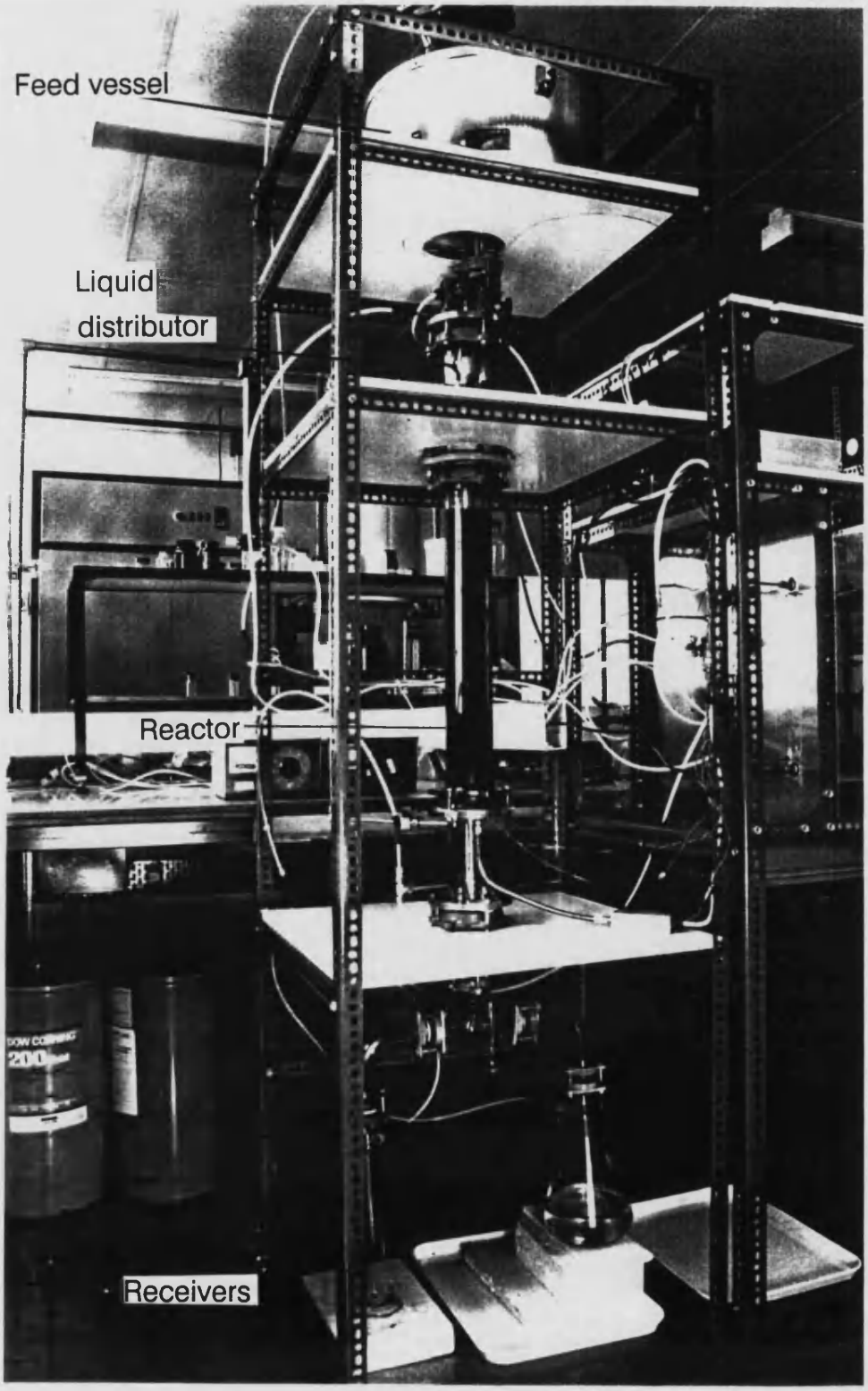

Plate 3.1 Photograph of the single channel flow reactor.

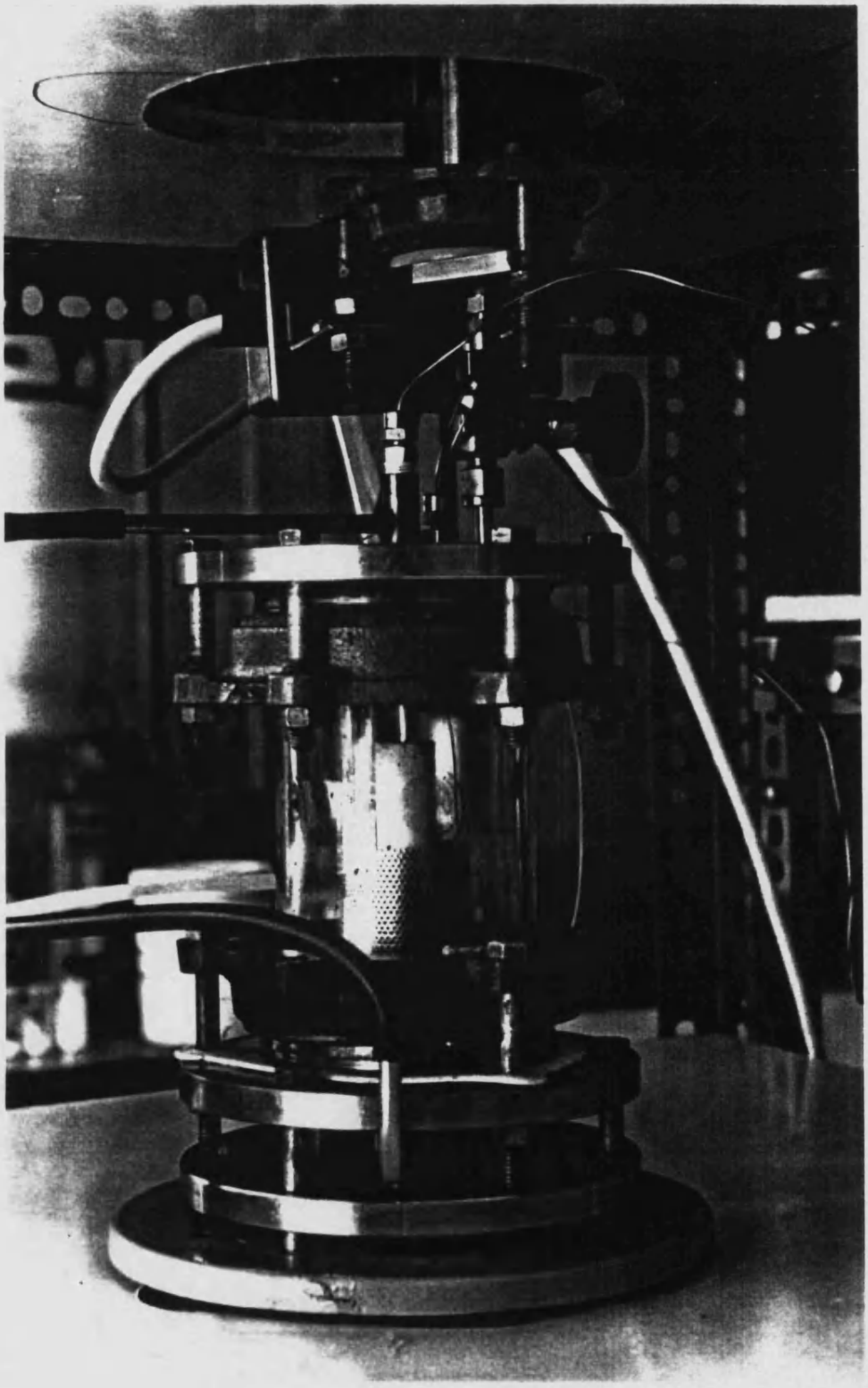

Plate 3.2 Photograph of the liquid distributor.

Plate 3.3 Photograph of the half-glass half-ceramic test tube.

CHAPTER 4

THE ONE DIMENSIONAL MODEL: VALIDATION AND SIMULATION RUNS

INTRODUCTION

In this chapter, the one dimensional model developed in Chapter 3 is validated with the experimental data. The one dimensional model is also used in simulation to compare the performance of a multi-channel system versus that of a packed bed reactor.

This chapter is presented under the following headings:

4.1 Validation of the model

4.2 Comparing modelling results with the experimental results

4.3 Comparing the performance of a monolith versus a packed bed reactor

4.4 Conclusions

4.1 VALIDATION OF THE MODEL

The one dimensional mathematical model has already been described in Chapter 3, see Section 3.1. For any j^{th} section of axial length in the single channel (see Figure 4.1), the steady state differential material balance

$$-\frac{\upsilon_l}{S_e}\frac{d(C_{OHb})_j}{dz_j} = (k_m)_j a\left\{(C_{OHb})_j - (C_{OHs})_j\right\} \qquad (3.12)$$

coupled with the material balance,

$$k_r(C_{OH_s})_j = (k_m)_j\left\{(C_{OH_b})_j - (C_{OH_s})_j\right\} \qquad (4.1a)$$

at the surface of the catalyst are solved.

At the surface of the catalyst the concentration of hydroxyl groups is calculated from equation (4.1a) since,

$$(C_{OH_s})_j = \frac{(C_{OH_b})_j}{1 + k_r/(k_m)_j} \qquad (4.1b)$$

The physical properties and transport parameters of the liquid are summarised in Table 4.1. Since the viscosity of the liquid changes during the reaction the physical properties were evaluated at each increment step, Δz, along the column. The mass transfer coefficient, $(k_m)_j$, and the reaction rate constant, k_r, are calculated from

$$(k_m)_j = \frac{(Sh)_j D_j}{\delta_j} \qquad (4.2)$$

$$k_r = A\exp\left(-\frac{E}{RT}\right) \qquad (4.3)$$

respectively.

Table 4.1 Physical properties and transport parameters

Density (supplied by Dow Corning Ltd.) $\rho = 970$ kg m^{-3}
Diffusion coefficient determined from (Schiebel, 1954) $D = \frac{8.2 \times 10^{-8}(T)}{\mu (V_B)^{(1/3)}} \{ 1 + \left(\frac{V_A}{V_B} \right)^{(2/3)} \} 10^{-4}$ (m^2 s^{-1}) at 413 K
Kinematic viscosity (experimentally correlated): $\nu = 6.3 \times 10^{-7} \left\{ \frac{C_{OH}}{10^3} \right\}^{-0.477}$ (m^2 s^{-1}) ; for T = 413 K
Chain length of the polymer *versus* average viscosity relation (supplied by Dow Corning Ltd., 1990) Chain length $= \frac{\nu - 0.865}{0.417}$

The Sherwood number is calculated from

$$(Sh)_j = 0.00178(Re)_j^{1.37}(Sc)_j^{1.27}\left(\frac{d_i}{\delta_j}\right)^{-0.32}\left(\frac{z_j}{\delta_j}\right)^{-0.32} \qquad (3.27)$$

and equation (3.12) was then solved together with the following initial condition:

$C_{OH} = 172$ mol m^{-3} ; at $z = 0$

by a fourth order Runge-Kutta for the step interval of 6×10^{-4} m. The tolerance value for the concentration of hydroxyl groups is accepted to be 1×10^{-3} mol m^{-3}. The flow chart and algorithm of the program are introduced in Appendix G, in Figures G.1 and G.2. The one dimensional model is used to simulate the performance of the single channel reactor. Examples of simulation studies are illustrated in Table 4.2, from which it is evident that at low liquid flowrates the concentration difference between bulk and the catalyst surface is high due to mass transfer effects. In Figure 4.2, C_{OH} is plotted as a function of reactor length at a liquid flowrate of 4.5×10^{-7} m^3 s^{-1} for the one of the simulations presented in Table 4.2.

Table 4.2 Using the one dimensional model to simulate the performance of the single channel trickle reactor.

Cell type		Circular
Cell diameter		0.015 m
Length of the channel		0.5 m
Inlet hydroxyl concentration		172 mol m^{-3}
Reactor temperature		413 K
v_l = 7.1 x 10^{-7} m^{-3} s^{-1}		
Length (m)	$(C_{OH})_{bulk}$ mol m^{-3}	$(C_{OH})_{surface}$ mol m^{-3}
0.5	154	135
1.0	138	117
1.5	124	103
2.0	112	92
v_l = 4.5 x 10^{-7} m^{-3} s^{-1}		
Length (m)	$(C_{OH})_{bulk}$ mol m^{-3}	$(C_{OH})_{surface}$ mol m^{-3}
0.5	146	116
1.0	125	95
1.5	108	79
2.0	93	67

Continue of Table 4.2

v_t = 3.8 x 10^{-7} m^{-3} s^{-1}		
Length (m)	$(C_{OH})_{bulk}$ (mol m^{-3})	$(C_{OH})_{surface}$ (mol m^{-3})
0.5	143	109
1.0	120	86
1.5	102	70
2.0	86	57
v_t = 1.6 x 10^{-7} m^{-3} s^{-1}		
Length (m)	$(C_{OH})_{bulk}$ (mol m^{-3})	$(C_{OH})_{surface}$ (mol m^{-3})
0.5	124	63
1.0	94	43
1.5	73	32
2.0	58	24

4.2 COMPARING THE MODELLING RESULTS WITH THE EXPERIMENTAL RESULTS

Making use of experimental data obtained in the series of experiments classified as Run 4 and presented in Table 3.2, the validity of the model was tested. This experimental data had not been used to evaluate any of the coefficients used in the model. The results are compared in Figure 4.3, and Table 4.3 from which it is evident that a close fit has been obtained. The one dimensional model could therefore be used with a degree of confidence to predict the performance of the reactor. Since the kinetics and mass transfer coefficients have been developed for a system at a constant pressure of 0.0789 bar, and a constant purge gas flowrate of 3.33×10^{-5} m^3 s^{-1}, care should be taken with the interpretation of the results when the program is run in simulation mode.

Table 4.3 Experimental simulation results to test validity of the model

	Experimental data (Outlet concentration)		Modelling results
Liquid flowrate (m^3 s^{-1}) x 10^7	$(C_{OH})_{initial}$ (mol m^{-3})	$(C_{OH})_{exit}$ (mol m^{-3})	$(C_{OH})_{bulk}$ (mol m^{-3})
7.1	123	109	111
4.5	107	98	93
3.8	105	88	86
1.6	90	65	58

4.3 COMPARING THE PERFORMANCE OF A MONOLITH VERSUS A PACKED BED REACTOR

Making use of operational data supplied by Dow Corning Ltd., (describing the performance of a packed bed catalytic reactor) simulation studies were performed to explore the performance of a multi-channel system. The process as previously described in Chapter 1, Section 1.3, occurs in two stages (see Figure 1.1). The feasibility of replacing the second reactor with a monolith support bed was studied in this thesis. Examples of possible operating conditions are shown in Table 4.4. The two reactors are identical in size and a schematic drawing (provided by Dow Corning Ltd., 1992) of one of the reactors is illustrated in Figure 4.4. The catalyst consisting of acidic clay is coated on irregular pellets (3 mm - 13 mm diameter). The catalyst charge in the bed is 1.35 kg m^{-3}. Although, the reactor was initially designed to operate as a trickle-bed, in practice, the settling of the catalyst bed restricts liquid flow causing hold-up and the reactor operates in flooded mode. In the event that throughput needs to be increased, empty space is available at the top of the bed enabling catalyst to be added. The pressure varies from 2 bar to 2.5 bar at the top of the bed and is of the order of 0.12 bar at the bottom of the bed.

The single-channel model is used to simulate the performance of a multi-channel monolith reactor and to compare its performance with that of the packed bed. In applying the single channel model to a multi-channel system the following assumptions are made:

(a) The flow of liquid and gas is uniformly distributed amongst the cells of the monolith and the performance of each channel is identical.

(b) The liquid trickles down the wall of the channels and all of the surfaces are covered with the liquid.

(c) That both the kinetics and mass transfer correlation developed for the single channel system are valid for the range of conditions simulated.

(d) In simulating the performance of monoliths with varying cell densities and channel diameters, the square cells were arranged on a square pitch, whereas the circular cells were arranged on a triangular pitch (see Appendix A, Section A.4).

The algorithm of the computer program and an example of the input and output parameters of one of the simulation runs are presented in Appendix G, in Figures G.3 and G.4. The results of one of these simulation studies (run number DC9 in Table 4.4) for a fixed channel diameter of 0.005 m is plotted in Figure 4.5. As expected, at a fixed value of ϵ_m, as the length of the bed is increased the fractional conversion of hydroxyl is observed to increase. To achieve a similar fractional conversion of 0.73, a monolith bed length of 1.23 m is required for an ϵ_m of 0.70 and around 1.8 m for an ϵ_m of 0.60. To increase fractional conversion, the channel diameter may also be reduced. Fixing the length of the monolith bed at 1.4 m, *i.e.* the same as the packed bed, the effect of channel diameter and ϵ_m on fractional conversion are illustrated in Figure 4.6. For the values of ϵ_m simulated, better performance is obtained for the monolith bed when:

$$(d_i)_{cell} \leq 0.006 \text{ m} \quad \text{for} \quad \epsilon_m = 0.7$$

Table 4.4 An example of plant data for a dimethylsiloxane process (based on information supplied by Dow Corning Ltd., 1992)

Measurement reference	Liquid flowrate $m^3 s^{-1} \times 10^4$	T_{in} (K)	$(C_{OH})_{in}$ (ppm)	(X_{OH})
DC1	5.20	408	81	0.84
DC2	6.83	408	170	0.72
DC3	8.58	388	409	0.56
DC4	6.83	388	409	0.56
DC5	5.07	408	275	0.61
DC6	6.83	413	337	0.59
DC7	5.07	421	192	0.70
DC8	8.58	417	243	0.68
DC9	***6.83***	***408***	***178***	***0.73***
DC10	8.58	408	411	0.60
DC11	5.07	408	202	0.53
DC12	8.58	423	159	0.75
DC13	5.07	428	30	0.90
DC14	6.83	423	69	0.89
DC15	6.83	435	41	0.80

4.4 CONCLUSIONS

(a) For the range of conditions tested the one dimensional model gives a good agreement with experimental data. Under reacting conditions since the mass transfer coefficients were enhanced, the correlation developed is only valid for the reacting system studied. Care should therefore be taken with the interpretation of results when the program is run in simulation mode *e.g.* when exploring the effects of channel diameter and bed length, since the influence of these parameters was not studied in the development of the correlation.

(b) For a fixed bed length of 1.4 m, the results of the simulation studies show that the monolith support system with the K_3PO_4 catalyst can achieve higher conversion than a commercial packed bed reactor.

CHAPTER 5

CONCLUSIONS

5.1 CONCLUSIONS

(a) A new method of coating the monolith pieces with a K_3PO_4 catalyst was developed. The catalyst dispersed in an alcohol slurry was dried on the support in an inert atmosphere.

(b) The results of the kinetic experiments in the spinning basket, semi-batch reactor demonstrate that in simplified form the condensation poymerisation reaction is overall first order with respect to C_{OH}, and may be represented by

$$r_{OH} = A\exp(-E/RT)C_{OH}$$

for C_{OH} = 20 to 169 mol m^{-3}

(c) From experiments in the spinning basket semi-batch reactor, calculated values of the reaction rate constant based on unit external surface area for the pellets and the single channel ring elements are similar. However, when reaction rates are calculated and compared based on unit volume for a packed bed reactor, then at high densities (> 20 cell cm^{-2}) the monolith support should achieve higher reaction rates per unit bed volume. The monolith support system shows potential as a catalyst support to be used in a three-phase reactor.

(d) In the chemical kinetically controlled region the results of the kinetic experiments in the single channel flow reactor (for a fixed pressure and purge gas flowrate) showed that the condensation polymerisation reaction is of first order with respect to hydroxyl groups and the reaction rate based on the external catalytic surface area may be represented by

$$r_{OH} = 4.2x10^{-4}\exp\left(-\frac{1.6x10^{4}}{RT}\right)C_{OH}$$

for

C_{OH} = 153 mol m^{-3}

T = 373 to 413 K, and

P = 0.0798 bar

(e) To evaluate mass transfer coefficients in the single channel monolith flow reactor, at a fixed pressure and purge gas flowrate, a semi-empirical correlation of the following form was developed:

$$Sh = 0.00178Re^{1.37}Sc^{1.27}\left\{\frac{d_i L}{\delta^2}\right\}^{-0.32}$$

for the ranges of:

$(C_{OH})_{feed}$ =139 - 172 $molm^3$

υ_l =1.7 x 10^{-8} - 7.1 x 10^{-7} m^3s^{-1}

Re =10^{-1} to $2x10^{-3}$

Sc =$5.4x10^4$ to $9.5x10^5$

d =0.015 m

L =0.5 m

(f) At a fixed pressure and purge gas flowrate, the co-current method of operation for the single channel flow reactor provides a higher reaction rate than the countercurrent method of operation.

(g) In both of the spinning basket and the single channel flow reactors the dramatic effect of the purge gas flowrate on the reaction rate confirms that the polymerisation reaction is very complicated. Although the reaction rate expression was shown to be well represented by a first order irreverible rate expression in terms of hydroxyl groups, the removal of water/volatile components (by higher purge gas flowrate) from the reaction mixtures was also shown to influence the overall rate.

(h) For the range of conditions tested the one dimensional model gives good agreement with experimental data. Under reacting conditions since the mass transfer coefficients were enhanced, the correlation developed is only valid for the reacting system studied. Care should therefore be taken with the interpretation of results when the program is run in simulation mode *e.g.* when exploring the effects of channel diameter and bed length, since the influence of these parameters was not studied in the development of the correalation.

(i) For a fixed bed length of 1.4 m, the results of the simulation stuides show that the monolith support system with K_3PO_4 catalyst can achieve higher conversion than a commercial packed bed reactor.

5.2 RECOMMENDATIONS FOR A FURTHER WORK

The study revealed that the following aspects would be worthy of further work as an extension of this study.

(a) The performance of experiments in a multi-channel monolith flow reactor.

(b) An investigation of how mass transfer coefficients for the single channel flow reactor are affected by channel length and diameter.

(c) A comprehensive study of catalyst to achieve a uniform coating.

(d) Experiments with different geometry of monolith structures in order to explore the effects of channel size and shape.

(e) The inclusion of energy balance in the one dimensional model.

(f) Performance of reaction experiments where the pressure is maintained constant and purge gas flowrate is varied.

(g) Determination of reaction kinetics for a reversible process.

REFERENCES

Barry A.J., Beck H.N. (1962). Silicone polymers. In: Inorganic polymers (F.G.H Stone and W.A.G. Graham, ed.) p. 191. London: Academic press

Bergles A.E., Collier J.G., Hewitt G.F., Mayinger F. (1981). Two phase flow and heat transfer in the power and process industries, pp. 6-23, USA: Hemisphere Puplishing Corporation

Billmeyer F.W.Jr.(1984).Textbook of polymer science, p.26,USA:John Wiley & Sons

Carothers, W.H. (1929).Polymerisation and ring formation. I. Introduction to the general theory of condensation poymers. *J. Am. Chem. Soc.*, **51**, 2548-2559

Charpentier J.C. (1976). Recent progress in two phase gas-liquid mass transfer in packed beds, *Chem. Eng. Journal*, **11**, 161-181

Charpentier J.C., Favier M. (1975) Some liquid hold-up experimental data in trickle bed reactor for foaming and non-foaming hydrocarbons, *AIChE Journal*, **21**(6), 1213-1230

Coulson J.M., Richardson J.F. (1978). Chemical engineering, Unit operations, Vol. 2, pp. 126-129, G.B: Pergamon Press.

Cussler E.L. (1984). Diffusion mass transfer in fluid systems, pp 237-240, USA: Cambridge University Press

Danckwerts, P. V. (1970). Gas-liquid reactions, p 73, USA: McGraw-Hill

DeLuca J.P., Campbell L. E. (1977). Advanced materials in catalyst. In: Monolithic catalyst supports, ed: Burton J.J. and Garten R.L., P. 317. USA: Academic Press.

DeVos R., Hatzaintoinou V., Schoon N.H. (1982). The cross flow catalytic reactor. An alternative for liquid phase hydrogenations, *Chem. Eng. Sci.* **37**(12), 1719-1925

Elms R. (1989). Method for preparing siloxane fluids with low silonal contents, US Patent 4831174 Assigned to Dow Corning ltd.

Flory, P.J. (1939). Kinetics of polyesterification, *J. Am. Chem. Soc.*, **61**, 3334-3344

Flory, P.J. (1953). Principle of polymer chemistry, pp 102-103, 12th edn., New York: Cornell University Press

Fogler H.S. (1983) Elements of Chemical Reaction Engineering, pp. 206-208, New Jersey: Printes-Hall Press

Fordam, S. (1960). Silicones. pp.5,107,145,148. London: George Newnes Ltd

Gianetto A., Specchia V. (1992). Trickle-bed reactors: State of art and perspectives, *Chem. Eng. Sci.*, **47**(13/14), 3197-3213

Goto S., Smith J. M. (1975). Trickle bed reactor performance, *AIChE J*, **21**(4), 706

Hatziantonio, V., Andersson B. (1984). The segmented two-phase flow monolithic catalyst reactor, *Ind. Eng. Chem. Fund.*, **23**, 82-88

Hatziantonio, V., Andersson B. (1982). Solid liquid mass transfer in segmented gas-liquid flow through a capillary, *Ind. Eng. Chem. Fundam.*, **21**, 451-456

Hatziantonio, V., Andersson B., Schoon N.H. (1986). Mass transfer and selectivity in liquid phase hydrogenation of nitro compouds in a monolith catalyst reactor with segmented gas-liquid flow, *Ind. Eng. Chem. Process Des. Dev.*, **25**, 964-970

Herskowitz M., Smith J.M. (1983). Trickle-bed reactors: A review, *AIChE Journal*, **29**, 1-18

Hewitt G.F., Hall-Taylor N.S. (1970). Annular two phase flow, pp 4-11, Edinburgh: Neil and Co. Ltd

Hoffman, H.P. (1978). Multiphase catalytic packed bed reactions, *Catal. Rev. Sci. Eng.*, **17**(1), 71-75

Hurd, C.B.(1946). Studies on siloxanes 1., *J. Chem. Soc.*, **68**, 364-368

Irandoust S., Andersson B. (1988). Monolithic catalyst, *Cat. Rev. Sci. Eng.*, **30**, 3, 341-392

Irandoust S., Andersson B., (1988)b. Mass transfer and liquid phase reactions in a segmented two-phase flow monolithic catalyst reactor, *Chem. Eng. Sci.*, **43**(8), 1983-1988

Irandoust S., Andersson B., Bengtsson E., Siverstrom M. (1989). Scaling up of a monolithic catalyst reactor with two-phase flow, *Ind. Eng. Chem. Res.*, **28**, 1489-1493

Jordan, G.D. (1968). Chemical process development, ed: Herbert M.S., McKetta J.J. vol. 1, ch. 4, USA: John Wiley and Sons

Kesselring J.P. (1986). Catalyst combustion. In: Advanced combustion methods ed: F. J. Weingberg, pp.248,251, London: Academic Press

Kirk R.E., Othmer D.F. (1982). Encyclopedia of chemical technology. 3rd edn. Vol. 20, p.922, New York: Interscience Press

Larkins R.P., White R.R., Jeffrey D.W. (1961). Two-phase cocurrent flow in packed beds, *AIChE J.*, **7**(2), 231-239

Lemcoff N.O., Cukierman A.L., Martinez O.M. (1988). Evaluation and application to the modelling of trickle bed reactor, *Cat. Rev.*, 393-456

Levenspiel, O. (1962). Chemical reaction engineering. ch.3, USA: John Wiley and Sons

Mazzarino I., Baldi G. (1988). Liquid phase hydrogenation on a monolithic catalyst, Proc. 2nd Int Chem Reac Eng Conf, Recent Trends in Chemical Reaction Engineering, ed: Kulkarni, Wiley Eastern India, Vol 1-2, 181-189

Meals R.N., Lewis F.M. (1959). Silicones. In: Reinhold plastic application series, ed: H.R. Simonds, pp. 92,143, USA: Chapman and Hall Ltd

Ng K.M. (1986). A model for flow regime transitions in cocurrent down flow trickle bed reactors, *AIChE Journal*, **32**(1) 115-122

Odian G. (1981). Principles of polymerisation. ch. 2, USA: John Wiley and Sons

O'Neal H.E., Ring M.A. (1966). Bond addivity properties of silicon compounds, *Inorganic chemistry*, **5**(3), 435-439

Pearce, C.A. (1972). Silicon chemistry and applications, pp. 6,50, London: Billing and Sons Ltd

Ramachandran P.A., Chaudhari R.V. (1983). Three-phase catalytic reactors, pp. 200-207, Great Britain: Gordon and Breach Science Publishers

Rase, H.I. (1977). Chemical Reactor Design for Process Plants, Principles and Techniques, pp. 195-198, USA: Wiley-Interscience Publication

Satterfield C.N. (1975). Trickle bed reactors, *AIChE Journal*, **21**, 209-228

Satterfield C.N., Ozel F. (1977). Some charecteristic of two-phase flow in monolithic catalyst structures, *Ind. Eng. Chem. Fundam.*, **16**(1), 61-67

Sato Y., Hirose T., Takahashi F., Toda M., Hashiguchi Y. (1973). Flow pattern and pulsation properties of cocurrent gas-liquid downflow in packed beds, *J. Chem. Eng. of Japan*, **6**(4), 315-319

Scardi S., Gerhard H., Hofmann H. (1979). Flow regime transition in trickle bed reactors, *Chem. Eng. J.*, **18**, 173-182

Scheibel, E.G. (1954). Liquid diffusivity, *Ind. Eng. Chem.*, **46**, 2007

Scheiver M.H., Pape P.G. (1982). Uses of silicones in process plants, *Chem. Eng.*, **89**(3), 123-128

Shah, Y.T. (1979). Gas-liquid-solid reactor design, pp. 149-180, USA: McGraw-Hill Inc

Skelland, A. H. P., (1974). Diffusional Mass Transfer, pp 131-139, USA: John Wiley and Sons

Smith J.M. (1981). Chemical engineering kinetics, pp. 298-301, Singapore: Fong and Sons Printers Ltd

Specchia V., Baldi G. (1977). Pressure drop and liquid hold-up for two phase concurrent flow in packed beds, *Chem. Eng. Sci.*, **32**, 515-523

Stark F.O., Flander J.R., Wright A.P. (1982). Silicones. In: Comprehensive organometallic chemistry, ed: Sir Geoffrey Wilwonson, vol.2, p.306, USA: Pergamon Press

Stevens, M.P. (1975). Polymer chemistry, pp. 13-17, Canada: Addision-Wesley Publishing Company

Tallmadge J.A., Gutfinger C. (1967). Entrainment of liquid films drainage withdraws and removal, *Ind. Eng. Chem.*, **59**(11), 19-34

Tosun, G. (1984). A study of cocurrent of non-foaming gas-liquid sytems in a packed bed, *Ind. Eng. Proc. Des. Dev.*, **23**, 29-33

Turbin J.L, Huntington R.L. (1967). Prediction of pressure drop for two-phase, two-component concurrent flow in packed beds, *AIChE Journal*, **13**(6), 1196-1202

Weekman V.W. Jr., Myers J.E. (1964). Fluid-flow charecteristics of cocurrent gas-liquid flow in packed beds, *AIChE Journal*, **10**(6), 951-957

Weekman, V.W. (1974). Laboratory reactors and their limitations, *AIChE Journal*, **20**, 833-840

APPENDICES

APPENDIX A Geometric properties of the pellets and monoliths: Calculation procedure adopted

A.1) Calculation of the bed void fraction in packed beds, and in monolith supports.

A.1a) In the pellet form of catalyst

Using acetone to fill the voids in the bed the void fraction of a bed packed with the pellet form of catalyst was estimated to be $\epsilon_p = 0.5$.

A.1b) In single channel ring elements

The bed void fraction was calculated from the "void volume / total volume" of the single channel which is

$$\epsilon_m = \frac{\pi d_i^2 L/4}{\pi (d_i + x_w)^2 L/4} = \frac{d_i^2}{(d_i + x_w)^2}$$

where x_w is the wall thickness (m), *e.g.* when d_i=0.015 m and x_w=5 x 10^{-3} m, then the bed void fraction of the single channel is found to be 0.56.

A.1c) In a square-cell, multi-channel monolith

Based on a method proposed by DeLuca and Campbell, 1977,

$$\epsilon_m = \frac{d_i^2}{(d_i + x_w)^2}$$

e.g. when $d_i = 0.002$ m and $x_w = 5 \times 10^{-4}$ m, then the bed void fraction of a square-cell monolith bed is 0.64.

A.1d) In a circular-cell, multi-channel monolith

The bed void fraction of a circular cell monolith was calculated from the geometry of a triangle pitch as follows (see Figure A.1):

Void volume of the cell on the triangle,

$$\frac{3}{6}\left(\frac{\pi d_i^2 L}{4}\right)$$

Figure A.1

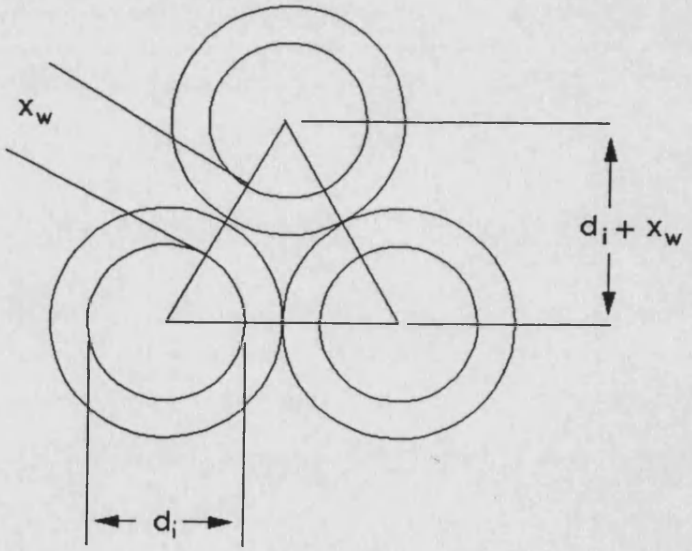

Total volume of the triangle,

$$\frac{\sqrt{3}(d_i + x_w)^2 L}{4}$$

hence bed void fraction is

$$\epsilon_m = \frac{\pi}{2\sqrt{3}} \frac{d_i^2}{(d_i + x_w)^2}$$

A.2) Calculation of the geometric surface area per unit bed volume, S_c

A.2a) For the pellet form of catalyst

The geometric external surface area per unit bed volume for the pellet form of catalyst was estimated using the following equation (Coulson and Richardson, 1978):

$$(S_c)_{pel} = \frac{6(1-\epsilon)}{\Phi d_p}$$

where ϕ is the sphericity which is determined approximately for the irregular pellet form of catalyst as follows:

From a sample of pellets, spherical shaped particles were selected and their total surface area per unit bed volume was measured by "Surface Area Analyser" to be 11.2 m_t^2 g^{-1}. This value was divided by the surface area of non-spherical particles which was determined using the same analyser to be 14 m_t^2 g^{-1}. The sphericity was determined to be 0.8. The geometric surface area per unit bed volume was then calculated as illustrated in the following example:

e.g. when $\epsilon_m = 0.5$ and $\phi = 0.8$ then $(S_c)_{pel}$ was calculated to be 1000 m_e^2 m_{bed}^{-3}

A.2b) For single-channel ring elements

For the single channel monolith $(S_c)_{sin-chan}$ is calculated by dividing the inside surface area of the channel that is coated with catalyst by the inside free volume of the channel, which gives

$$(S_c)_{sin-chan} = \frac{\pi d_i L}{\pi d_i^2 L/4}$$

e.g. when d_i =0.015, then $(S_c)_{sin-chan}$ was calculated to be 266.66 $m_e^2\ m_{bed}^{-3}$.

A.2c) For a circular-cell, multi-channel monolith

For a circular monolith the geometric surface area per unit bed volume was calculated from the geometry of a triangle pitch (see Figure A.1) considering only the inside surface area of the circular channels on the triangle pitch as "inside surface area of the channels on the triangle pitch / total volume of the triangle" . This gives

$$(S_c)_{cir-mon} = \frac{\frac{3}{6}(\pi d_i L)}{(\sqrt{3}(d_i + x_w)^2 L)/4} = \frac{2\pi d_i}{\sqrt{3}(d_i + x_w)^2}$$

e.g. when d_i = 0.005 m, x_w = 0.001 m, then $(S_c)_{cir-mon}$ was calculated to be 136 $m_e^2\ m_{bed}^{-3}$. In this calculation, it is assumed that the liquid is only free to flow inside the circular channels.

A.2d) For a square-cell, multi-channel monolith

Based on the method proposed by DeLuca and Campbell, 1977.

$$(S_c)_{sq-mon} = 4\frac{(\sqrt{\epsilon_m} - \epsilon_m)}{x_w}$$

e.g. when ϵ_m=0.64 and x_w=0.0005 m, then $(S_c)_{sq-mon}$ was calculated to be 1280 $m_e^2\ m_{bed}^3$.

A.3) Calculation of the external catalytic surface area, S_e

A.3a) For the pellet form of the catalyst

The external surface area of the pellet form of catalyst was calculated as follows:

$$(S_e)_p = \frac{(S_e)'_p}{\phi}$$

where $(S_e)'_p$ is the total external geometric surface area of the spherical pellets.

By sieve tray analysis the average diameter of the particles was estimated to be 0.003 m and the external catalytic surface area of each pellet was calculated as if it were spherical. Hence,

$$(S_e)_{pellet} = \pi 0.003^2 = 2.82 x\, 10^{-5} \quad m^2$$

where $(S_e)_{pellet}$ is the average surface area of one pellet. The total external surface area of the pellets is calculated by

$$(S_e)'_p = (N_p)(S_e)_{pellet}$$

where (N_p) is the number of pellets in the bed. In the experiments 2 and 3.58 g amounts of pellets were used. The average number of pellets (N_p) was therefore estimated to be 88.84 for 2 g of pellets and 151.69 for 3.58 g of pellets. The total external surface areas were therefore

$$(S_e)'_{pel} = (2.8x10^{-5})(88.84) = 2.5x10^{-3} \quad m^2$$

for 2 g of catalyst, and

$$(Se)'_{pel} = (2.8x10^{-5})(159.0) = 4.5x10^{-3} \quad m^2$$

for 3.58 g of catalyst.

The sphericity of the pellets was estimated to be 0.8, so the actual total external catalytic surface area of the pellets was estimated to

$$(Se)_{pel} = \frac{2.5x10^{-3}}{0.8} = 3.1x10^{-3} \quad m^2$$

for 2 g of catalyst

$$(Se)_{pel} = \frac{4.5x10^{-3}}{0.8} = 5.6x10^{-3} \quad m^2$$

for 3.58 g of catalyst

A.3b) For the square-cell, multi-channel monolith

The total external catalytic surface areas were determined for three different pieces of monolith (See Figure A.2).

Monolith piece 1,

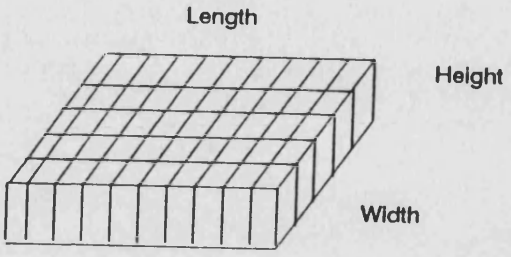

Figure A.2

Length = 51.0 mm

Width = 9.0 mm

Height = 11.5 mm

Cell dimension = 2 x 2 mm^2

Number of cells = 57

$(S_c)_1$ = (4 x (11.5 x 2) x 57) + 2 x (11.5 x 51) + 2 x (11.5 x 9) = 6624 mm^2

Monolith piece 2,

Length = 40.0 mm

Width = 9.0 mm

Height = 12.0 mm

Cell dimension = 2 x 2 mm^2

Number of cells = 45

$(S_c)_2$ = (4 x (12.0 x 2) x 45) + 2 x (12.0 x 40.0) + 2 x (12.0 x 9) = 5496 mm^2

Monolith piece 3,

Length = 49.0 mm

Width = 9.0 mm

Height = 12.5 mm

Cell dimension = 2 x 2 mm^2

Number of cells = 57

$(S_e)_3$ = (4 x (12.5 x 2) x 57) + 2 x (12.5 x 49) + 2 x (12.5 x 9) = 7150 mm^2

The total external surface area for the three pieces of monolith that were housed in the basket was therefore

$(S_e)_{sq\text{-}mon} = (S_e)_1 + (S_e)_2 + (S_e)_3$

$(S_e)_{sq\text{-}mon}$ = 19270 mm^2 = 0.019 m^2

A.3c) For the single channel, ring elements

For the form of ceramic ring illustrated in Figure A.3,

Outside diameter = 20 mm

Inside diameter = 15 mm

Wall thickness = 5 mm

Length = 8 mm

Figure A.3

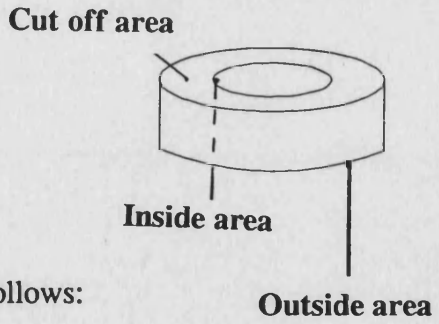

The geometric surface areas were calculated as follows:

Inside area

$(S_e)_1 = \pi d_i L$ = 376.9 mm^2

Outside area

$(S_e)_2 = \pi d_i L = 502.6 \text{ mm}^2$

Cut off area

$(S_e)_3 = 2\pi d_i L = 235.6 \text{ mm}^2$

The total external catalytic surface area of a ring (single channel, circular monolith)

$(S_e)_{sin-chan} = 1115.3 \text{ mm}^2$

For 3 rings in the basket, then

$(S_e)_{sin-chan} = 3345 \text{ mm}^2 = 3.34 \times 10^{-3} \text{ m}^2$

for 4 rings in the basket

$(S_e)_{sin-chan} = 4460 \text{ mm}^2 = 4.46 \times 10^{-3} \text{ m}^2$

A.4) Calculation of the number of cells per unit area, N_c

A.4a) For a circular-cell monolith

If the cells are positioned on a triangular pitch as illustrated in Figure A.1, then the number of cells per unit area was calculated from

$$N_c = \frac{1}{\frac{\sqrt{3}}{4}(d_i + x_w)^2}$$

e.g. when d_i=0.015 m and x_w=0.005 m then the number of cells was calculated to be

5773.5 cell m^{-2}.

A.4b) For a square-cell monolith

Based on the method proposed by DeLuca and Campbell (1977).

$$N_c = \frac{1}{(d_i + x_w)^2}$$

e.g. when d_i=0.002 m and x_w=0.0005 m then the number of cells was calculated to be 160000 cell m^{-2}.

A.5) Calculation of the reaction rate per unit bed volume, R_{OH}

The reaction rate per unit bed volume in terms of hydroxyl groups, R_{OH}, is calculated at a point in the bed when X_{OH}=0.3 . Since

$$(R_{OH})|_{x=0.3} = (r_{OH})_e S_c$$

which may be written as:

$$R_{OH}|_{X=0.3} = k_r (C_{OH})_o (1 - X_{OH}) S_c$$

For pellets, when k_r= 1.47 x 10^{-4} m^3 m^{-2} s^{-1}, then

$$(R_{OH})_{pel} = 1.47 \times 10^{-4} (C_{OH})_o (1 - X_{OH})(S_c)_{pel}$$

For a multi-channel, circular cell monolith, when $k_r = 1.13 \times 10^{-4}$ m^3 m^{-2} s^{-1}, then

$$(R_{OH})_{cir-mon} = 1.13 \times 10^{-4} (C_{OH})_o (1 - X_{OH})(S_c)_{cir-mon}$$

For a multi-channel square cell monolith, when $k_r = 1.13 \times 10^{-4}$ m^3 m^{-2} s^{-1}, then

$$(R_{OH})_{sq-mon} = 1.13 \times 10^{-4} (C_{OH})_o (1 - X_{OH})(Sc)_{sq-mon}$$

The results of these calculation are given in Tables A.1, A.2 and A.3 for the pellet, circular and square cell multi-channel monolith supports respectively.

Table (A.1) Predicted reaction rates per unit bed volume for a packed bed (ϵ_m= 0.5) in a flow reactor at a point in the bed when X_{OH} = 0.30.

Diameter of the pellets (mm)	$(S_c)_{pel}$ ($m_e^2\ m_{bed}^{-3}$)	R_{OH} mol $m_{bed}^{-3}\ s^{-1}$
1.0	3750	66.5
1.5	2500	44.4
2.0	1875	33.3
2.5	1500	26.6
3.0	1250	22.2
3.5	1071	19.0
4.0	937	16.6
4.5	832	14.8
5.0	750	13.3
5.5	682	12.1
6.0	625	11.1
6.5	577	10.2
7.0	500	9.5
7.5	469	8.8
8.0	469	8.3

Table (A.2) Predicted reaction rates for a circular cell monolith support (ϵ_m=0.5) in a flow reactor at a point when X_{OH}=0.30.

N_c cell cm^{-2}	d_i cm	$(S_c)_{mon}$ $m_e^2 m_{bed}^{-3}$	R_{OH} mol m^{-3}_{bed} s^{-1}
10	0.36	560	7.6
15	0.29	686	9.4
20	0.25	793	10.8
25	0.23	886	12.1
30	0.21	971	13.2
35	0.19	1048	14.3
40	0.18	1121	15.3
45	0.17	1189	16.2
50	0.16	1253	17.1
55	0.15	1314	17.9
60	0.14	1373	18.7
65	0.14	1429	19.5
70	0.13	1483	20.2
75	0.13	1535	20.9
80	0.12	1585	21.6

Table (A.3) Predicted reaction rates for a square cell monolith support (ϵ_m=0.5) in a flow reactor at a point when X_{OH}=0.30.

N_c cell cm^{-2}	d_i cm	$(S_c)_{mon}$ $m_e^2 m_{bed}^{-3}$	R_{OH} mol m^{-3}_{bed} s^{-1}
10	0.22	894	12.2
15	0.18	1095	14.9
20	0.16	1263	17.2
25	0.14	1414	19.3
30	0.13	1549	21.1
35	0.12	1673	22.8
40	0.11	1788	24.4
45	0.10	1897	25.8
50	0.10	2000	27.3
55	0.95	2097	28.6
60	0.09	2190	29.8
65	0.09	2280	31.1
70	0.08	2366	32.3
75	0.08	2449	33.4
80	0.07	2529	34.5

APPENDIX B Analytical method and error analysis

B.1) Determining the total concentration of hydroxyl (-OH) groups

This was determined (using a procedure recommended by Dow Corning Ltd) by titrating with lithium aluminium dibutylamide (0.16 M in dimethoxyethane) with 4-phenylazodiphenylamine (operating over the range pH 1.2 - 2.5) as the indicator. The indicator was made up with toluene (1 % w/w) and both the indicator and titrant were kept in a dark bottle.

B.1a) Procedure

(1) Place 20 ml of Tetrahydrofuran into a septum bottle with a vent. (The septum bottle has an inverted septum stopper on the top).

(2) Add sufficient indicator to get yellow colour.

(3) Add a few drops of titrant to get red colour.

(4) Add known weight of sample to the bottle (should make the colour turn yellow).

(5) Titrate until colour returns to the same starting red colouration, and make a note of the volume used.

B.1b) Calculation method to determine the concentration of hydroxyl groups

The following equation (based on a procedure used by Dow Corning Ltd) was used to determine the concentration of hydroxyl groups:

$$C_{OH} = \frac{(V_{titr.})F}{w_s}$$

where:

V_{tit} is the volume of the titrant

F is the Factor (17000)

w_s is the weight of the sample

The calculation gives ppm of total hydroxyl groups (i.e. it includes water).

The factor, F, was obtained by titration of known amount of 2-naphthol and using the following equation:

$$F = \frac{11.8(w_{nap})}{(V_{tit})1.7}$$

where w_{nap} is the weight of the 2-naphthol (approximately 0.1 g).

B.2) Error analysis for the measurement of hydroxyl concentration

For the data in Table B.2

Sum of samples = 38986.19

Number of samples = 15

Average of samples = 2599.07

Sum of deviation = 1854.72

Average of deviation = 123.648

Relative deviation = (123.648 / 2599.07) x 100 = 4.75 %

Table B.2 Measurement of concentration values and their deviations from the average value

C_{OH} (ppm)	Deviation
2471.38	127.69
2650.87	51.79
2661.09	62.01
2837.72	238.64
2375.27	223.8
2621.96	22.8
2398.14	200.93
2684.2	85.12
2599.66	0.58
2500.80	98.27
2430.40	168.67
2839.64	240.56
2667.36	68.28
2707.50	108.42
2540.20	58.89

B.3) Error Analysis for the viscosity measurement

Viscosities were measured with the calibrated *Technico* Viscometers at 25°C in a water bath. For the data in Table B.3

Sum of samples = 2199.06

Number of samples = 15

Average of samples = 146.604

Sum of deviation = 3.367

Average of deviation = 0.224

Relative Deviation = (0.224 / 146.604) x 100 = 0.153 %

B.4) Relationship between viscosity and concentration of hydroxyl groups

The concentration of hydroxyl groups is plotted versus viscosity in Figure B.1. Applying linear regression analysis the following equation was developed:

$$C_{OH} = 918043.45\nu^{-1.1515}$$

where:

standart error of estimating concentration = 0.0236

standart error of estimating viscosity = 0.024

number of observations = 21

degrees of freedom = 19

regression coefficient = 0.99

Table B.3 Measured values of viscosity values and their deviations from the average value

Viscosity, cst	Deviation
146.60	0.004
146.85	0.246
146.62	0.016
146.09	0.514
146.60	0.004
146.21	0.394
146.60	0.004
147.40	0.795
145.90	0.704
146.60	0.004
146.58	0.024
146.60	0.004
146.96	0.356
146.79	0.186
146.66	0.056

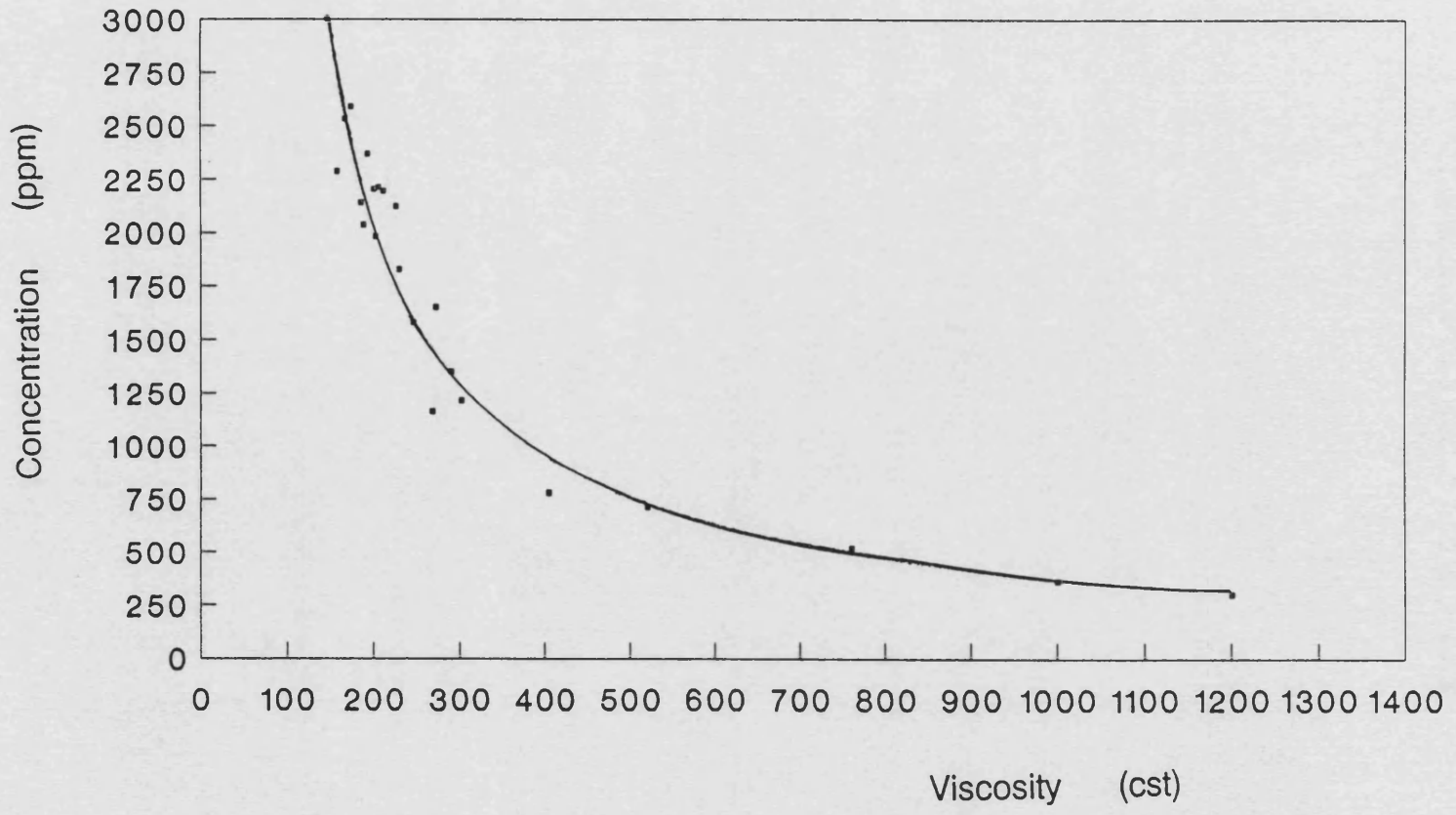

Figure B.1 Hydroxyl groups concentration versus viscosity relationship at 298 K.
(▪ represents measured data ; continuous line represents regression curve).

APPENDIX C Determining the order of the reaction for the pellet form of catalyst: Details on the example calculation presented in Section 2.5.1

C.1) Experimental measurements and calculated parameters

Table C.1 and C.2 gives the measurement and calculated data to determine the order of reaction for the pellet form of catalyst

Table C.1 Experimental measurements

Operating and initial conditions	
Liquid volume	1 litre
Catalyst mass	19 g
Initial OH concentration	169 mol m^{-3}
Volume of volatilise material	120 m*l*
Volume of sample taken at 10 min. intervals	17 m*l*
Vacuum pulled	61 cm Hg
Rotameter readings for gas flowrate at the vacuum condition	6 m*l* min^{-1}
Geometric external surface area of 19 g of pellets, S_c	0.03 m^2

Table C.2 Calculated parameters that changed as a function of time during the reaction

Time (min)	ν (cst)	C_{OH} (mol m^{-3})	V_l (m^3)x10^3	N_{OH} (mol)	X_{OH}	$V/S_e \ln(1-X_{OH})$ (m_l^3 m_e^{-2})
10	200	116	0.880	0.102	0.396	0.015
20	314	71	0.863	0.062	0.635	0.030
30	520	41	0.846	0.035	0.794	0.044
40	824	27	0.829	0.022	0.867	0.055
50	1000	20	0.812	0.016	0.90	0.063

*V_l is the liquid volume remaining in the reactor.

C.2) Applying the method of equal-area graphical differentiation

From the plot of N_{OH} / S_e as a function of time (presented in Figure 2.11, Chapter 2) the slope of the curve $\frac{d(N_{OH}/S_e)}{dt}$ was determined at a number of intervals. In Table C.3 the calculation steps are tabulated for the method of equal-area differentiation. This technique was used to analyse the data in Figure C.1. The order of reaction was then calculated from the plot of $[\ln \frac{d(N_{OH}/S_e)}{dt}]$ *versus* $[\ln C_{OH}]$ which is presented in Figure 2.12 in Chapter 2.

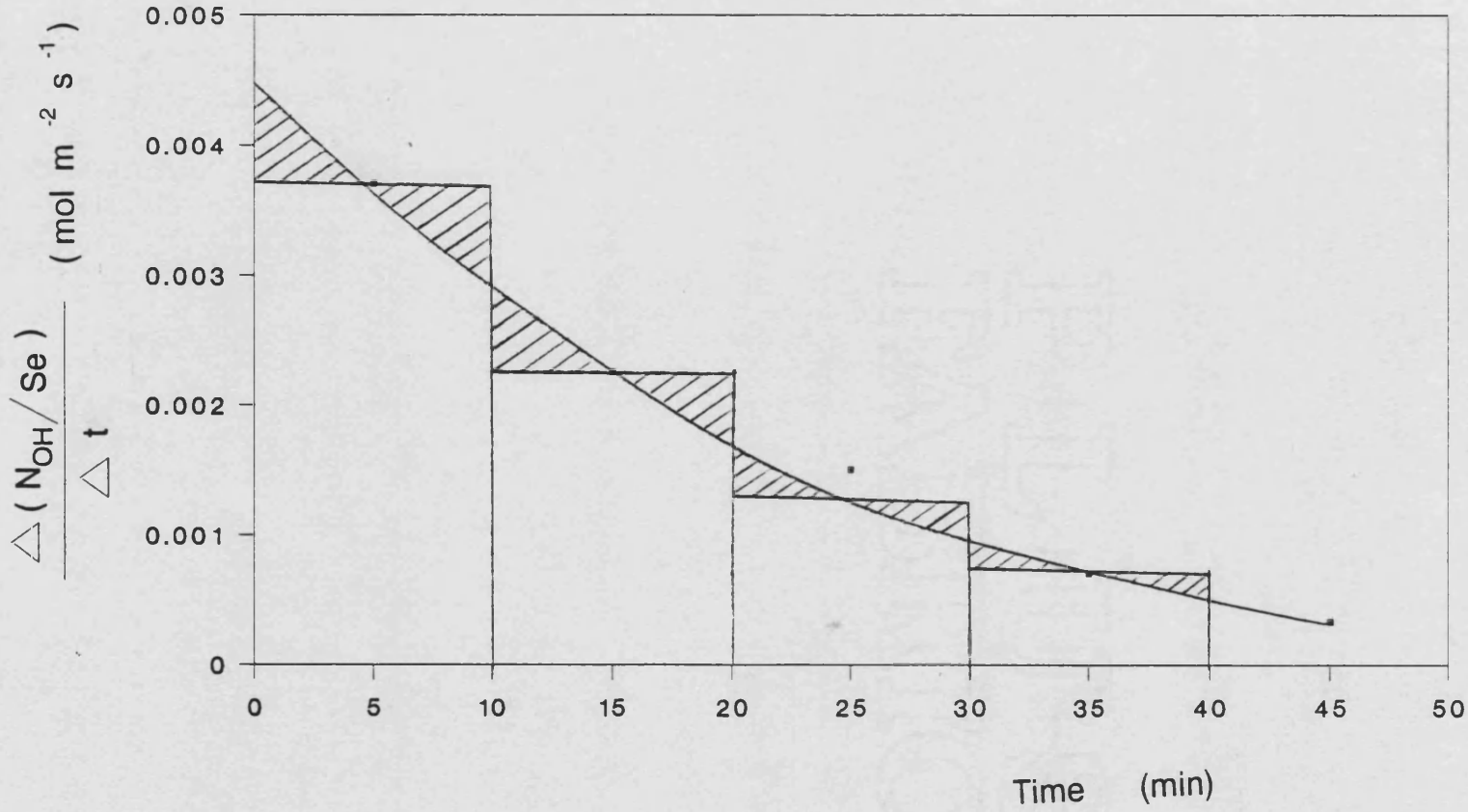

Figure C.1 Applying the method of equal-area graphical differentiation.

Table C.3 Applying the method of equal-area graphical differentiation

Time (min)	N_{OH}/S_e (mol m^{-2})	$\frac{\Delta(N_{OH}/S_e)}{\Delta t}$ (mol m^{-2} s^{-1})	$\frac{d(N_{OH}/S_e)}{dt}$*
0	5.63		4.50×10^{-3}
		3.71×10^{-4}	
10	3.40		2.96×10^{-3}
		2.25×10^{-3}	
20	2.05		1.83×10^{-3}
		1.50×10^{-3}	
30	1.15		5.68×10^{-4}
		7.05×10^{-4}	
40	0.73		2.35×10^{-4}
		3.30×10^{-4}	
50	0.53		

* values calculated from Figure (C.1)

APPENDIX D Determining the reaction rate constant in the spinning basket, semi-batch reactor by the integral method of analysis : Details on the example calculation presented in Section 2.5.1.2.

Experimental measurements and calculated parameters are given in Table D.1. The results of a sample calculation for one of these runs is tabulated in Table D.2.

D.1) Experimental measurements and calculated parameters

	Measurements for the pellet form of catalyst						
	Viscosity (cst)						
Sample taken	Run 1	Run 2	Run 3	Run 4	Run 5	Run 6	Run 7
1	168	163	169	174	180	189	199
2	177	187	190	195	199	207	224
3	186	192	198	220	230	268	291
4	188	199	232	278	295	344	544
5	191	204	285	336	360	750	896
	Measurements for the multi-channel monolith						
	Viscosity (cst)						
Sample taken	Run 8	Run 9	Run 10	Run 11	Run 12	Run 13	Run 14
1	178	176	180	180	195	189	198
2	199	203	206	207	204	215	223
3	212	217	220	219	220	272	325
4	228	250	267	287	247	423	626
5	245	279	320	367	278	712	760
	Measurements for the single-channel monolith						
	Viscosity (cst)						
Sample taken	Run 15	Run 16	Run 17	Run 18	Run 19	Run 20	Run 21
1	161	164	173	189	194	190	190
2	167	182	196	206	207	215	218
3	180	193	210	231	243	275	284
4	192	227	278	312	357	453	515
5	196	260	315	537	678	720	752

Table D.2 Measured and calculated parameters for experiments Number 1.

Time (min)	ν (cst)	C_{OH} (ppm)	C_{OH} (mol m^{-3})	V_l (m^3)x 10^3	N_{OH}	X_{OH}	$\ln(1-X_{OH})$	k_r ($m^3{}_l m^2{}_e s^{-1}$) x10^5
10	168	2500	143	0.910	129	0.23	0.264	12.7
20	177	2385	136	0.893	121	0.28	0.330	7.82
30	186	2250	128	0.870	111	0.34	0.417	6.42
40	188	2210	126	0.845	106	0.37	0.462	5.18
50	191	2177	124	0.820	101	0.39	0.507	4.41

From Table D.2 the value of reaction rate constant, k_r, at any time, t, was evaluated from

$$k_r = \frac{\ln(1 - X_{OH})V_l}{t \quad S_e}$$

For the example calculation when t= 10 min, then

$k_r = 1.3 \times 10^{-4}$ $m_l^3 m_e^{-2} s^{-1}$

and the average value of k_r is calculated to be

$k_r = 7.3 \times 10^{-5}$ $m_l^3 m_e^{-2} s^{-1}$

APPENDIX E The single channel trickle-flow reactor: Temperature measurements

Preliminary experiments were made to confirm that the liquid and gas temperatures approached each other at the exit of the reactor. In this series of experiments the power inputs to the electrical heaters at the inlet and outlet of the reactor were varied in order to select optimum operating conditions. As can be seen in Table E.1 there is no need for additional electrical heat when the temperature of the heated jacket is 140°C.

Table E.1 Temperature measurements for the single channel, trickle flow reactor

Gas inlet	Liquid inlet	Gas outlet	Liquid outlet	Setting of the electrical heaters (ohm)		Heated jacket temperature
°C	°C	°C	°C	top	bottom	°C
96	149	102	101	3	1.5	25
102	151	108	106	3	1.5	25
110	150	117	114	3	2.0	25
117	150	129	127	3	2.5	25
119	147	146	142	3	3.0	25
116	144	151	147	3	3.0	25
94	141	135	131	3	3.0	25
90	120	122	124	0	0	125
95	134	127	125	0	0	130
115	142	140	140	0	0	140
116	141	139	139	0	0	140
117	140	140	139	0	0	140

APPENDIX F The single channel, trickle flow reactor: An example of applying regression analysis to a concentration versus liquid flowrate plot.

For a single channel, trickle flow reactor operating at a temperature of 413 K applying regression analysis to tha data presented in Figure F.1.

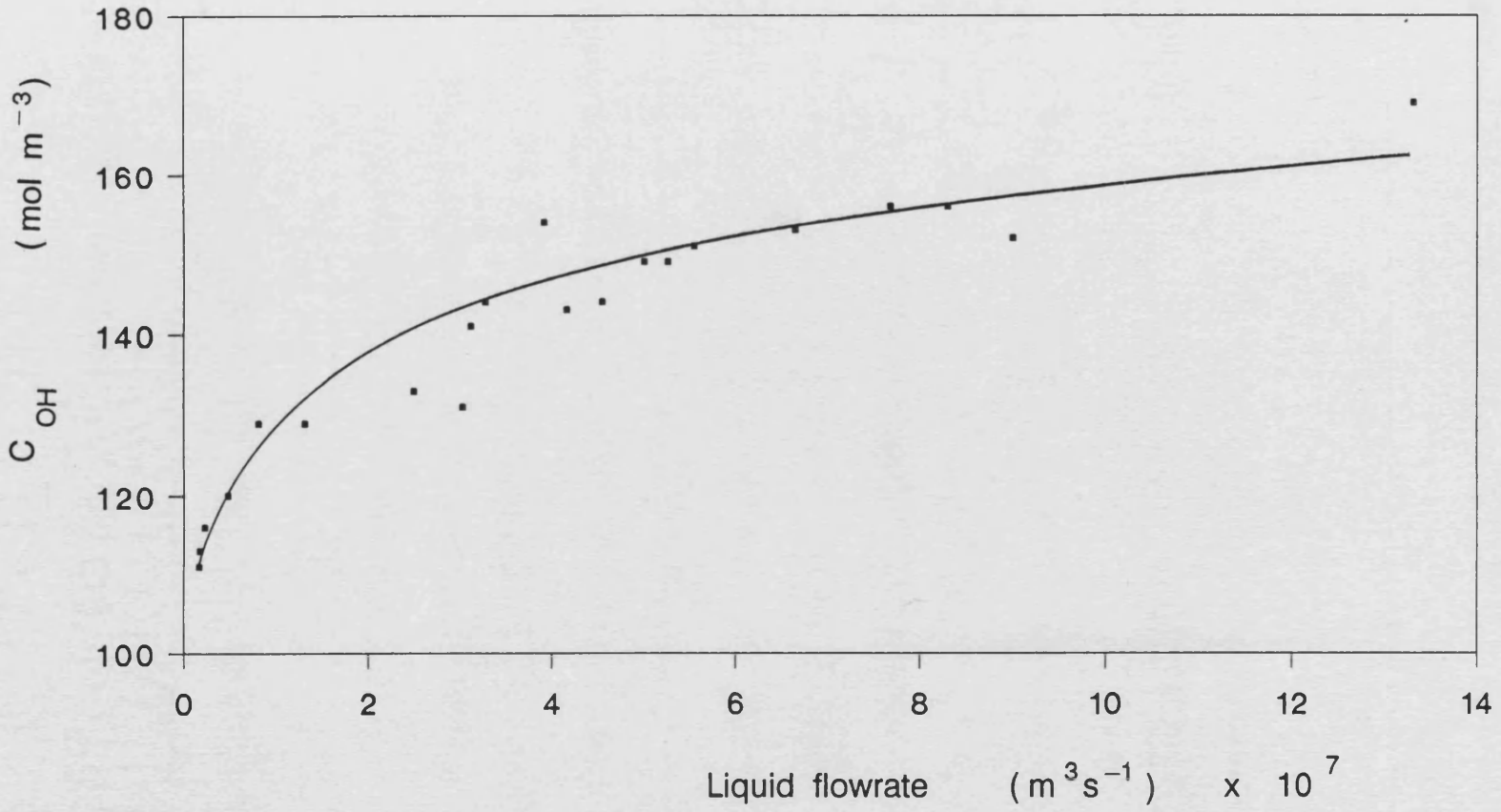

Figure F.1 Reactor outlet concentration as a function of inlet liquid flowrate (T=413 K ; P=0.079 bar ; ▪ represents data points ; continuous line represents non-linear regression curve).

APPENDIX G The flowchart, algorithm and print out of the computer programs

The language used was Q-Basic and the program ran on an PCSX Opus Technology personal computer.

Figure G.1 gives the flowchart of the one dimensional model for the single channel, catalytic flow reactor.

Figure G.2 gives the algorithm of the program : Modelling of the single channel catalytic flow reactor. This routine is used in Chapter 4, Section 4.2

Figure G.3 gives the algorithm of the multi-channel monolith program: Simulation of the single channel catalytic flow reactor to a multi-channel monolith reactor. This routine is used in Chapter 4, Section 4.3.

Figure G.4 gives the print out of one of the simulation runs.

Figure G.1 **The flowchart of the one dimensional model for the single channel, catalytic flow reactor.**

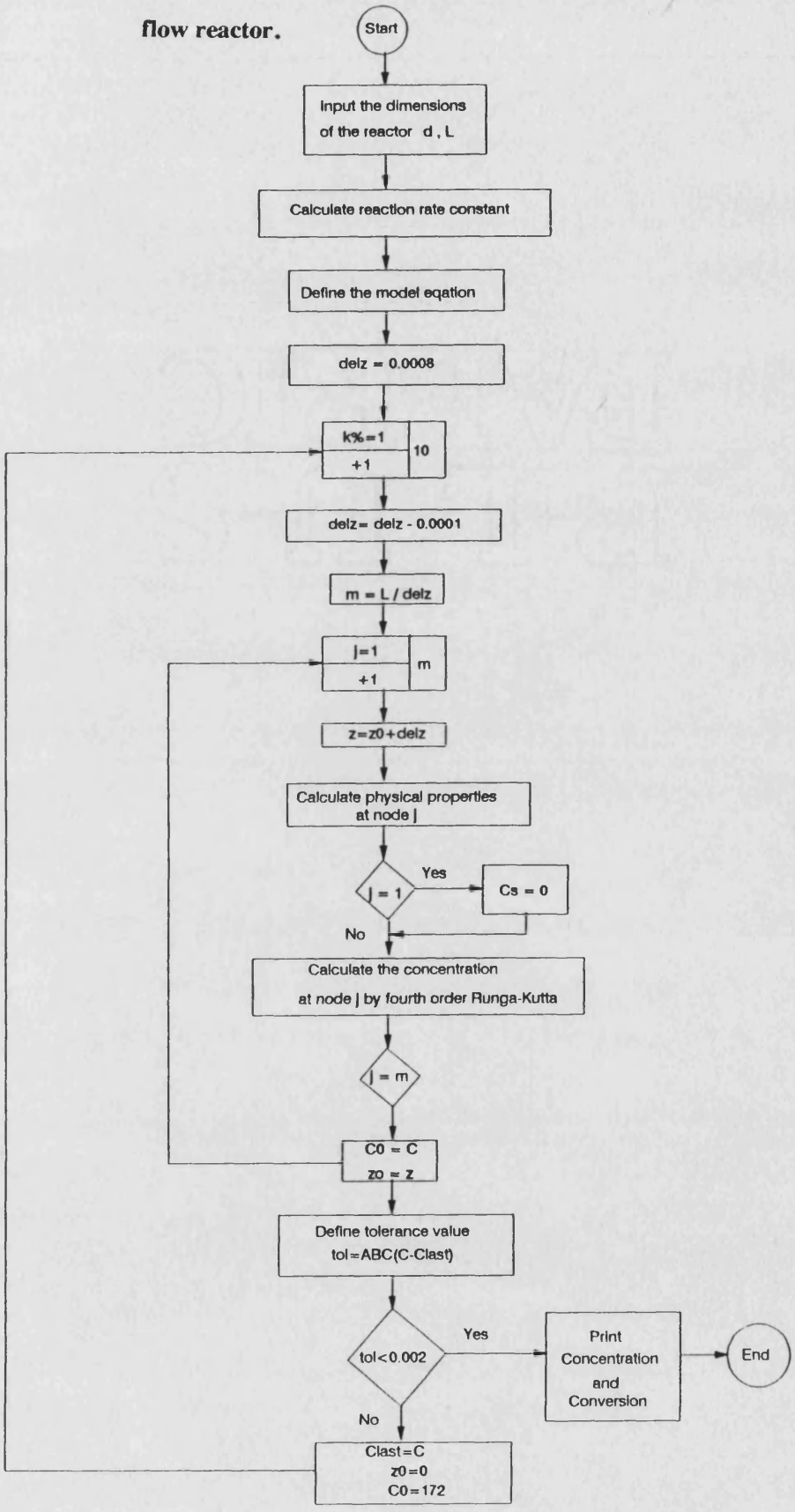

Figure G.2 **The algorithm of the program : Modelling of the single channel catalytic flow reactor.**

```
SCREEN 0: WIDTH 80: CLS : KEY OFF
PRINT "*************************************************"
PRINT "*                                               *"
PRINT "*        MODELLING OF THE SINGLE CHANNEL        *"
PRINT "*            CATALYTIC REACTOR                  *"
PRINT "*                                               *"
PRINT "*               MODEL.BAS                       *"
PRINT "*                                               *"
PRINT "*************************************************"

'*******REACTOR DIMENSIONS (m)*********
READ d, L
DATA .015,2

'*******CALCULATION OF THE REACTOR SIZE*******

'CROSS SECTIONAL AREA
S = (3.14159 * d ^ 2) / 4!

'SURFACE AREA
P = 3.14159 * d * L

'VOLUME
v = S * L

'SURFACE AREA PER FREE UNIT VOLUME
a = P / v

'*******DATA FOR ARRHENIOUS EQUATION*****
READ Ar, E, R, t
DATA 4.188E-4, 16126.64, 8.314, 413

'*******INITIAL CONDITIONS*******
'CONCENTRATION (mol/m^3) AND AXIAL LENGTH (m)
C0 = 172.4: z0 = 0

PRINT "ENTER LIQUID FLOWRATE, Vl  (m^3/s)"
INPUT "liquid flow rate, Vl="; Vl

'****CALCULATION OF AVERAGE VISCOSITY****
'****FROM THE INLET CONCENTRATION****
avis = 63 * (C0 / 1000) ^ -.47692

'****CALCULATION OF REACTION RATE CONSTANT (m/s)****
kr = Ar * EXP(-E / (R * t))

CLS
LOCATE 3, 10: PRINT "TABLE OF THE RESULTS"
LOCATE 5, 2:  PRINT "Volumetric flowrate="; Vl; "m3/s"
LOCATE 8, 1:  PRINT "Length"
```

```
 LOCATE 9, 3:  PRINT "z, m"
 LOCATE 8, 14: PRINT "Exit Concent."
 LOCATE 9, 15: PRINT "Cl, mol/m3"
 LOCATE 8, 30: PRINT "Surface Concen."
 LOCATE 9, 32: PRINT "Cs, mol/m3"

'****DEFINITION OF THE DIFFERENTAL EQUATION*****
 DEF fneqn (QQ, LCONS, SCONS) = -QQ * (LCONS - SCONS)

'****INITIAL STEP INTERVAL VALUE***
 delz = .0008

 Clast = 170
'****CHANGING THE STEP INTERVAL****
 FOR K% = 1 TO 10
 delz = delz - .0001

 m% = L / delz

 FOR i% = 1 TO m% STEP 1
 z = z0 + delz

'****CALCULATION OF THE CHAIN LENGTH****
 Cn = (LOG(avis) - .865448) / .417816

'****CALCULATION OF THE MOLECULAR WEIGHT****
 MW = 240 + 74 * Cn ^ 2

'****CALCULATION OF THE DIFFUSION COEFFICIENT (m^2/s)****
 vis1 = (avis / (1000 ^ 2))
 mw1 = (MW / .97) ^ (1 / 3)
 Tem = (vis1 * 10000 * .97 * mw1)
 Diff = (8.53369E-05 / Tem) / (100 ^ 2)

'****CALCULATION OF FILM THICKNESS (m)****
 fth = ((3 * vis1 * Vl) / (3.14159 * d * 9.8)) ^ (1 / 3)

'****CALCULATYION OF VELOCITY  (m/s)****
 vel = Vl / (3.14159 * ((d / 2) ^ 2 - ((d / 2) - fth) ^ 2))

'****CALCULATION OF SCHMIDT NUMBER****
 Sc = vis1 / Diff

'****CALCULATION OF REYNOLDS NUMBER****
 Re = vel * fth / vis1

'CALCULATION OF SHERVOOD NUMBER****
 lt = ((z * d) / fth ^ 2) ^ (-.32379)
 Sh = .00178 * Re ^ 1.378 * Sc ^ 1.276 * lt

'****CALCULATION OF MASS TRANSFER COEFFICIENT (m/s)****
 km = Sh * Diff / fth
```

```
'****CALCULATION OF OVERALL RATE CONSTANT (m/s)***
 K = 1 / ((1 / km) + (1 / kr))


'****CALCULATION OF SURFACE CONCENTRATION (mol/m^3)***
 Cs = C0 / ((kr / km) + 1)

'****SOLUTION OF DIFFERENTIAL EQUATION****
'****USING RUNGE-KUTTA              METHOD****

 IF i% = 0 THEN Cs = 0
 QQ = (km * a * S) / Vl
 LCONS = C0
 SCONS = Cs
 h = delz
 k1 = h * (fneqn(QQ, LCONS, SCONS))
 LCONS = C0 + (1 / 2) * k1
 k2 = h * (fneqn(QQ, LCONS, SCONS))
 LCONS = C0 + (1 / 2) * k2
 k3 = h * (fneqn(QQ, LCONS, SCONS))
 LCONS = C0 + k3
 k4 = h * (fneqn(QQ, LCONS, SCONS))
 C = C0 + (1 / 6) * (k1 + 2 * k2 + 2 * k3 + k4)

 dels% = m% / 4

 IF i% = dels% THEN j = 1: GOTO 10
 IF i% = dels% * 2 THEN j = 2: GOTO 10
 IF i% = dels% * 3 THEN j = 3: GOTO 10
 IF i% = dels% * 4 THEN j = 4: GOTO 10
 IF i% = dels% * 5 THEN j = 5: GOTO 10

 GOTO 20

10
'***PRINTING THE RESULT****
 LOCATE 6, 2: PRINT "Step interval="; delz
 LOCATE 10 + j, 2: PRINT USING "#.#"; z
 LOCATE 10 + j, 16: PRINT USING "###.#####"; C
 LOCATE 10 + j, 32: PRINT USING "###.#####"; Cs


20
 avis = 63 * (C / 1000) ^ -.47692
 z0 = z
 C0 = C
```

```
        NEXT i%
        LOCATE 20, 20: PRINT : INPUT "press to any key", kk$
        tol = ABS(C - Clast)
        IF tol < .002 GOTO 30
        Clast = C
        z0 = 0: C0 = 172.4
        NEXT K%

30
        END
```

Figure G.3 The algorithm of the multi-channel monolith program: Simulation of the single channel catalytic flow reactor to a multi-channel monolith reactor.

```
SCREEN 0: WIDTH 80: CLS : KEY OFF
LPRINT "*************************************************"
LPRINT "*                                               *"
LPRINT "*       SIMULATION OF THE SINGLE CHANNEL        *"
LPRINT "*       FLOW REACTOR TO A MULTI- CHANNEL        *"
LPRINT "*         MONOLITH SUPPORT REACTOR              *"
LPRINT "*                                               *"
LPRINT "*              SIMUL.BAS                        *"
LPRINT "*                                               *"
LPRINT "*************************************************"
LPRINT

'*******Enter the reactor dimensions**********
LPRINT : LPRINT "    Enter the reactor type"
LPRINT : LPRINT "         1. Circular cell monolith"
LPRINT : LPRINT "         2. Square cell monolith"
5    LPRINT :

LPRINT "Enter your choice  (1 or 2)"
INPUT "Enter your choice(1-2)"; RQ
IF RQ < 1 OR RQ > 2 THEN GOTO 5

LPRINT : LPRINT "Enter dimensions of the reactor"

INPUT "Inside diameter of the cell"; di
LPRINT : LPRINT "Inside diameter of the cell="; di; "m"

INPUT "Length of the monolith bed"; L
LPRINT : LPRINT "Length of the monolith bed="; L; "m"

INPUT "Diameter of the column"; Dc
LPRINT : LPRINT "Diameter of the column="; Dc; "m"
LPRINT

INPUT "Step interval"; delz
LPRINT : LPRINT "Step interval="; delz; " m"

'****CALCULATION OF WALL THICKNESS****
tw = .138 * di

LPRINT : LPRINT "wall thickness="; tw; " m"

hdo = di + tw

IF RQ = 1 THEN GOTO 6: LPRINT
IF RQ = 2 THEN GOTO 7: LPRINT
```

```
'****INITIAL CONDITIONS****
 C0 = 38: z0 = 0: T = 408
 Cin = C0

 LPRINT "Enter the initial conditions"

 LPRINT : LPRINT "Volumetric liquid flowrate="; Vl; " m^3 / s"

 Vlt = Vl / Nt
 Spt = Ac * 1.5 / Vl

'***Calculate the average viscosity from the inlet concentration
 avis = 63 * (C0 / 1000) ^ -.47692

'****Calculation of reaction rate constant*****
 kr = Ar * EXP(-Pr / (R * T))

'*****Calculate the number of steps******
 m% = L / delz
 CLS
 LPRINT
 LPRINT "Inlet concentration="; Cin; " mol/m^3"
 LPRINT
 LPRINT "Reactor temperature="; T; "K"
 LPRINT "Exit concentration of OH ="; C; "mol / m ^ 3"
 LPRINT
 LPRINT "TABLE OF THE RESULTS"
 LPRINT

'****Definition of the differential equation*****
 DEF fneqn (QQ, LCONS, SCONS) = -QQ * (LCONS - SCONS)

 FOR i% = 0 TO m% STEP 1
 z = z0 + delz

'****Chain length****
 Cn = (LOG(avis) - .865448) / .417816

'****Molecular weight****
 MW = 240 + 74 * Cn ^ 2

'****Diffusion cefficient****
 vis1 = (avis / (1000 ^ 2))
 mw1 = (MW / .97) ^ (1 / 3)
 Tem = (vis1 * 10000 * .97 * mw1)
 Diff = (8.53369E-05 / Tem) / (100 ^ 2)

'****Film thickness****
 fth = ((3 * vis1 * Vlt) / (3.14159 * di * 9.8)) ^ (1 / 3)
```

```
'****CALCULATION OF THE REACTOR SIZE*****
6
 LPRINT : LPRINT
 LPRINT "Your choice =>  CIRCULAR CELL MONOLITH "
 LPRINT

'****CALCULATION OF VOID FRACTION****
 e = (3.14159 * di ^ 2) / (2 * (3 ^ .5) * hdo ^ 2)

'****CALCULATION OF CELL DENSITY****
 Nc = 2 / (3 ^ .5 * hdo ^ 2)

'****CALCULATION OF CROSS SECTIONAL AREA OF A CELL***
 A = (3.1416 * di ^ 2) / 4

'****CALCULTION OF SURFACE AREA PER UNIT BED VOLUME***
 S = 4 * di * (1 - e) / (hdo ^ 2 - di ^ 2)

 LPRINT
 LPRINT "Cell density="; Nc; "cell / m ^ 2"
 LPRINT
 LPRINT "Void fraction of the monolith bed="; e
 LPRINT

 GOTO 8
7
 LPRINT : LPRINT
 LPRINT "Your choice =>  SQUARE CELL MONOLITH"


 e = di ^ 2 / hdo ^ 2
 Nc = 1 / (hdo ^ 2)
 A = di ^ 2
 S = 4 * (e ^ .5 - e) / tw

 LPRINT "Cell density="; Nc
 LPRINT
 LPRINT "Void fraction of the monolith bed="; e

8
'****CALCULATION OF CROSS SECTIONAL AREA OF COLUMN***
 Ac = (3.1416 * Dc ^ 2) / 4

'****CALCULATION OF NUMBER OF CELL****
 Nt = Nc * Ac
 St = A * Nt

'****CALCULATION OF BED VOLUME****
 Vt = St * L

 LPRINT "Total number of the cells="; Nt

'****DATA FOR ARRHENIOUS EQUATION****
 Ar = .0004188: Pr = 16126.64: R = 8.3144
```

```
'****interstitial velocity****
 vel = Vlt / ((3.14159 * ((di / 2) ^ 2 - ((di / 2) - fth) ^ 2)))

'****Schmidt number****
 Sc = vis1 / Diff

'****Reynolds number****
 Re = vel * fth / vis1

'****Sherwod  number****
 lt = ((z * di) / fth ^ 2) ^ (-.32379)

 Sh = .00178 * Re ^ 1.378 * Sc ^ 1.276 * lt

'****Mass transfer coefficient****
 km = Sh * Diff / fth

'****Overall rate calculation****
 K = 1 / ((1 / km) + (1 / kr))


'****Surface concentration calculation****
 Cs = C0 / ((kr / km) + 1)

'Solution of the differential equation

 IF i% = 1 THEN Cs = 0
 QQ = ((km * A * Nt * S) / Vl)
 LCONS = C0
 SCONS = Cs
 h = delz
 k1 = h * (fneqn(QQ, LCONS, SCONS))
 LCONS = C0 + k1 * 1 / 2
 k2 = h * (fneqn(QQ, LCONS, SCONS))
 LCONS = C0 + k2 * 1 / 2
 k3 = h * (fneqn(QQ, LCONS, SCONS))
 LCONS = C0 + k3
 k4 = h * (fneqn(QQ, LCONS, SCONS))

 C = C0 + (1 / 6) * (k1 + 2 * k2 + 2 * k3 + k4)

 dels% = m% / (4)

 IF i% = m% GOTO 9

 GOTO 10
9
'****PRINTING THE RESULTS****

 LPRINT "Volume of the reactor ="; Vt
 LPRINT
```

```
   Rate = (Ac * L) / 1.33

   LPRINT "(V)mon/(V)pel="; Rate
   LPRINT
   Con = (Cin - C) / Cin

   LPRINT "Exit concentration of hydroxyl groups="; C; "  mol / m^3"
   LPRINT

   LPRINT "Conversion of hydroxyl groups ="; Con
   LPRINT : LPRINT

   END

10
   avis = 63 * (C / 1000) ^ -.47692
   z0 = z
   C0 = C

   NEXT i%
```

Figure G.4 **The print out of one of the simulation runs.**

```
**********************************************************************
*                                                                    *
*              SIMULATION OF THE SINGLE CHANNEL                      *
*              FLOW REACTOR TO A MULTI- CHANNEL                      *
*                 MONOLITH SUPPORT REACTOR                           *
*                                                                    *
*                        SIMUL.BAS                                   *
*                                                                    *
**********************************************************************

Enter the reactor type

        1. Circular cell monolith

        2. Square cell monolith

Enter your choice  (1 or 2)

Enter dimensions of the reactor

Inside diameter of the cell= .005 m

Length of the monolith bed= 1.4 m

Diameter of the column= 1.1 m

Step interval= .0006  m

wall thickness= .00069  m

Your choice =>  CIRCULAR CELL MONOLITH

Cell density= 35665.21 cell / m ^ 2

Void fraction of the monolith bed= .7002842

Total number of the cells= 33893.86

Enter the initial conditions

Volumetric liquid flowrate= .000683  m^3 / s

Inlet concentration= 38  mol/m^3

Reactor temperature= 408 K

TABLE OF THE RESULTS

Volume of the reactor = .9317084

(V)mon/(V)pel= 1.000352

Exit concentration of hydroxyl groups= 8.917166   mol / m^3

Conversion of hydroxyl groups = .7653378
```